This thesis, “Crater lake evolution during volcanic unrest: case study of the 2005 phreatic eruption at Santa Ana volcano, El Salvador,” is hereby approved in partial fulfillment of the requirements for the Degree of MASTER OF SCIENCE IN GEOLOGY.

Department:

Geological and Mining Engineering and Sciences

Signatures:

Thesis Co- Advisor _____

Typewritten Name *Dr. William I. Rose*

Thesis Co- Advisor _____

Typewritten Name *Dr. Matthew R. Patrick*

Department Chair _____

Typewritten Name *Dr. Wayne Pennington*

Date _____

ABSTRACT

Santa Ana volcano in El Salvador hosts a small acid crater lake and fumaroles in its summit crater. From 2000 to 2004, volcanic activity was characterized by relative quiescence interrupted by episodes of hydrothermal venting. Degassing took place via wet and dry ascent paths. Aqueous chemistry analyses and temperature measurements revealed an acid (pH~1) sulfate-chloride (SO_4/Cl~1.5) lake that was consistently several degrees warmer than ambient temperature. Energy budget modeling elucidated the stark contrast between the relatively cool crater lake with a small heat input (< 15 MW) and the adjacent high temperature fumaroles (875 degrees C). In June 2004, unrest began and progressed into a volcanic crisis in late August 2005 when incandescence was observed in the crater fumaroles. The volcanic crisis was marked by anomalously high sulfur dioxide fluxes and uncharacteristic seismicity (VT, LP, "banded" tremor). The month-long crisis ultimately culminated in a phreatic eruption (VEI 3) on 1 October 2005. The 2005 eruption significantly changed the crater geometry. Satellite images and visual observations show that the lake changed color and position, drowning the adjacent high temperature fumaroles. Degassing directly into (and through) the lake at the newly subaqueous fumarole caused the lake to acidify (pH>0.5) and warm (<65 degrees C, <830 MW), resulting in periodic evaporations during 2006 and 2007.

Eruption precursors could be interpreted to signify an arrival of new magma within a few kilometers of the surface prior to the October 2005 eruption, but lack of a conclusive magmatic component among eruptive products and lack of geochemical evidence of water-magma interaction suggest that new magma was not involved, or

alternatively, that an intrusion of new magma stalled at depth below the hydrothermal system. Continued lake instability post-2005, i.e. lake evaporations, suggests that magma may still reside at shallow levels in the edifice. The reality of a magmatic intrusion becomes more likely the longer high lake temperatures and high heat flow continue to be recorded in the lake.

ACKNOWLEDGEMENTS

I am grateful for the support and encouragement I have received from many people during the course of my graduate studies. I am grateful for the guidance of my thesis committee: Dr. Bill Rose, Dr. Matt Patrick, Dr. Ann Maclean, and Dr. Joop Varekamp. I am especially thankful for my advisor Dr. Bill Rose, who has shown me my potential and encouraged me to develop into a creative, thoughtful, and independent scientist. I also owe thanks to MTU professors Dr. John Gierke and Dr. Jose Luis Palma who provided the motivation and assistance to finish up.

This project would never have been possible without the collaborations with Salvodoran volcanologists Demetrio Escobar, Eduardo Gutierrez, and Francisco Montalvo of Servicio Nacional de Estudios Territoriales. I also wish to thank Rodolfo Olmos and his students and the Universidad de El Salvador, and Carlos Pullinger and Marvin Garcia of LaGeo S.A. de C.V., for their collaborations in the field.

This project comes forth from the collaborative research environment fostered by the Remote Sensing for Hazards group at Michigan Tech, and I am thankful for the many fruitful conversations I have had with my fellow graduate students and for the vision of the professors who have made these exchanges possible. Finally, I would like to thank my family and friends who have supported me throughout this endeavor.

TABLE OF CONTENTS

LIST OF TABLES Page

LIST OF FIGURES Page

CHAPTER 1

1. Introduction

1.1 Problem statement

This study investigates the evolution of the crater lake at Santa Ana volcano (Illamatepec) in El Salvador during 2000 to 2007, focusing on a period of unrest in 2004 and 2005. The Santa Ana crater lake is used as a window into the subterranean hydrothermal and magmatic systems to infer driving processes at depth. At other crater lakes, it has been demonstrated that volcanic lake parameters (chemistry, temperature, size) often change prior to an eruption and can be used to monitor volcanic activity during unrest (*Delmelle & Bernard, 2000*).

At Santa Ana, volcanic unrest escalated into volcanic crisis, and finally culminated in a phreatic eruption on 1 October 2005 after 100 years of repose. A short-lived (1 hr. duration) ash-and-gas column rose to an altitude of 14 km and the crater lake breached the crater rim generating a hot acidic lahar. The 2005 eruption occurred after 16 months of unrest observed in the crater lake and fumaroles, but without any apparent short-term (days) precursors. Approximately 5000 people were evacuated and two people lost their lives. Communities on the eastern flank in particular were severely affected. Heavy rains from Hurricane Stan in the days following the eruption remobilized recently deposited ash, causing lahars (volcanic mudflows) to flow down the slopes of the volcano and inundate these communities with upwards of 2 m thick deposits of mud and rock.

The 2005 eruption was deemed phreatic as no conclusive magmatic component was identified among its eruptive products at that time (*D. Escobar, pers. comm.*). Historical records and phreatomagmatic deposits exposed in the crater suggest that larger

phreatomagmatic central vent eruptions are characteristic of historic activity in the last 500 years (*Smithsonian Eruptive History*). Eruptions in the last century have been small to moderate in magnitude (up to Volcanic Explosively Index (VEI) 3), with the last phreatomagmatic eruption occurring in 1904. During the study period three phreatic eruptions took place; the 1 October 2005 eruption was moderate in magnitude (VEI 3) while the other two were minor (VEI 1).

Long term baseline datasets are lacking at Santa Ana volcano; Santa Ana volcano has only been monitored since 2002, and only a few research studies had been conducted. *Meyer-Abich (1956)* first reported on the geology of the El Salvador and Guatemala, including the geology and eruptive history of Santa Ana volcano. Detailed petrology of the Santa Ana volcanic complex was presented over the course of several papers published in the 1980's by W.I. Rose & M.J. Carr's research groups (*Halsor & Rose, 1988; Carr & Pontier, 1981; Carr et al., 1981*), and more recently *Pullinger (1998)* reconstructed the eruptive history of the Santa Ana volcanic complex. Santa Ana volcano was a focus in the *Natural Hazards in El Salvador* GSA Special Paper (2004), with *Bernard et al. (2004)* presenting the first peer-reviewed publication on the geochemistry of the crater lake, *Siebert et al. (2004)* revisiting the Acajutla debris avalanche, and *Salazar et al. (2004)* reporting on diffuse degassing of CO_2 in the Santa Ana volcanic complex. Other recent studies include *Rodriquez et al. (2004)* presenting COSPEC measurements of SO_2 degassing during 2001 and 2002.

Despite the fatalities and damages caused by the 2005 eruption of Santa Ana, only two studies have been published which focused on the precursory activity leading up to this event. *Olmos et al. (2007)* presented SO_2 mini-DOAS degassing data before and

during the eruption, and discussed correlation with RSAM seismicity, and *Hernandez et al. (2007)* presented crater lake temperatures measured with a FLIR thermal camera in September 2005 and February 2006.

1.2 Volcanic hazards, society, and science in El Salvador

El Salvador is prone to a variety of geological and meteorological hazards, and volcanic hazard is one of the most potentially destructive phenomena. Though large scale volcanic events may occur infrequently, when they do occur their effects can be devastating. Volcanic risk is high in El Salvador owing to high population density and economic reasons. El Salvador is the smallest country in Central America, 21,040 km^2, with a population of ~5.7 million (May 2007) (*DIGESTYC, 2007)* and has the highest population density in Central America (*Rose et al., 2004*). Industry and agriculture are major sources of income, and fertile volcanic soils attract coffee, corn and sugarcane growers to the flanks of the volcanoes. Seventy percent of Salvadorans live within 20 km of potentially active volcanoes, with the largest cities taking their names from the active stratovolcanoes near which they are located: San Salvador (1.8 million people), San Miguel (455,000 people), and Santa Ana (522,000 people) (*Pullinger, 1998*). Furthermore, poorer people often have no choice but to live closer to the volcanoes or along steep walled valleys (*quebradas*), where they are at higher risk to volcanic explosions or debris flows/flash flooding.

Poverty, crime, and civil war, prevented scientific research and hazard awareness during the 1970s-early 1990s, but El Salvador is beginning to address the need for technical research and education about geohazards. After Hurricane Mitch (Nov. 1998)

and the 2001 earthquakes, the government created The National Service for Territorial Studies/*Servicio Nacional de Estudios Territoriales* (SNET) with the objectives of disaster prevention and risk reduction through technical research, land use planning, and dissemination of information to the public. A significant obstacle in the development of this agency is the lack of university degree programs in geosciences and, consequently, the lack of trained Salvadoran geoscientists. Currently, SNET employs three volcanologists charged with monitoring the country's active volcanoes. The demands of monitoring of these volcanoes preclude substantial time devoted to research.

Hazard-related scientific research is especially needed at Santa Ana volcano because: 1) Santa Ana is El Salvador's most active volcano; 2) Santa Ana volcano has a high surrounding population density with a total population of 1 million within a 25 km radius of the volcano, or 17% of the country's total population, including the cities of Santa Ana (population 522,000) 20 km to the north and Sonsonate (population 420,000) 20 km to the south (*Pullinger, 1998*); and 3) few hazard studies have been conducted.

1.3 Background on crater lakes and associated hazards

Fifty-five volcanoes worldwide host crater lakes with eruptive activity, occurring in a diversity of settings including Central America, New Zealand, Indonesia, the Philippines, Japan, and Africa (*Simkin & Siebert, 1994*). This represents approximately 7% of the world's 714 Holocene-age volcanoes (*Simkin & Siebert, 1994*). The existence of a volcanic lake depends on a delicate hydrologic balance between volcanic inputs, climatic effects, and hydrodynamic conditions (*Pasternack and Varekamp, 1997).* Volcanic lakes may persist in such a state of dynamic equilibrium for decades, but

perturbations to this balance may result in evaporation (e.g. Poas, *Rowe [1992]*, Santa Ana, *this study*). A generic conceptualized model of processes occurring in and below a crater lake is reproduced in Figure 1.1 (*Pasternack and Varekamp, 1997).* In this model, degassing from a magma body at depth ascends in the volcanic conduit in multi-phase flow and/or via a heat pipe mechanism. Degassing and recirculation of lake waters through a zone of sublimnic alteration below the lake leads to water-rock interaction and precipitation of sulfides & native sulfur as volcanic brines are injected into the lake at subaqueous vents.

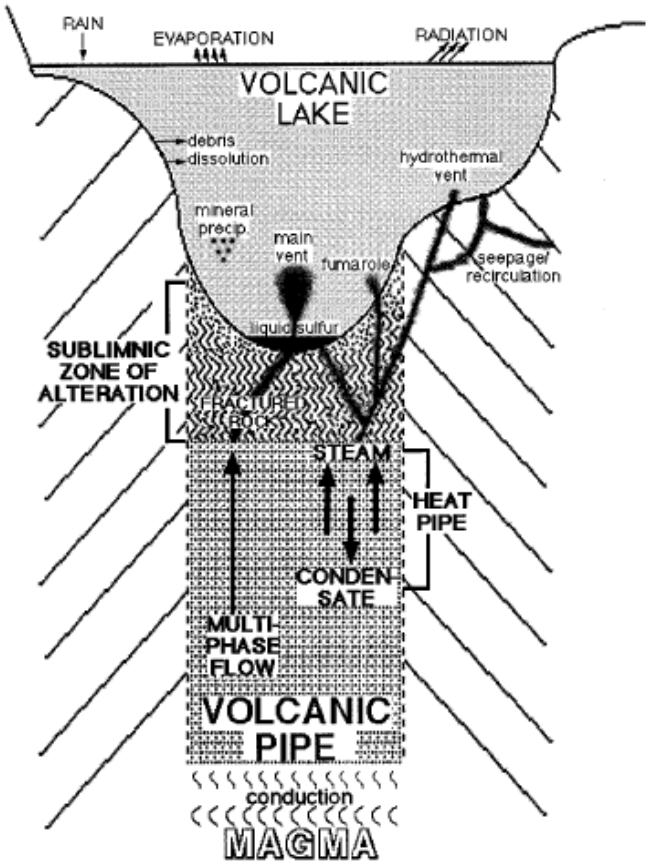

Figure 1.1: A generic conceptual model of processes occurring in and below crater lake. Figure reproduced from Figure 5 in *Pasternack and Varekamp (1997)*. With kind permission from Springer Science+Business Media: Bull. Volc., Volcanic lake systematics I. Physical constraints, 58, 1997, G.B. Pasternack & J.C. Varekamp, Figure 5.

Crater lakes on active volcanoes are windows into hydrothermal and magmatic systems. The composition of volcanic lake water ranges from cool dilute meteoric waters to hot concentrated acidic brines. This acidification comes from magmatic gases ascending from a shallowly degassing magma body below.

The modes of acidification often depend on the geometry (depth, extent) of the magmatic and hydrothermal systems. Condensing magmatic gases may form acidic fluids in-situ upon cooling which subsequently mix with groundwater where an extensive hydrothermal system overlies a deep magma body (e.g. Keli Mutu, *Pasternack & Varekamp [1994]*). If the magma body is very shallow, magmatic gases may be injected directly into the hydrothermal system (e.g. Kawah Ijen, *Demelle and Bernard [1994]).* Gases may even be injected directly into the lake if the magma breaches the lake bottom (e.g. Ruapehu, *Giggenbach [1974]*). In most cases, both mass and energy transfer occur in the volcanic conduit as water vapor and other gases ascend from magma at depth. However, for some systems a heat pipe requiring energy transfer without mass flow has been proposed (e.g. Ruapehu, *Hurst et al. [1991]*). A layer of native sulfur will often accumulate on the lake bottom where subaqueous fumaroles discharge into the lake (*Takano et al., 1994*).

Acidification of hydrothermal waters by hydrolysis of readily soluble volcanic gases (e.g. SO_2, HCl) promotes dissolution of wallrock or fresh magmatic intrusion by water-rock interaction, and enables precipitation and redissolution of secondary minerals. Lake hydrology contributes to a crater lake's size and composition via dilution by meteoric or glacial meltwater, concentration by evaporation, and mass loss by outflow or seepage. Few minerals tend to be saturated in acid lake waters, and lake chemistry is

mainly controlled by acidification by volcanic gas counterbalanced by neutralization by water-rock interaction with overprints of dilution and evaporation.

Volcanic lake hazards include phreatic activity, phreatomagmatic activity, lahars, base surges, wet ashfall, seepage of toxic fluids, and release of noxious gases to the atmospheric. The type of hazards associated with a particular lake depends on physical and chemical processes occurring at the lake at a given time. The physiochemical lake classification scheme of *Pasternack & Varekamp (1997)* facilitates identification of potential hazards and appropriate research and/or monitoring parameters (Table 1.1). Key parameters for classifying a particular lake include its eruption history, lake temperature, pH, and total dissolved solids (TDS) (*Pasternack & Varekamp, 1997*). High activity lakes may evolve into peak activity or variable mass lakes, resulting in variant hazards and a need to reevaluate necessary monitoring parameters.

Lake Type	Lake Subtype	Representative Values			Main Hazards	Research/Monitoring
		Temp	pH	TDS		
Variable Mass					Volcanic eruptions, lahars	Lake level, temperature, history, Mg/Cl
Peak Activity	hot acid-hyperbrine	>45ºC	< 0.3	>30%	Volcanic/phreatic eruptions, lahars, seepage of toxic fluids	Temperature, Mg/Cl, watershed monitoring
High activity	hot acid brine	35 to 45ºC	0.3 to 1.0	15-25%	Seepage of toxic fluids, evolution to peak activity	Temperature, volcanic flux estimates, Mg/Cl, sulfur isotopes, polythionate abundances, watershed monitoring
	cool acid brine	Tair to 35ºC	0.3 to 1.0	4-15%		
Medium activity	reduced acid-saline	Tair to 35ºC	1.0 to 3.0	1-4%	Atmospheric pollution, seepage of toxic fluids	Air and watershed monitoring
	oxidized acid-saline	Tair to 35ºC	1.0 to 3.0	1-4%		
Low activity				<1%	Lake explosions	Water column monitoring

Table 1.1: Crater lake classification scheme used for identifying potential hazards and appropriate monitoring parameters at volcanic lakes, adapted from *Pasternack and Varekamp (1997).*

Peak activity and variable mass lake types carry potential hazards of phreatic and phreatomagmatic volcanic eruptions. *Phreatic* eruptions are steam-and-gas driven explosions whose ejecta consist entirely of pre-existing wall rock and lack juvenile magmatic material, whereas *phreatomagmatic* eruptions generate eruptive products with juvenile material produced by direct interaction of magma with groundwater (*Barberi et al., 1992*). Phreatic eruptions occur when expansion of a confined overpressurized fluid ruptures an overlying impermeable caprock/carapace, usually formed by authigenic mineral precipitation from a geothermal fluid. Steam generated by boiling of groundwater is the main vapor phase constituent, e.g. at geothermal fields, but noncondensible magmatic gases, especially CO_2 and H_2S, can contribute significantly to overpressurization (*Wohletz & Heiken, 1992*). Caprock failure is commonly triggered by one or a combination of the following: fracturing following seismic events that reduces lithostatic load and/or increases heat flow as hot fluids flow through fractures, ascending magma heating shallow aquifers thereby reducing lithostatic load, and vaporization of surface waters infiltrating hot fractured rocks or a plugged conduit (*Barberi et al., 1992*). Phreatic activity can be very destructive, e.g. Bandai volcano, Japan in 1888 (*Yamamoto et al., 1999*); Agua Shuca geothermal vent, El Salvador in 1990 (*Handal & Barrios, 2004*).

Phreatic eruptions which occur at active volcanoes with hydrothermal systems are often triggered by magmatic intrusion, blurring the textbook distinction between phreatic and phreatomagmatic activity. At andesite volcanoes, “failed” magmatic eruptions generate minor phreatic eruptions (e.g. Soufrière Hills, Monserrat, *Sparks, 2000;* La Soufrière, Guadeloupe, *Heiken et al., 1980*), but modifications of the state of stress in the

upper crust prevent eruption of magma (*Pinel & Juapart, 2005*). Phreatic eruptions resulting from "failed" magmatic eruptions often have the same precursors as magmatic or phreatomagmatic eruptions (*Barberi et al., 1992*), making it difficult to accurately forecast events. Additionally, phreatic activity may herald the imminence of subsequent larger phreatomagmatic or magmatic eruptions, (e.g. Mount Saint Helens (May 1980), *Stoiber et al. [1981]*; Mount Pinatubo (June 1991), *Wolfe & Hoblitt [1996]*).

Phreatic-phreatomagmatic hazards at "peak activity" and "variable mass" lakes (see Table 1.1) may be effectively monitored with appropriate parameters of lake temperature, lake level, lake and watershed chemistry, and knowledge of lake history (*Pasternack & Varekamp, 2000*). For instance, long-term data sets obtained at crater lakes on Ruapehu, Poas, and Kusatsu-Shirane volcanoes have unambiguously demonstrated that geochemical and physical processes are strongly linked (*Varekamp et al., 2000; Rowe et al., 1992; Ohba et al., 1994*). Lake water chemistry often changes prior to an eruption and can be used to monitor volcanic activity (*Giggenbach, 1974*). Crater lakes respond to increased heat and gas fluxes with anomalous temperature, volume, and chemistry changes months to weeks before the onset of eruptive activity. Increased heat and gas fluxes can be caused by an increase in enthalpy of geothermal fluids entering the lake, an increase in gas flow rate or the injection of new magma. Increases in temperature prior to eruptions have been identified at several lakes, (e.g. Raoul Island, Kermadac Islands; Ruapehu, New Zealand, *Giggenbach, [1983]),* and concurrent increases in Mg/Cl ratio has been identified at Ruapehu (*Giggenbach, 1983*). Lake level may drop prior to an eruption due to enhanced seepage. Temperature changes, or changes in chemistry of acid fluids entering lake, can also alter lake composition by

changing the degree of saturation of minerals and promoting precipitation or dissolution reactions (*Bernard et al., 2004*).

Other parameters appropriate for monitoring phreatic-phreatomagmatic eruptions include seismicity, fumarolic gases, and sulfur dioxide emissions. Magmatic and hydrothermal activity generates a seismic signature that includes volcano-tectonic seismicity, long period seismicity, tremor, and banded tremor. Volcanic tremor is often the most reliable short term precursor to phreatic eruptions, occurring days to hours prior to eruption (Kusatu-Shirane, 1932, 1 hour before; Ruapehu, 1969, half an hour before, *Barberi et al. [1992]*). Composition of fumarolic gases directly provides information on magmatic gases discharge, though direct sampling may be difficult and dangerous during periods of elevated activity. Remote detection of volcanic gases provides a safer alternative to direct sampling, and volcanic SO_2 is commonly monitored at active volcanoes (*Symonds et al., 1994*).

1.4 Objectives & Methodology

1.4.1 Objectives

There are five primary research objectives for my thesis project: 1) to improve monitoring capabilities at Santa Ana volcano; 2) to identify long-range and short-range precursors to 2005 eruption; 3) to interpret possible eruption triggering mechanisms for 2005 eruption; 4) to evaluate the impact of the 2005 eruption on the crater lake and fumaroles; and 5) to provide eruption hazard assessment for Santa Ana and to provide suggestions for future monitoring.

1.4.2 Methodology

To improve monitoring capabilities at Santa Ana volcano, I will first analyze seven years of archived crater lake temperature and chemistry time series. I will then integrate these datasets with seismic and volcanic SO_2 degassing datasets to see if the combination of datasets reveals new insights. Seismic and SO_2 degassing datasets will provide crucial information on volcanic activity immediately preceding and following the 2005 eruption when crater lake data were not available. In addition to evaluating existing archived data, I will improve monitoring capabilities by providing new remote sensing monitoring tools. Spaceborne thermal infrared remote sensing will be used to investigate new ways to monitor crater lake temperature and size. The ASTER satellite sensor will be targeted as an appropriate remote sensing monitoring tool.

Once I have analyzed and integrated existing and new datasets, I will need to develop a physical model of the magmatic and hydrothermal systems to achieve the remaining four objectives. The physical model will provide a framework within which to link observed events/dataset trends with plausible physical processes. This physical model will provide a context to identify an eruption triggering mechanism. This model will also shed light on whether the 2005 eruption can be classified as a phreatic eruption, a phreatomagmatic eruption, or a failed magmatic eruption resulting in a phreatic eruption. Mineralogical analysis of tephras and lake bottom ejecta will provide critical information on magmatic and hydrothermal alteration components in erupted products.

To provide a current eruption hazard assessment, I will need to evaluate how the 2005 eruption changed the magmatic and hydrothermal systems. The physical model will provide a context in which to identify those changes. Classifying the lake during pre-

eruptive, and post-eruptive periods using the physiochemical classification scheme of *Varekamp et al. (2000)* will facilitate identification of potential hazards for the prevailing magmatic-hydrothermal conditions. Lake classification will also facilitate choosing appropriate monitoring parameters. This eruption hazard assessment will assist with planning for future disasters at Santa Ana.

1.5 International Collaboration

An additional objective of this thesis project is to develop sustainable relationships with Salvadoran counterparts in several institutions in El Salvador—Servicio Nacional de Estudios Territoriales (SNET), Universidad de El Salvador (UES), and LAGEO (private geothermal company). This objective is cultural rather than scientific in nature, but is nonetheless an important aspect of working abroad that is sometimes overlooked. This objective is very much in line with the aims of the NSF OISE/PIRE project which is funding this research, *Remote Sensing for Hazard Mitigation and Resource Protection in Pacific Latin America*, and is also in line with the "broader impacts" criteria of NSF itself.

To achieve the goal of establishing sustainable relationships, I will work in such a way with Salvadoran counterparts so that the collaboration is mutually beneficial. I will work closely with Salvadoran scientists via email and in person, so that trust is established. I will benefit by having access to archived data, from guidance in the field, and from their personal experience during the 2005 eruption crisis. Salvadoran counterparts will benefit from final outcome of my study—an assessment of eruption hazards and suggestions for future monitoring, as well as enhanced understanding of

physical volcanic processes at Santa Ana—as well as from my expertise in remote sensing of active volcanoes. I will transfer my knowledge of satellite remote sensing techniques by holding workshops for each collaborating institution. These relationships will pave the way for further collaborations between Salvadoran institutions and Michigan Technological University.

1.6 Thesis outline

In chapter 2, I will summarize the eruptive history of Santa Ana volcano. I will briefly describe the geologic setting, then report on the eruptive history of the Santa Ana complex, focusing on Santa Ana volcano itself. I will provide a detailed account of the events leading up to, during, and after the October 2005 eruption, including visual observations of SNET personnel and myself.

In chapter 3, I will present data collection &analytical methods. I will present results of lake temperature, lake chemistry, mineralogy of erupted products, as well as SO_2 fluxes and seismicity.

In chapter 4, I will present data analysis. Data analysis includes modeling the both the saturation state of the lake and the energy budget of the lake.

In chapter 5, I will provide interpretations of the data analysis. Comparison to other similar volcanoes will provide analogs to understanding the Santa Ana magmatic – hydrothermal systems. I will present a new physical model for the Santa Ana magmatic – hydrothermal systems. Based on this model, I will identify eruption precursors and propose eruption triggering mechanisms for the 2005 event. I will conclude with an

assessment of the current phreatic and phreatomagmatic eruption hazard and provide suggestions for future research.

In chapter 6, I will synthesis the conclusions of this research project.

CHAPTER 2

2. Eruptive history of Santa Ana volcano

2.1 Geological Setting

Santa Ana volcano (13.853ºN, -89.63ºE, 2381 m summit elevation) is located approximately 40 km west of the city of San Salvador, the capital of El Salvador (Figure 2.1). Santa Ana volcano is part of a volcanic complex in northwestern El Salvador situated in the Central American volcanic front, resulting from oblique convergence of the Cocos plate beneath the Caribbean plate along the Middle America trench at a rate of ~8 cm/yr (*DeMets et al., 1990*). The front is the locus of nearly all volcanic activity, and extends in linear, right-stepping segments 1100 km from the Mexico-Guatemala border to Costa Rica parallel to the trench (*Carr, 1984, Carr et al., 1982*). The Santa Ana volcanic complex lies on the southern boundary of the Central Graben, a tectonic depression which runs the length of the country, between the Apaneca Range to the west and San Salvador volcano to the east.

The main eruptive vents in the Santa Ana volcanic complex are the Santa Ana and Izalco stratovolcanoes, and the Coatepeque collapse caldera (Figure 2.2). The complex also contains the parasitic cones Cerro Verde, San Marcelino, Chino, El Astillero, and Conejal to the southeast, and cinder cones and explosion craters to the northwest in the Chalchupa graben (*Pullinger, 1998*). Like most other volcanoes in El Salvador, the Santa Ana central vent is located at the intersection of two major structural features: an E-W fault system, which delineates the southern boundary of the "Central Graben," and a NW-SE regional fault system (*Wiesemann, 1975*). The NW-SE fault system is also evident

from the alignment of late Pleistocene eruptive vents to the northwest and southeast of Santa Ana volcano (*Pullinger, 1998*). The Santa Ana complex is younger than ~200 ka (*Pullinger, 1998*), and is underlain by the Miocene-Pliocene Bálsamo Formation and the Quaternary San Salvador Formation (*Siebert et al., 2004*).

2.2 Eruptive history of the Santa Ana volcanic complex

It has previously been proposed that below each of the three main eruptive vents in the Santa Ana volcanic complex are three magma plumbing systems fed by a common deep-seated parental magma body (*Carr & Pontier, 1981; Halsor & Rose, 1988, Pullinger, 1998).* Like other across-arc paired volcanoes associated with rhyolitic calderas in Central America, such as Cerro Quemado-Santa María-Almolonga, Tolimán-Atitlán-Atitlán caldera, and Acatenango-Fuego-Barahona, separate but contemporaneous magma bodies present below each volcano evolved and ascended through the crust at different rates *(Halsor & Rose, 1988). Carr & Pontier (1981)* first reported on the composition of the three magma types in the Santa Ana volcanic complex: LILE-rich basaltic andesite to andesite magma beneath Santa Ana volcano (52-62% SiO_2), LILE-poor basaltic andesite magma beneath Izalco (52-57% SiO_2), and rhyolite magma beneath Coatepeque. *Pullinger (1998)* later reported basaltic lavas at Santa Ana with as low as 50% SiO_2.

From the Pleistocene to the present, magmatism shifted progressively seaward from Coatepeque to Santa Ana to Izalco (Figure 2.2). The 6.5 x 10.5 km ENE-WSW Coatepeque caldera formed in two stages during paroxysmal rhyodacitic ignimbrite-forming Plinian eruptions ~15,000 years apart during the late Pleistocene. These Plinian

eruptions produced four voluminous tephra deposits, the Bellavista and Arce tephras (77±2 ka and 72±3 ka, respectively, both high precision $^{40}Ar/^{39}Ar$ age-dates; *Rose et al. (1999)*) and Congo and Conacoste tephras (Congo is 56.9±2.8–2.1 ka, [*Rose et al. (1999)*] or 53±3 ka [*Kutterolf et al. (2008)],* both high sensitivity ^{14}C age dates; and Conacoste is ~51 ka [*Kutterolf et al. (2008)]*, determined by dating from offshore sedimentation rates.)

Bimodal SiO_2 content of Santa Ana basaltic to andesitic lavas has been interpreted by *Carr & Pontier (1981)* as open system fractionation of a graded magma chamber with a silicic top and uniformly basaltic base *(McBirney, 1980)*. Static magmatic evolution was punctuated by injection of mafic magma and rapid eruption (*Halsor & Rose, 1988)*. Disequilibrium textures in mafic lavas have been interpreted as incomplete magma mixing (*Carr & Pontier, 1981)*.

Edifice sector collapse of Santa Ana volcano in the late Pleistocene at 10 ka produced the 16±5 m^3 Acajutla debris avalanche (*Pullinger, 1998*). Sector collapse has been attributed to hydrothermal alteration, regional earthquakes, unstable steep slopes, and shallow magma intrusions (*Siebert et al., 2004*). The Acajutla debris avalanche traveled ~50 km south to the Pacific Ocean, covering 390 km^2 on land and extending the coastline by 7 km (*Siebert et al., 2004*). The main conduit reactivated quickly due to lithostatic unburdening and the collapse scar was quickly filled in as Santa Ana grew to its present size (*Pullinger, 1998)*.

Following the edifice sector collapse, the main conduit became obstructed and vents were emplaced along NW-SE trending fissure (*Pullinger, 1998*). NW vents in the Chalchuapa graben were active until the pre-Colombian occupation of Tazumal around

300 BC (*Pullinger, 1998*). The SW vents have been active until recently; the last eruption was at San Marcelino in 1722 (*Pullinger, 1998*). A shift in volcanism away from the central vent may have caused collapse along four ring faults in the main edifice of Santa Ana, probably during 1525-1575, producing the nested craters observed presently (*Meyer-Abich, 1956*).

In 1770, the main center of volcanism shifted 4 km southward to Izalco volcano, though the Santa Ana central vent remained active simultaneously (*Meyer-Abich, 1956).* Izalco exhibited nearly continuous Strombolian activity from 1770 to 1965, earning the title "Lighthouse of the Pacific" (*Meyer-Abich, 1956; Pullinger, 1998).* Eruption of more mafic, completely mixed lavas probably occurred due to frequent recharging of the magma chamber below Izalco (*Halsor & Rose, 1988).*

2.3 Historic Activity at Santa Ana volcano

The massive (165 km^3) Santa Ana stratovolcano is the site of current eruptive activity in the complex. Santa Ana's flat-topped summit is marked by four semi-circular nested craters (Figure 2.3). The presently active vent is the steep-walled central explosion crater from 1904 (100 m depth). Figures 2.4a and 2.4b provide oblique and orthogonal views, respectively, of the explosion crater containing a small (~200 m diameter) acidic lake and adjacent high temperature fumaroles on the western crater wall. Figure 2.4a shows phreatomagmatic tephras overlying the summit crater. The 1904 phreatomagmatic eruption deposited phreatomagmatic tephra along the crater rim and up to 5km west of the crater over the course of two weeks, leaving behind a 0.5 km diameter explosion crater (*Smithsonian Eruptive History*). The 1904 eruption at Santa Ana occurred

simultaneously with activity at Izalco volcano, and was probably triggered by an earthquake (*Meyer-Abich, 1956*). Following the 1904 eruption, a volcanic lake appeared in the explosion crater and has existed ever since. A bathymetric survey carried out in 2000-2002 confirmed a bowl-shaped lake with a maximum depth of 27 m and a volume of 4.7 x 10^5 m^3 (black lake outline in Figure2.4b) and several bubbling hot springs have been observed along the shoreline (T ~ 80ºC) (*Bernard et al., 2004*). Intense fumarolic degassing in the explosion crater along the western crater wall has been observed in the last few decades (*since 1978, Stoiber GVP*). *Meyer-Abich (1956)* reports fumarolic activity since 1950, and postulates that crater fumarolic activity has probably occurred since the time of the Spanish Conquest in the 1500's. A gas plume driven by NE trade winds was often observed about the summit during 2000-2005, and vegetation and coffee plantations have been affected by acid rain, especially on the south and southwest flanks.

Historic activity at Santa Ana volcano in the last ~500 years is typified by phreatomagmatic or phreatic central vent eruptions, suggesting a hydrothermal system is present at shallow depths below the vent (*Pullinger, 1998*). Negative Bouguer anomalies and incompatible element geochemistry (*Carr & Pontier, 1981; Halsor & Rose, 1988*) support the presence of a large shallow magma chamber at a depth of 3-7km (*Carr et al., 1981*). Persistent passive degassing from fumaroles located in the crater and the presence of an acidic crater lake imply that shallow young magma bodies reside within or below the base of the cone (*Wohletz & Heiken, 1992*). Eruptions in the last century in have been small to moderate in magnitude (up to VEI 3), but phreatomagmatic tephras exposed in crater wall suggest larger eruptions have occurred in the recent past (Figure 2.4a).

Historical records document at least 12 explosive eruptions since 1520, yielding an average eruption rate 1-2 eruptions every 100 years (*Smithsonian Eruptive History*).

In the last hundred years, volcanic activity in the lake and fumaroles has been reported periodically. Activity has been limited to hydrothermal or phreatic activity since the last phreatomagmatic eruption in 1904. In 1920, boiling and considerable evaporation was observed in the lake (*Meyer-Abich, 1956; cf. Larde, 1923*). In July-August 1992, an increase in fumarolic activity and an order of magnitude increase in dissolved sulfate and chloride in the lake were observed (*SNET, unpublished data*). From May 2000 to February 2002, increased activity in the fumaroles, hot springs and lake without increased seismic activity was previously interpreted to be due to increased venting of the hydrothermal system (*BVGN 26:04*). Fumaroles, which in January 2000 had a temperature of 523ºC, were observed to be incandescent in glowing cracks in the fumarole field on 17 January 2001 (*BVGN 26:04)*. In June 2002, even higher fumarole temperatures were measured of up to 875ºC (*Bernard et al., 2004*). Incandescence was followed by an increase in SO_2 degassing, and one month later on 8-9 February 2001 SO_2 fluxes were measured by stationary and vehicular COSPEC at 393-244 tons/day (*BVGN 26:04*). Sulfur spherules were also observed in the lake at this time during February 2001. Interestingly, a 6 m decrease in lake level occurred between observations in January 2000 and February 2002. This episode of increased fumarolic activity without erupted lava and with retreating lake levels has been previously interpreted as leaking or cracking of an impermeable authigenic mineral cap in the hydrothermal system (*BVGN 26:04*).

2.4 The 2005 eruption crisis & visual observations

2.4.1 Precursory activity, June 2004 to August 2005

Beginning on 08 June 2004, Santa Ana volcano began to show signs of unrest. Intense degassing produced gas plumes that rose to 2000 m and were accompanied by a strong sulfur smell. While in the crater, SNET scientists reported hearing loud noises associated with degassing which were likened to a jet engine. The lake turned from green to brownish yellow, and lake level rose 1 m. Intense degassing, "jet engine noises," and a strong to moderate sulfurous smell continued to be observed throughout 2004 and into 2005 up until the eruption on 1 October 2005. Periodic gas plumes reached increasingly elevated heights of 500-600 m above the summit. Degassing occurred episodically throughout the pre-eruptive period, with pulses of variable duration, e.g. pulses ranging from 2 to 25 minutes observed in March 2005. There were also periods of sustained degassing in December 2004, February 2005 and April-May 2005, which were accompanied by floating rafts of sulfur in the lake in December 2004 and April 2005.

On the night of 15 June 2005, a minor phreatic eruption occurred in the crater. The explosion was registered seismically at 11:56 pm local time (*SNET Informe Especial*, *2005a)* and intense gas emission was observed the next day (*SNET Informe Especial*, *2005b*). The explosion generated a moderately sized rockfall on the western crater wall. The rockfall was composed of ash and altered talus from the fumarole field. A thin layer (<1mm) of ash was deposited on the northern flank (*SNET Informe Especial, 2005b*).

Beginning on 23 August, just one month prior to the 1 October 2005 eruption, the fumarole field was observed to be incandescent (Figure 2.5). The radiant heat output of the fumarole field reached a maximum at this time (1.02-1.05 $W*sr^{-1}*um^{-1}$, at-sensor

radiance, MODIS images). Concentric, circular incandescent cracks were observed from the crater rim on 23 August (SNET visual), 27 August (ITER FLIR), 28 & 29 August (SNET visual), 8 Sept (SNET visual) (Figure 2.5). Incandescence was observed in the fumarole field up until the eruption. By 27 September 2005 the lake had turned from green to chocolate brown color, but the lake level did not change significantly.

2.4.2 Phreatic eruption, 1 October 2005

Santa Ana volcano reawakened from100 years of repose with a moderately-sized phreatic eruption (VEI 3) on the morning of 1 October 2005 at 1420 UTC (8:20 am local time) (Figure 2.6). Although the volcano had exhibited 16 months of anomalous behavior, the eruption caught SNET volcanologists by surprise as there were no apparent precursors identified in the days preceding the eruption.

The phreatic eruption proceeded in two stages, thought the exact eruptive mechanism remains unclear. First, an initial lateral blast ejected the crater lake, breaching the crater rim to the east. The acid lake waters formed a hot boiling mudflow that flowed for 3 km down Las Minas drainage on the eastern flank (Figure 2.7) (*SNET report, October 2005*).

After the initial lateral blast, a gas-and-ash plume was generated high above the volcano (Figure 2.6). The Washington VAAC reported that ash was visible in MODIS satellite imagery to an altitude of 14 km. SNET visually estimated that the plume rose to 10 km above the volcano (*D. Escobar, pers. comm.).* The short-lived eruption plume (~1 hr. duration) deposited ballistics and ash up to 5 m thick at the crater rim and deposited ash up to 40 km to the west. Ashfall of 3-5 cm thick was reported in Los Naranjos, 5 km

NW of the summit (*Olmos et al., 2007*). SNET estimated a total volume of 1.5 * 10^4 m^3 of ash, which damaged 1,400 hectares of crops (*SNET, Eruption Chronology, BGVN 30:09*).

Approximately 5000 people within a 5 km radius around the volcano were evacuated, including San Blas (~1 km SE of the summit) and Coatepeque lakeshore communities. Communities on the eastern flank in particular were severely affected. Heavy rains from Hurricane Stan in the days following the eruption (2-10 October 2005) remobilized recently deposited ash, causing secondary lahars to flow down the slopes of the volcano primarily to the east towards Coatepeque. Los Planes de la Laguna was inundated with upwards of 2 m thick deposits of mud and rock, damaging houses and washing out the bridge in Caserio de Javillal (*BGVN 30:09*). Rainfall of > 100 mm per day was recorded in Los Naranjos during 3-6 October, with a maximum of 320 mm recorded on 5 October 2005 (*BGVN 32:04*). Local witnesses reported seeing the first lahar, carrying blocks up to 2 m in diameter, on the night of 2 October 2005. SNET seismically registered a total of 22 lahar events following the eruption, all of which were confirmed by local residents (*BGVN 32:04*). Two people lost their lives to landslides in Palo Campana.

2.4.3 Activity subsequent to the phreatic eruption, October 2005 to 2007

The 1 October 2005 eruption significantly changed the geometry of features within the crater (Figures 2.10a and 2.10b). The eruption destroyed the main fumarolic area on the western crater wall and left behind a flooded lake floor with a vigorous subaqueous fumarole (Figure 2.10a). An orthorectified ASTER image (4 Feb 2007)

shows that the crater lake shifted in position to the west (Figure 2.10b). In February 2006, weak crater fumaroles on the western crater wall where previously incandescent fumaroles had been observed had an average of 120ºC (SNET monthly report). Other fumaroles on the western crater wall measured at 75-81ºC. By July 2007, weak low temperature (92.0ºC to 95ºC) crater fumaroles on the western and southern walls emitted mostly water vapor, though some sulfur crystals and a weak sulfurous smell were present. The prominent subaqueous hot spring was observed in the center of the lake at the end of a peninsula of exposed sediments caused by a rockfall from the south wall sometime between 20 April and 2 May 2006. The hot spring exhibited activity ranging from bubbling to episodic upwelling to intense degassing.

Evaporation and degasification through the lake continued during the post-eruptive period, resulting in several evaporations of the lake in January -May 2006, April 2007 and August 2007 (e.g. April 2007 evaporation in Figure 2.8) and a geyser-like minor phreatic eruption on 15 March 2007. The phreatic event was captured on a webcam to the SE on Cerro Verde between 6:05 and 6:12 pm. The eruption deposited a fine layer of ash on the summit area. On 23 March 2007, following tremor the day before, enhanced evaporation and pulses of gas columns rising to 400 m were observed. A sulfur smell was not detected in the gas columns.

Following the March 2007 eruption, sulfur spherules were observed in suspension and along the shorelines from May 2007 to July 2007 (Figure 2.9). Spherules had also been observed during a period of hydrothermal activity in 2001. The sulfur spherules were yellow to gray, and round without tails. A layer of wet native sulfur was also observed along the lakeshore in July 2007.

The lake changed color from turquoise to gray after the minor phreatic eruption, and then to yellow on 15 May 2007. The significance of these color changes is not fully understood, but crater lakes worldwide have been observed to exhibit a wide range of colors—turquoise blue, emerald green, white, brown, and blood red—and color changes. Lake color is related to dissolved and/or suspended organic and inorganic sediment content (*Oppenheimer, 1997*). Lake color changes are attributed to changing oxidation state of lake waters caused by seasonality (e.g. Lake Voui, Vanuatu [*BGVN 31:05*]; Keli Mutu Lakes, Indonesia [*Pasternack & Varekamp, 1994*]), or volcanic activity (e.g. Poas, Costa Rica [*BGVN 32:12*]).

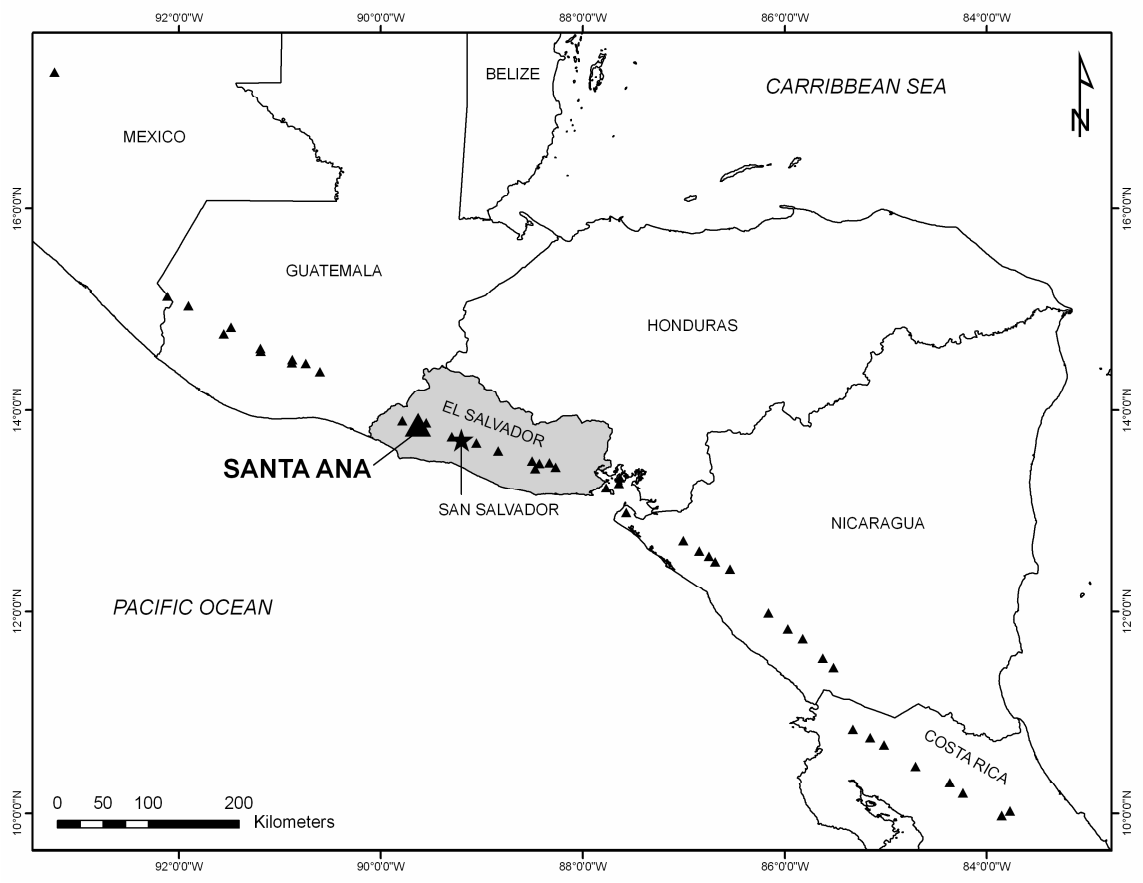

Figure 2.1: Location map of Santa Ana volcano (large black triangle) situated in the Central American volcanic front (small black triangles). Star denotes the city of San Salvador. Add coordinates. Figure created by author from data from the GIS Data Depot (vector data), and the Smithsonian Institute Global Volcanism Program volcano database (volcano locations).

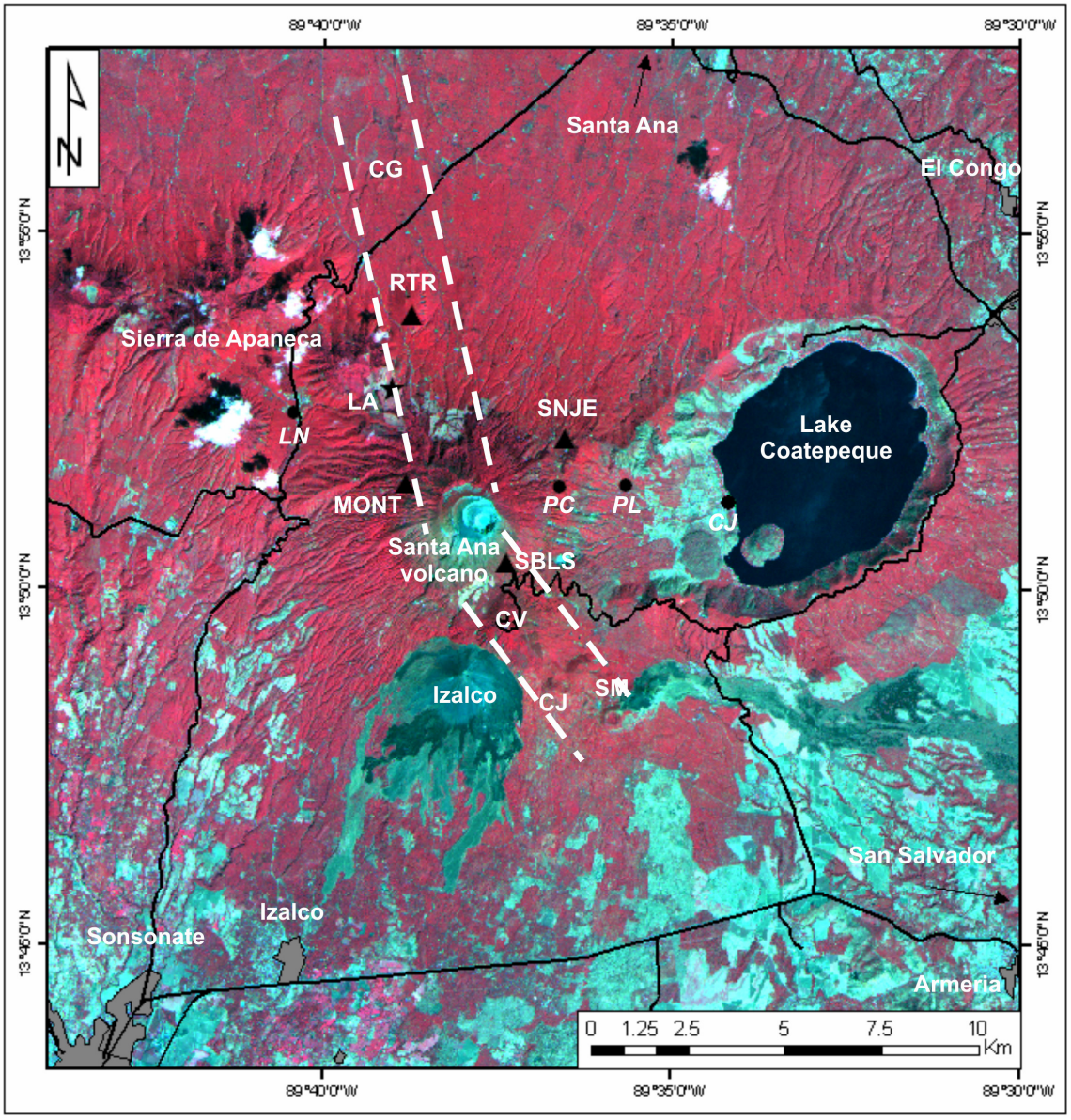

Figure 2.2: Map of the Santa Ana volcanic complex. ASTER image acquired on 3 February 2001 displayed with 321 RGB false color combination. ASTER image orthorectified with a 10 m DEM digitized from 10 m elevation contours of 1:25,000 topographic quadrangles (Instituto Geographico Nacional).Volcanic features: CV=Cerro Verde, SM=San Marcelino, CH=Chino, EA=El Astillero, CJ=Conejal, CG=Chalchupa graben. Seismic stations are denoted by triangles: SBLS=San Blas, SNJE=San José, MONT=Ecomontaña, RTR=Retiro. Meteorological station is denoted by a star: LA=Los Andes. Villages are denoted by solid circles: CJ= Caserio de Javillal, LN= Los Naranjos, PC=Palo Campana, PL= Los Planes de la Laguna. Figure created by author from data from NASA/JPL (ASTER imagery) and SNET (vector data & DEM).

Figure 2.3: Flat topped summit of Santa Ana with nested craters. Photograph courtesy of La Prensa Gráfica.

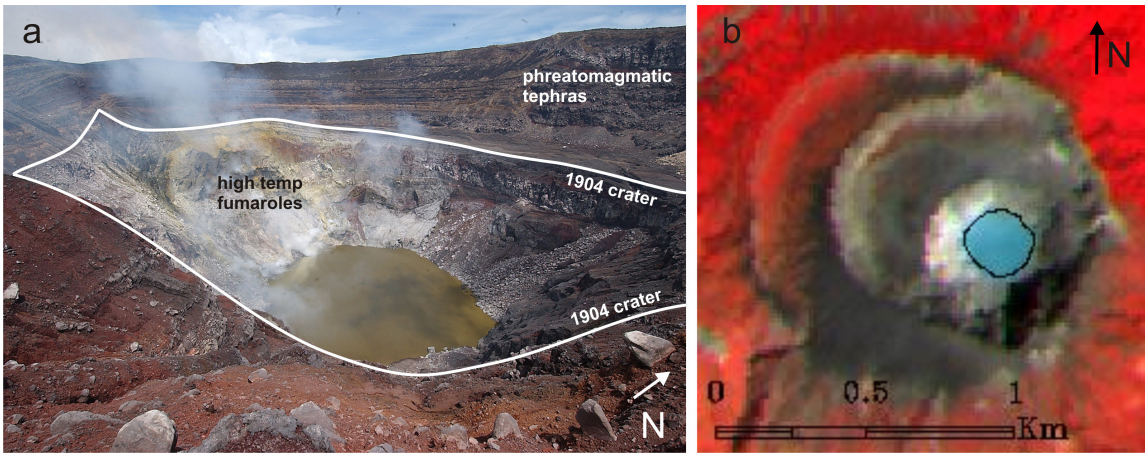

Figure 2.4: Oblique photographs and orthorectified ASTER imagery showing summit geometry prior to October 2005. A: Digital photograph from 31 August 2005 showing explosion crater overlain by phreatomagmatic tephras. Crater contains a volcanic lake and adjacent high temperature fumarole field. Photograph courtesy of El Diario del Hoy. B: ASTER image from 3 Feb 2001, showing a nearly circular lake (blue) and adjacent fumaroles to the west (white). Superimposed lake outline (black line) from bathymetric surveys 2000-2002 by Bernard et al., 2004.

Figure 2.5: A: Incandescence observed in the fumarole field in late August. B: Concentric, glowing cracks in the fumarole field. Photos taken on 31 August 2008, courtesy of La Prensa Gráfica.

Figure 2.6: Eruption column captured on 1 October 2005. Photo courtesy of La Prensa Gráfica.

Figure 2.7: Hot, acidic lahar flowing down Quebrada Las Minas on 1 October 2005. Photograph by Demetrio Escobar (SNET).

Figure 2.8: Lake evaporation in April 2007. a) Lake evaporated from its entire surface and lake volume was greatly diminished. b) Periodic strong degassing pulses observed originating from a point at the tip of the sediment peninsula. Photograph by Rodolfo Olmos (UES).

Figure 2.9: Sulfur spherules observed on the lakeshore on 05 July 2007. Pen for scale. Photograph taken by author.

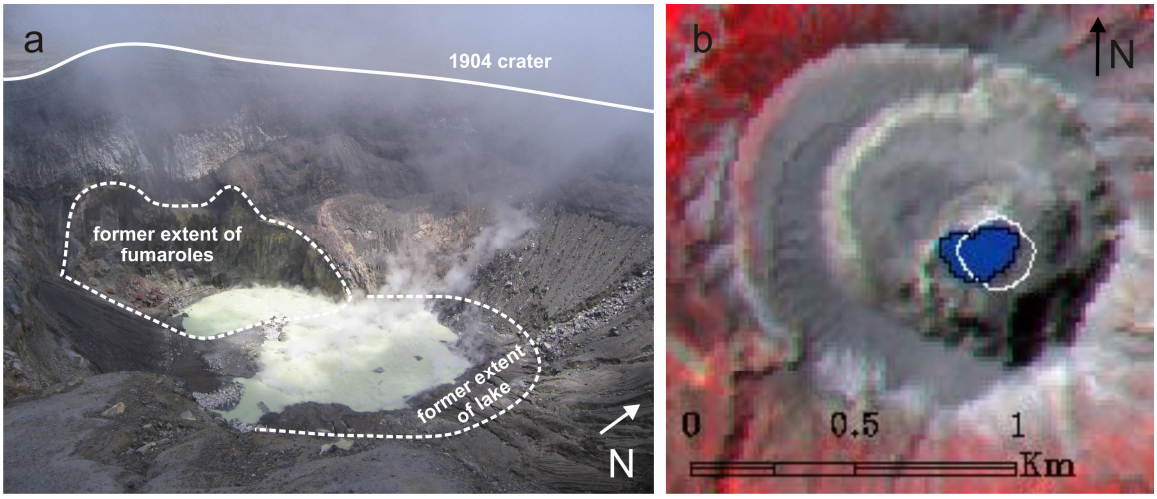

Figure 2.10: A: Post-eruption crater, 28 June 2007, showing an intensely degassing yellow-green lake which has shifted in lake position to the west. The eruption destroyed the main fumarolic area, and was subsequently drowned by the lake. B: Post-eruption crater, 04 Feb 2007, showing the heart-shaped post-eruption lake (blue with black outline) shifted to the west. Pre-eruption lake outline (white) shown for comparison. Figure created by author from data from NASA/JPL (ASTER imagery).

CHAPTER 3

3. Results

3.1 Introduction

In this section, I present crater lake thermal and geochemical methods and results from 2000 to 2007, with the aim of: 1) improving understanding of these archived datasets; 2) identifying precursory activity to the 2005 eruption; 3) evaluating the impact of the 2005 eruption; and 4) proposing a physical model of the magmatic and hydrothermal systems. These data are compared to an earlier study carried out by *Bernard et al. (2004)*, which documented crater lake behavior during 2000-2002. The periods of low level activity and hydrothermal activity observed by *Bernard et al. (2004)* during 2000-2002 serve as a basis for comparison for subsequent periods of similar low level and hydrothermal activity in 2002-2005.

Crater lake temperature and chemistry are available for the duration of the study period, but with a significant data gap from one and a half months prior to about 10 months following the 1 October 2005 eruption (16 August 2005 – 31 July 2006). However, seismic and sulfur dioxide flux data are available during two critical time periods, when, first, incandescent fumaroles (late August 2005) were observed immediately preceding the eruption, and, second, lake evaporation (January -May 2006) was observed shortly after the eruption. Therefore, crater lake data are integrated with seismicity and sulfur dioxide fluxes to further achieve the goals of identifying precursory activity and evaluating the impact of the 2005 eruption. Timing of datasets relative to observed events are presented in Figure 3.1.

Results from a brief investigation into the mineralogy of suspended material in the lake waters and erupted products (tephra and lake vent rocks) are also presented in this section. Mineralogical results are compared to results of geochemical modeling (Chapter 4.5) and are also used in the development of the physical model (Chapter 5.4) and in interpreting eruption triggering mechanisms (Chapter 5.5).

3.2 Data collection & analytical methods

3.2.1 Direct lake water temperature measurement methods

Lake temperatures were acquired by three methods during 2000-2007: continuous *in-situ* temperature sensor, discrete *in-situ* thermocouple, and satellite remote sensing (Figure 3.2). *In-situ* measurements are presented in this section (Chapter 3.2a) and remote sensing measurements are presented in the next section (Chapter 3.2b).

Beginning in 2002, crater lake water temperature was recorded continuously at five, ten or thirty minute intervals by an Onset StowAway Tidbit Temperature Logger sensor (MicroDAQ.com, Ltd.) floating at a depth of 1 m in the middle of the lake. The temperature sensor was not telemetered; data were manually recovered on a regular basis. Temperature sensor data are continuous from May 2002 to May 2005 (with a data gap in February-April 2004 due to sensor failure), February to May 2007, and November 2007 to April 2008. The sensor was lost in the 15 June 2005 eruption, and a new one was reinstalled after the eruption in February, 2007.

Lake temperature was measured *in-situ* with a thermocouple at the lake shore. *In-situ* thermocouple measurements provide supplementary measurements when temperature sensor data are unavailable. Temperature sensor and thermocouple

measurements agree fairly well (average error is 2.24ºC), but the thermocouple mostly yields temperatures that are greater than the sensor. This is probably because the lake is not completely thermally homogenous, and spot temperatures may be affected by proximity to hot springs along the shore, fluctuations in mixing rates within the lake, or vertical stratification.

Lake temperatures were integrated with meteorological data to assess seasonal and climactic effects that are not readily evident from lake temperature measurements alone. Annual averages of meteorological data are presented in Table 3.1 and monthly averages are presented in Table 3.2 and Figure 3.2. Meteorological data consist of daily maximum, minimum and average air temperature and precipitation recorded at Los Andes Meteorological Station (13.88ºN, -89.65ºE, 1770 m.a.s.l.), which is 4 km NNW of Santa Ana volcano and is the closest weather station to the summit (Figure 2.2). The meteorological dataset is nearly complete with full daily coverage for the duration of the study period, except during 1 January 2002 - 1 July 2002 and 1 October 2005 - 20 November 2005. Additionally, the maximum air temperature was not recorded 17 August 2002 - 17 March 2003.

The climate in El Salvador is tropical savannah with the dry season in the low sun winter (Type Aw in Koeppen classification, *Aguado & Burt, 2007*). The Los Andes weather station has a mean temperature of 16-18ºC, which is much lower than typical in El Salvador because it is higher in elevation (1770 m.a.s.l.). It receives ~2 m rain per year during the rainy season, with typical tropical storms or hurricanes generating ~ 100-200 mm per day. The Santa Ana summit receives additional orographic rain, so the weather data from the Los Andes station are only an approximation of weather conditions at the

crater lake. The winter dry season (November to April) and the summer rainy season (May to October) carry minor seasonal temperature differences which correlate with the northern hemisphere summer and winter. During the study period, dry season air temperatures ranged from 10ºC to 18ºC and wet season temperatures ranged from 14ºC to 25ºC (Figure 3.2).

The average annual atmospheric temperature recorded at the weather station over the seven year study period was 16.9ºC. However, the weather station is 130 m below the elevation of the lake, so the air temperature at the elevation of the crater lake will be cooler than air temperature at the elevation of the meteorological station. To correct for this elevation difference, an environmental lapse rate for region was determined. An empirically derived average environmental lapse rate of 6ºC/1000 m calculated for the study period from radiosonde data collected at Phillips Goldston International station (78583), Belize City, Belize, yielded a correction of 0.78ºC for the 130 m difference in elevation between the Los Andes meteorological station (1770 m.a.s.l.) and the crater lake (1900 m.a.s.l.). Though climactic conditions in Belize City are different to those at Santa Ana volcano, this empirically derived lapse rate of 6ºC/1000 m compares well to the international environmental lapse rate of 6.6ºC/1000 m established by the International Civil Aviation Organization. The elevation correction yielded an average atmospheric temperature of 16.12ºC for the study period in the Santa Ana crater.

As might be expected at a lake with a volcanic heat source, the Santa Ana crater lake was consistently warmer than air temperature for the duration of the study period. The magnitude of the difference between lake temperature and air temperature is called here the “lake temperature anomaly” (LTA) (Figure 3.4). LTA is calculated simply as:

LTA = Lake temperature (ºC) – Average atmospheric temperature (ºC)

where lake temperature is daily sensor, thermocouple, or satellite measurement, and average atmospheric temperature at Los Andes is corrected for the 130 m elevation difference (described above) and smoothed using a 30 day Hanning window.

Whereas lake temperature is a key parameter used in quantifying contributions from a volcanic heat source to the lake (Chapter 4.6), LTA is useful to: 1) demonstrate that the volcanic lake is above ambient, 2) quantify how much above ambient, and 3) compare changes in lake temperatures under variable atmospheric conditions. Change in absolute lake temperature may result from variability of the volcanic heat source and/or variability in climatic conditions. The LTA parameter incorporates atmospheric temperature and begins to account for climatic factors.

3.2.2 Direct lake water temperature measurement results

Daily averages of direct lake temperature data for 2000-2008 are plotted with daily averages of atmospheric temperature and precipitation data in Figure 3.2a. Pre-eruptive and post-eruptive periods are plotted with expanded scales in Figures 3.2b and 3.2c, respectively. The high temporal resolution lake temperature data reveal a lake that changed temperature rather slowly over the course of one day compared to diurnal changes in atmospheric temperatures, especially during the dry season. The lake had an average diurnal variation of < 2ºC during the dry season and 5-7ºC during the rainy season, compared to the atmospheric temperature diurnal variation of 5-15ºC during the dry season and 2-10ºC during the rainy season. These differences are essentially related to the higher specific heat of water compared soil or rock (factors of 5-6). In general the

monthly temperature of the lake is influenced by the solar incidence (higher in the summer, lower in the winter) and by the cooling effects of heavy rainy season rains (higher in the summer, but causing cooling, and absent in the winter).

From February 2002 to June 2004, the lake exhibited low level activity, similar to activity in early 2000 reported by *Bernard et al. (2004)*. During February 2002 - June 2004, the LTA was 0.5-8ºC, with lake temperatures of 16-25.5ºC. The size of the anomaly during February 2002 - June 2004 is comparable to the LTA calculated from *Bernard et al. (2004)* during early 2000 (LTA = 1.5-4ºC, lake temperature ~19ºC). During this period, lake temperature rose with air temperatures in the spring and fell in the autumn. Lake warming in the spring was suppressed by rainfall and the lake cooled episodically by ~4ºC in response to large rainfall events (>50 mm/day), especially early in the rainy season (dashed lines in Figure 3.2b). The lake recovered to equilibrium temperature within a few days. As the rainy season progressed, the lake temperature responded less drastically to large rainfall events.

During a period of hydrothermal activity during June 2004 to August 2005, lake cooling by rainfall was apparently not as effective as it had been in previous years—in fact the lake temperature anomaly increased during the rainy months. The LTA was 4-12ºC, with lake temperatures of 20-28ºC, which is comparable to temperatures and LTAs calculated from *Bernard et al. (2004)* during a heating period in late May 2000 to February 2002 (LTA=10-13ºC, lake temperature 26-30ºC). Taking into account seasonal and climatic effects, anomalous gradual heating was observed from June 2004 to November 2004, prior to the eruption (Figure 3.4a). During the time period of November 2004-August 2005, the lake did not continue warming. Instead, the lake temperature

anomaly dropped and mimicked the pattern of ambient air temperature. In fact, the temperature of the lake declined from January 2005 to March 2005, following the winter cooling pattern, and then began warming with the March through May period. The sensor loss in the 15 June 2005 minor phreatic event resulted in an unfortunate data gap, but direct measurements of the lake in 16 August 2005 determined a relatively cool lake temperature of 21ºC (LTA of 4.3ºC). This was the last direct temperature measurement prior to the eruption and indicated that the lake was relatively cool on 16 August 2005.

Direct lake temperature measurements were unavailable from late August 2005 to the eruption on 1 October 2005 because the crater was determined to be too dangerous to visit. The crater lake continued to be deemed too unsafe to visit for 17 months after the eruption and temperature monitoring did not resume until February 2007. Direct temperature measurements revealed that the lake was much hotter than before the eruption, with lake temperatures as high as 65ºC, resulting in lake temperature anomalies of 10-48ºC. Such high temperatures and temperature anomalies had never before been observed or documented at Santa Ana crater lake.

The temperature sensor recorded a rise and fall in temperature about the minor phreatic event on 15 March 2007. The temperature began to rise rapidly on 8 March 2007, one week prior to the event. By 14 March 2007, lake temperature had reached a maximum of 61.5ºC with a lake temperature anomaly of 46ºC. Temperatures remained elevated following the phreatic activity, leading to near complete evaporation on two occasions—April 2007 and August 2007. By late 2007, lake temperatures remained high but stable with temperatures of 28-48ºC and LTA of 15-33ºC.

3.2.3 ASTER temperature and area retrieval method

Lake surface temperatures and areas were obtained remotely from the ASTER (Advanced Spaceborne Thermal Emission Radiometer) satellite sensor. ASTER is a multispectral sun-synchronous sensor aboard the Terra satellite platform (*Pieri & Abrams, 2004*). The Terra satellite was launched in December 1999 and began acquiring imagery in February 2000. ASTER has 14 bands spanning the visible to the thermal infrared portions of the electromagnetic spectrum. The bands are divided into three subsets, the very near infrared (VNIR) (0.52-0.86 μm) with a spatial resolution of 15m/pixel, the short wave infrared (SWIR) (1.6-2.43 μm) with a spatial resolution of 30m/pixel, and the thermal infrared (TIR) (8.125-11.65 μm), with a spatial resolution of 90m/pixel (*Pieri & Abrams, 2004*). Unique features of the ASTER sensor include its off-nadir pointing capability and its stereo viewing capability to create digital elevation models (DEMs) with a spatial resolution of 30 m. ASTER provides high spatial resolution imagery in the visible bands (VNIR) which will be used in this study to delineate lake areas. ASTER also provides excellent spatial resolution in the thermal bands (TIR), which will be used to retrieve lake temperatures. Along with Landsat ETM+ thermal bands (spatial resolution = 60m/pixel), ASTER TIR bands provide the best spatial resolution currently available from civilian (non-military) thermal satellite imagery.

Two types of ASTER imagery products were used in this study: L1A products, which are at-sensor radiance that has not been registered to a geographic coordinate system, and AST04 products, which are brightness temperatures recorded at the sensor. A total of 60 archived ASTER images containing Santa Ana volcano were available for 2000-2007 from the Land Processes Distributed Active Archive Center (LPDAAC) Earth

Observing System (EOS) Data Gateway at http://edcimswww.cr.usgs.gov/pub/imswelcome/. However, only 18 images, or 30% of the total number of images, were useable cloud-free images. These 18 cloud-free images consist of 12 daytime and 6 nighttime images, averaging 2-3 images per year. ASTER lake temperatures and lake size from the 18 cloud-free images, spanning 2000 to 2007, are presented in Table 3.3.

ASTER images were processed using ENVI (ITT Visual Information Solutions) and ArcGIS (ESRI) software. Image processing methodology is presented schematically in Figure 3.5 and is described in the following paragraphs. After satellite imagery was acquired, several image processing procedures were used to obtain atmospherically corrected lake water temperatures and lake areas: 1) image orthorectification; 2) lake pixel identification; 3) correction for ASTER sensor degradation; and 4) correction for atmospheric effects.

ASTER images were orthorectified by modeling the nature and magnitude of geometric distortions in the imagery to remove the distortions caused by topography, camera geometry, and sensor-related errors (*ITT, 2008)*. In this study, orthorectification with a high resolution DEM was necessary to precisely locate the volcano summit in each image of the time series. Various types of models can be used to orthorectify imagery from pushbroom sensors, e.g. rigorous sensor models, rational polynomial functions, affine transformations *(Poli, 2004)*, and in this case orthorectification was carried out in ENVI using a rational polynomial coefficient model (RPC). The PRC model relates object-space (latitude, longitude, height) to image space (line, sample) through quotients of cubic polynomials (*Grodecki & Dial, 2003*). The RPC model was chosen because

images can be orthorectified easily with or without ground control points, and ground control points were not available for the field area in El Salvador.

In ENVI, both types of ASTER imagery products were orthorectified—L1A images (unregistered, at-sensor radiance) and AST04 (brightness temperature at sensor)—using the RPC model. The RPC coefficients and elevation information are needed to build an RPC model for ASTER images in ENVI. Like other spaceborne pushbroom sensors (e.g. IKONOS, OrbView-3, QuickBird, SPOT, and CARTOSAT-1), the ASTER sensor data includes ancillary rational polynomial coefficients calculated from ephemeris data (satellite position) (*ITT, 2008*). A 10 m digital elevation model (DEM) (WGS 84, UTM 16N) was used for elevation information. The DEM was digitized from 10 m elevation contours of 1:25,000 topographic quadrangles by the Instituto Geographico Nacional de El Salvador. A nearest neighbor resampling method was used to resample the elevation values.

A high spatial resolution 10 m DEM was used to ensure good spatial registration among the images. However, spatial registration was good for daytime images but poor for nighttime images. Good quality spatial registration for nighttime images was especially important to accurately identify the crater lake pixel(s). In nighttime images, features were displaced geographically and topographically in varying amounts. Displacement was often, but not always, in the same direction. I speculate that poorer spatial registration may be due to one or more of the following: error arising from nighttime satellite ephemeris; error arising from relating satellite ephemeris to ground position when the TIR is pointed off-nadir (max ±24º); or other sensor-related errors

during night-time acquisition. Therefore, a manual spatial correction was applied to nighttime images.

In ArcGIS, lake pixels were identified in the orthorectified L1A high spatial resolution very near infrared (VNIR, 15 m/pixel). Volcanic lake pixels have generally been identified in satellite images by one of two methods: (1) applying a user-defined threshold; or (2) identifying the hottest pixel, assuming the crater lake is the hottest feature in the landscape (*Oppenheimer, 1996).* The high temperature fumarole field directly adjacent to the crater lake precludes the use of method (2), and so method (1) is employed here.

The lake pixel identification methodology used here is as follows: First, a user-defined threshold is applied to distinguish lake pixels from land pixels. Band 3 (0.75-0.86 μm) was chosen to identify lake pixels because water is highly absorptive in the near infrared. Second, geolocated lake outlines were manually digitized from the user-defined threshold. Lake area and equivalent radius were calculated for each daytime image (no visible bands during the night). Third, using the geolocated lake outlines, the purest lake pixel was identified in the orthorectified AST04 thermal infrared bands (TIR). Santa Ana lake is relatively small (~200 m diameter) compared to ASTER TIR pixels (90 m/pixel), and at best the lake occupies only one pure lake pixel. A circular lake with a minimum diameter of 128 m is needed to encompass one TIR pixel, and a diameter of 254 m is needed to always guarantee a pure lake pixel (*Oppenheimer, 1993*). If the lake did not encompass one pure lake pixel, the pixel that occupied the largest percentage of the lake was taken as the lake pixel or several partial lake pixels were averaged. Finally, Band 13 and Band 14 brightness temperatures were noted for lake pixels.

A correction for degradation of the ASTER sensor was applied to AST04 Band 13 and Band 14 lake pixels using lookup tables obtained from the Japan ASTER Science Team website (http://deco.cis.ibaraki.ac.jp/RECAL/) (*Tonooka, 2003).* A detailed explanation of the application of the correction for sensor degradation is given in *Appendix A*.

After accounting for sensor degradation, an atmospheric correction was applied to Band 13 and Band 14 TIR lake pixels. An atmospherically corrected temperature (T_s) is obtained when the algorithm is applied to Band 13 and Band 14 lake pixels using the equation (*Trunk, 2005; Trunk & Bernard, 2008*):

$$T_s=(0.050900273*(T_{Band\ 13recal}*100))-(0.040517907*(T_{Band\ 14recal}*100))+0.897764116$$

where $T_{Band\ 13recal}$ and $T_{Band\ 14recal}$ are recalibrated temperatures in degrees Celsius.

The atmospheric correction is based on a widely used empirical split-window algorithm originally developed to retrieve sea surface temperatures (*Njoku, 1990;Yu et al., 2000).* The empirical split-window algorithm applied here was developed specifically for crater lakes by *Bernard (2005)* and validated by *Trunk (2005). Bernard (2005)* developed the algorithm at Taal volcano (Philippines) by correlation of ASTER and MODIS imagery. *Trunk (2005)* validated the method at Lake Yugama at Kusatsu-Shirane, (Japan), and applied the atmospheric correction to Kawah Ijen (Indonesia), Crater Lake at Ruapehu (New Zealand), Laguna Caliente at Poas (Costa Rica), and Copahue (Argentina). *Trunk (2005)* reported an average inaccuracy of ± 1.5ºC with a precision of ± 1.9ºC, and a maximum inaccuracy of 6.3ºC for Lake Yugama, noting that larger errors may arise under extreme environmental conditions. The results of *Bernard (2005)* and *Trunk (2005)* have recently been combined in a joint publication *Trunk & Bernard (2008).*

3.2.4 ASTER lake temperature and area results

The results of the lake surface temperature retrieval for the 18 ASTER images are plotted with direct temperature measurements in Figure 3.2. Twelve (8 day, 4 night) of 18 total images have corresponding ground truth temperature measurements at the same time as ASTER acquisition, and 4 images (4 day, 2 night) lack corresponding ground truth. For the 12 images for which ground truth is available, ASTER surface temperatures compare fairly well to ground measurements, comparable temperature comparisons reported by *Trunk (2005)*. Difference in ASTER temperatures and ground temperatures ranges from 0.03ºC to 3.93ºC error, with an average error of ± 2.1ºC (Figure 3.6). This average error is slightly higher than the average error of ± 1.5ºC reported for Lake Yugama by *Trunk (2005)*, but well within their maximum reported error of 6.3ºC.

Discrepancy between direct temperature measurements and ASTER surface temperatures arises from several factors. ASTER temperatures are impacted by a variety of environmental conditions, such as variable skin temperature due to variable windspeed, ambient air temperature, and weather conditions; daytime solar heating; and "mixed pixels," or contamination by the hot fumarole field, or cool fumarole gas plume/meteorological clouds. In this case, mixed pixels are probably the greatest source of environmental error.

Direct temperature measurements by thermocouple or temperature sensor measure 'bulk' temperature of several centimeters to a meter below the water surface, whereas radiometers, such as ASTER, measures the temperature of the top millimeter of the water surface, or "skin temperature." The skin temperature varies from the bulk temperature by a few tenths of a degree to several degrees (Bernard, 2005; Oppenheimer, 1997) because

the skin temperature is partly influenced by the temperature of the air above the lake surface (*Bernard, 2005*). Although nighttime images lack solar heating and theoretically provide more accurate temperatures, the average error for nighttime images (2.7ºC) is slightly higher than the average error for daytime images (1.8ºC). This is probably due to the poorer quality geolocation of nighttime images resulting in contamination from the hot adjacent fumaroles or cool surrounding rock/plume. Additional error arising from ASTER instrumental error (NEΔT of ± 0.3ºC resulting in precision of ± 1.9ºC) and error associated with the application of atmospheric correction (difference between environmental conditions at Taal and Santa Ana) is estimated to be within average error (*Trunk, 2005*).

The available cloud-free ASTER temperature time series demonstrates that ASTER temperatures are reasonable estimates of lake temperature within a few degrees (±2ºC). In the absence of ground data, ASTER can provide viable lake temperature information at Santa Ana. For example, the ASTER sensor provided several important temperature estimates after the 2005 eruption, especially in January 2006, when the crater lake was inaccessible to sample directly (Figure 3.2a). Few cloud-free images were available during this period; 11 other cloudy ASTER images were acquired during October 2005 - December 2006, but cloudy weather conditions, including orographic clouds at the summit, and the adjacent steam plume prevented clear views of the lake. The ASTER sensor revealed a lake with a temperature of 23.8ºC± 2.1ºC on 16 January 2006, which was within the temperature range observed prior to the eruption. The ASTER sensor also revealed post-eruption lake warming during 2006. Subsequent ASTER images in 2006 revealed that the lake warmed to 24.6ºC 15 October 2006 and

26ºC on 2 December 2006. By January 2007, temperatures of 30-35ºC were registered by ASTER and ground methods, surpassing all temperatures measured prior to the eruption. If the lake continues to exist at elevated temperatures (30-60ºC) and once again becomes too dangerous to sample, ASTER lake temperatures will become exceedingly useful.

In addition to a temperature record, orthorectified ASTER images with 15 m/pixel resolution provide excellent estimations of lake size. ASTER images show that since 2003, lake size has remained fairly constant with an average equivalent radius of ~100 m from 2003-2007. (Equivalent radius = Sqrt.(Area/π)). However, visual observations of the lake following the eruption verify extreme lake evaporations, up to 30% normal size, which were not captured by the ASTER sensor. Better constraint on lake size during evaporation periods could be achieved if more frequent daytime ASTER images are acquired in the future.

3.2.5 Lake water chemistry analytical methods

Lake water was sampled monthly on the north shore of the crater lake by personnel from Centro de Investigaciones Geotecnicas del Ministerio de Obras Publicas (2000-2001) and subsequently by Servicio Nacional de Estudios Territoriales (SNET) (2002-2007). The results of these measurements are presented in Table 3.4. pH was measured i*n-situ* on a monthly basis via glass electrode. Within days of collection unfiltered water samples were analyzed for anions (Cl, SO_4, F, B, S^{-2}) and selected cations (Mg, Ca, K, Na, total Fe, Si) by the SNET Hydrology division following standard methods described in *Eaton et al. (1995).* SO_4, Cl, Ca, and Mg were measured for the duration of the study period: SO_4 was determined by colorimetry, Cl was determined by

argentometry, Ca was measured by EDTA titration and Mg was estimated from total hardness - calcium differencing. Beginning in June-July 2004, Si, B, and F were determined by colorimetry. Additionally, total dissolved solids (TDS), K, Na, S^{-2} and total Fe were analyzed beginning in 2006: TDS, K and Na were measured by selective ion electrodes, and sulfide and total Fe were determined by colorimetry.

Chemistry results of six samples from January - July 2007 analyzed for additional cations and trace elements are also presented in Table 3.4. Filtered (0.45 μm) samples were analyzed for major elements by inductively coupled plasma atomic emission spectrometer (ICP-AES) and for trace elements by inductively coupled plasma mass spectrometry (ICP-MS) at SGS Laboratories, Toronto, Canada. Charge balance is within ±10% for all 2007 samples except June and July samples, which have charge balances of 25% and 35%, respectively. Precision errors are only available for cations analyzed by SGS Laboratories, and are provided in Table 3.4 as relative standard deviation (RSD) expressed as a percentage (RSD=100*Standard Deviation/Mean).

3.2.6 Lake water chemistry results

Chemical analyses of lake waters 2000-2007 are presented in Figure 3.7 (anions) and Figure 3.8 (cations). Anion data presented includes sulfate (SO_4), chloride (Cl), fluoride (F), boron (B), as well as total dissolved solids (TDS). Cation data presented includes rock forming elements magnesium (Mg), calcium (Ca), total iron (Fe), sodium (Na), potassium (K), and silicon (Si), though only Mg and Ca were measured during 2002-2006. Results of these analyses for 2002-2007 are compared with results from 2000-2002 from the previous study of *Bernard et al. (2004)*. Discussion in the following

paragraphs focuses on primarily on anion datasets; cation results from 2002-2007 are noiser than anion results, and less confidence is placed in cation analyses.

Santa Ana's lake chemistry during 2000-2002 was described by *Bernard et al. (2004)* as containing cool acid-sulfate-chloride waters with pH ~1, SO_4 = 11,000 mg/kg, Cl = 7000 mg/kg, SO_4/Cl ~1.5, and TDS = 23,000 mg/kg (Figure 3.7). The major cations in the lake water were derived from congruent dissolution of andesite host rock at about 100ºC. This "background" data may represent a relatively stable period of low level activity which lasted through mid-2004.

During low level activity in February 2002-June 2004, crater lake chemistry was comparable to that reported by *Bernard et al. (2004),* with concentrations of pH ~ 1.1, SO_4 = 10,000 ppm, Cl = 6,000 ppm and SO_4/Cl = 1.0-1.5 (Figure 3.7). Chloride and sulfate co-varied during this period and $SO_4 > Cl$. Similar to temperature, seasonal dilution was evident in anion trends, temporarily driving up SO_4/Cl ratio and pH during the rainy season. Sulfate exhibited logarithmic recovery, while Cl recovered more quickly.

Departures from this stable low level of activity occurred during May 2000-February 2002 and June 2004-August 2005 when hydrothermal activity was observed in the lake. Despite gaps in data collection, anomalously high temperatures were observed during periods of hydrothermal activity, which represented a departure from typical temperatures recorded during low level activity. The lake reached a maximum temperature of 30ºC during May 2000-February 2002, but lake chemistry did not show significant changes. However, when reached a maximum temperature of 28ºC during June 2004-August 2005, the lake did exhibit significant changes in anion trends. Constant

anion concentrations and constant SO_4/Cl ratios were observed, and seasonal dilution was not observed (Figures 3.7a and 3.7b). This represents a major departure from the seasonal dilution trend that had been a prominent feature during low level activity. In fact, in appears that both Cl and SO_4 concentrations increased slightly in early 2005. Constant to slightly increasing anions concentrations suggest that more acid fluids reached the lake, causing the lake waters to acidify (minimum pH = 0.7 on 17 June 2005) (Figure 3.7c) and the lake to warm. Other anions—fluorine and boron—exhibited similarly constant trends lacking seasonal dilution in late 2004 and early 2005 (Figure 3.7a). The minor phreatic event on 15 June 2005, seems to have had a slight impact on lake chemistry. The event apparently caused anion concentrations, and therefore acidity, to decrease (Figure 3.7), and Mg concentration to increase (Figure 3.8), though these variations were well within the range of concentrations measured during the previous several years.

Lake chemistry definitely changed after the 2005 eruption, though perhaps not immediately. These changes were probably related in some way to the October 2005 eruption, though the data gap from August 2005 to July 2006 precludes determining whether the changes took effect immediately and whether there was a direct causal relationship between the eruption and subsequent lake behavior. Although the 2005 eruption and the post-eruption lake activity may not be directly related, the October 2005 eruption and subsequent lake instabilities may have both been caused by larger scale, longer term unrest at the volcano, or the October 2005 eruption may have enabled the subsequent change in lake chemistry. The most extreme changes in lake chemistry were not recorded until after the phreatic eruption on 15 March 2007 (VEI 1).

Following the phreatic eruption in March 2007, lake was relatively hot (max T ~65ºC), acidic (min. pH = 0.5) and concentrated (max. TDS ~150,000 mg/kg). The 2007 lake chemistry represented a further departure from low level activity, exhibiting dynamic chemical trends not previously observed. Not only were dilution trends not observed during this post-eruptive period, but the lake continued acidifying and anion concentrations steadily increased as more volcanic fluids were delivered to the lake via hotsprings and a newly subaqueous central fumarole. Despite increasing acidity of lake waters, increases in magnesium or other cations were not observed (Figure 3.8).

When the lake was first sampled post-eruption, Cl and SO_4 concentrations were low as the summit had received ample rainfall in June-July. However, Cl soon recovered to ~ 10,000 ppm, and SO_4 recovered to ~7000 ppm Cl. The minor phreatic event on 15 March 2007 apparently had a significant impact on lake chemistry. The lake abruptly became more acidic, reaching pH = 0.5 in July 2007, and Cl abruptly reached a maximum concentration of ~22,000 ppm.

However, while Cl increased to unprecedented values, SO_4 did not increase proportionally, which drove the SO_4/Cl ratio below 1. $SO_4 <$ Cl had not been observed in the lake previously during the study period. $SO_4/Cl < 1$ cannot be explained by dilution by rainwater alone because element ratios are unaffected by dilution or evaporation; these ratios must be caused by a different process.

3.2.7 Sulfur dioxide fluxes and seismicity methods & results

Sulfur dioxide fluxes and seismicity data are presented in conjunction with the lake temperature anomaly (LTA) in Figure 3.9. All available gas flux and seismic data,

which spans 2004 to 2007, is presented in Figure 3.9a. Pre-eruptive and post-eruptive periods are plotted with expanded scales in Figures 3.9b and 3.9c, respectively. SO_2 fluxes have units of tons per day. Seismic events are classified as long period (LP) and volcano-tectonic (VT), and are presented in number of events per day.

Volcanic sulfur dioxide fluxes are commonly quantified by correlation spectrometry (COSPEC) and miniaturized UV spectrometry (mini-DOAS) remote sensing techniques. At Santa Ana volcano, pre-eruptive and post-eruptive volcanic SO_2 fluxes were measured by both techniques. Stationary COSPEC, on loan from INSIVUMEH, Guatemala, was used to measure SO_2 fluxes on several occasions during the pre-eruptive period. Beginning in late August 2005, and lasting thru November 2006, daily measurements were made with vehicular mini-DOAS operated by the Universidad de El Salvador (UES). SO_2 flux measurements from late August 2005 to December 2005 have been presented previously by *Olmos et al. (2007)*.

As degassing intensified in June 2004, a COSPEC was sent from Guatemala to El Salvador to quantify SO_2 degassing. COSPEC measurements on 24-27 June 2004 yielded SO_2 fluxes of up to 586 tons/day (*Olmos et al., 2007*) (Figure 3.9a), which were higher than the SO_2 fluxes measured previously during low level activity in 2002 (30-80 tons/day) (*Rodriguez et al., 2004*). SO_2 fluxes were measured again by Guatemalan COSPEC on 13-15 April 2005, and yielded SO_2 fluxes of 523-581 tons/day, which were similar to June 2004 measurements (*Olmos et al., 2007*).

Degassing increased again in late August 2005, and SO_2 output increased dramatically. SO_2 flux quickly reached a maximum of 4285 tons/day on 24 August 2005, one day after incandescence was first observed in the fumarole field (Figure 3.9b). This

value represented a seven fold increase from earlier pre-eruptive estimates of ~600 tons/day. Daily monitoring with mini-DOAS showed increases to peak values of > 4000 tons/day on three occasions during the month of September 2005, and degassing maximums corresponded with maximums in number of LP events/day.

The Ozone Monitoring Instrument (OMI) aboard NASA's Aura satellite detected the sulfur dioxide emission associated with the 2005 eruption. Figure 3.10 shows combined sulfur dioxide emissions on October 1 and 2, 2005. The total eruption cloud mass on October 1 was reported to be about 10,000 tons (*NASA Earth Observatory, 2005)*. The gas plume was displaced to the west and southwest over the Pacific and soon dissipated by October 2 (Figure 3.10). A total mass of 10,000 tons is a relatively small SO_2 output, considering pre-eruptive SO_2 emission rates of ~4000 tons/day and also when compared to larger eruptions, e.g. Anatahan (April 5-6, 2005) (*NASA Earth Observatory, 2005*).

Following the 1 October 2005 eruption, SO_2 output abruptly declined to < 750 tons/day, but recovered to 2500-1500 tons/day during the end of 2005 (Figure 3.9b). After reaching a maximum of 2695 tons/day on 07 January 2006, SO_2 fluxes gradually decreased to low levels in May 2006 and remained at low levels through September 2006. Renewal of vigorous degassing in early 2006 corresponded with concurrent progressive evaporation of the crater lake. Degassing resumed once more following the 15 March 2007 phreatic event, and SO_2 fluxes remained below 600 tons/day during March – September 2007 (Figure 3.9c). By November and December 2007, SO_2 fluxes approached lower limits of detection at 15-20 tons/day.

Temporal trends in number of events per day of high frequency volcano-tectonic (VT) and low-frequency (LP) seismicity registered at San Blas seismic station during the study period are presented in Figure 3.9. The seismic station is a short period vertical component seismometer and is managed by SNET. Beginning on 8 June 2004, LP microseismicity was detected for the first time since 2001. Cell phone communication in March 2005 between SNET seismologists in San Salvador and scientists on the crater rim confirmed that observed strong gas pulses corresponded with microseismic signals. LP microseismicity was interpreted to be associated with degassing of the hydrothermal system and had been recorded previously at Santa Ana in 2001 and 1992 when increased hydrothermal activity was observed in the lake, but had been absent from 2002 to May 2004.

As degassing intensified in June 2004, LP microseismicity associated with degassing rose to ~200 events/day. LP trends mirrored LTA trends during this period, rising June-November 2004 and declining November 2004-June 2005 (Figure 3.9b). During the month of November 2004, microseismic events increased in amplitude and duration, and the "smell of bleach" emanating from a subaqueous fumarole in the NWN sector of the lake, inferred to be HCl, was reported by SNET scientists. During January 2005, 2 minutes of low frequency tremor comprised of 6 events was recorded and villagers from San Blas and Salvanatura park guards reported smelling rotten eggs (indication of H_2S). Low frequency tremor lasting for 100 seconds was recorded again on 3 May 2005. Few VT events (<5 events/day) were registered during this period.

LP events jumped abruptly from ~100 to ~200 events/day on 1 August 2005, and again from ~200 to ~350 events/day on August 25, one day after SO_2 reached maximum

values, and two days after incandescence was first observed in the fumarole field (Figure 3.9b). VT swarms were registered on 18, 22 & 27 August 2005, before and during incandescence was observed. Banded tremor was registered on 27 August. During the month of September, the number of LP events/day remained very high at ~400-600 events/day. LP events reached a maximum of 622 events/day on 12 Sept. 2005, progressively decreasing in number to ~200 events/day 1 October 2005 while VT events remained low (<10 events/day).

Following the eruption, the number of LP events quickly dropped to < 50 events/day whereas the number of VT events quickly reached a maximum of 42 events/day on 7 October 2005. LP events remained at that low persistent level until they doubled to ~100 events/day on 1 January 2006. LP events maintained ~100 events/day for the next 6 months as the lake degassed from a central subaqueous fumarole and progressively evaporated. During this time VT events exhibited cyclic behavior, reaching progressively lower maximums. High frequency banded tremor lasting less than 20 minutes was recorded on 20-23 March 2006.

LP and VT events resumed low levels for the remainder of 2006 until both types of seismicity exponentially increased during the week prior to a minor phreatic eruption on 15 March 2007 (Figure 3.9c). The number of LP events reached its zenith on 12 March 2007, while VT events continued rising until 14 March 2007. The eruption generated an LP event with larger amplitude than had been registered previously (*SNET Informe Especial*, *2005a*). LP activity that began on 8 March 2007 transitioned into tremor in April during three periods of tremor (1, 15, 24 April) each lasting 30 minutes.

3.2.8 Mineralogy of erupted products

Mineralogy of filtered suspension of samples from January -July 2007, tephra from the 15 June 2005 and 1 October 2005 eruptions, and lake bottom ejecta from the 1 October 2005 eruption were determined by polarizing light microscope, scanning electron microscope (SEM) with an energy dispersive (EDS) detector, and X-ray diffraction (XRD) at Michigan Technological University.

Gypsum crystals were identified in the filtered suspension by XRD and SEM for all six samples from 2007, and bladed crystals of gypsum were found along the shoreline in July 2007. No additional minerals were identified, possibly because only < 50 mls of sample was available for filtration. It is plausible that the filtered suspension would be monomineralic, but one might also expect that more than one phase might be present, given that in an earlier study, *Bernard et al., (2004)* identified trace amounts of amorphous silica, Pb+Sr-rich barite (BaSO4), pyrite, and gypsum in suspension, and sporadic precipitates of tamarugite [$NaAl(SO_4)_2 \cdot 6(_{H2O})$] along the shoreline.

Oil immersion of tephra samples from the 15 June 2005 and 1 October 2005 eruptions revealed that tephras were composed of altered aluminosilicates, equant plagioclase phenocrysts, quartz phenocrysts, and equant glass shards lacking bubblewall features. Ash fraction (< 2 mm) samples from both eruptions had very similar x-ray patterns, and cristobalite and minor anhydrite were identified in the < 4 phi size fraction. Plagioclase phenocrysts and glass shards may possibly suggest a magmatic component, but a significant amount of advanced argillic alteration clay minerals would also be expected from a magmatic eruption. Samples were prepared for clay mineral identification by XRD in the fines fraction (< 2 μm) following standard procedures

(*Moore & Reynolds, 1989)*, but no clay minerals were present. Clay minerals are not stable at low pHs encountered in the upper vent region below the lake, and would not be expected if the eruption was sourced from this region. However, clay minerals are likely to be found deeper in the hydrothermal system, perhaps contributing to formation of an impermeable authigenic mineral layer, and would be a potential component in erupted tephra if the eruption was sourced from deep in the system.

Several lake bottom ejecta from the October 2005 eruption were collected on the summit and in the lahar drainage in Los Planes de la Laguna in July 2007. Ejecta were composed of altering wallrock with interstitial native sulfur and other alteration minerals, or composed of secondary alteration minerals only. Minerals identified in lake bottom ejecta by XRD and SEM include cristobalite, gypsum, alunite, natroalunite, native sulfur, and iron sulfides. Neither jarosite nor diaspore were identified.

3.3 Data summary

A summary of data results is provided below and in Table 3.5. Santa Ana crater lake chemistry was similar from 2002 until the 2005 events, with most of the characteristics described by *Bernard et al. (2004).* Seasonal variation with dilution by meteoric water during the rainy season was evident in temperature and chemistry trends during low level activity from February 2002 to June 2004. However, beginning in June 2004 the lake experienced anomalous heating (T=28ºC; LTA=12ºC) and subtle changes in geochemical trends during a period of hydrothermal activity which lasted until August 2005. During this time, long period seismicity was also registered (~200 events/day) concurrent with lake temperature and geochemical changes. Additionally, volcanic

degassing fluxes (< 600 t/d SO_2) associated with venting of the hydrothermal system were greater than degassing fluxes (30-80 t/d SO_2) obtained during periods of low level activity. The observed trends during this period of hydrothermal activity were similar to a period of increased hydrothermal activity in 2001 reported by *Bernard et al. (2004)*, when anomalous heating (T=30ºC, LTA=13ºC), anomalous SO_2 flux (< 400 t/d), and LP seismicity occurred.

In late August and September 2005, seismic activity and SO_2 degassing increased dramatically, marking a one month period of intense fumarolic activity prior to the 1 October 2005 eruption. (Crater lake data were not available for this time period). This period initiated with three volcano-tectonic swarms on 18, 22, and 27 August 2005 and concurrent observations of incandescence in the main fumarole field beginning on 23 August, followed by sudden increases in SO_2 flux on 24 August (> 4000 t/d) and LP seismicity on 25 August (from 200 to 350 events/day). Finally, banded tremor was observed on 27 August 2005. During September 2005, SO_2 flux and LP seismicity remained at very high levels, while VT events were minimal. Immediately following the 1 October eruption, SO_2 and LP seismicity decreased substantially and a VT swarm occurred on 7 October shortly after the eruption.

During 2007, the lake chemistry began to change. Most significantly, the lake acidified following the 15 March 2007 phreatic eruption and chloride concentrations surpassed previously observed levels. Sustained LP seismicity followed by banded tremor was registered in January -April 2006 and March-April 2007, coincident with periods of lake evaporation. A week-long rapid ramping up of lake temperature, LP, and

VT seismicity heralded a minor phreatic eruption on 15 March 2007. This event accelerated increasing anion trends and facilitated acidification of the lake.

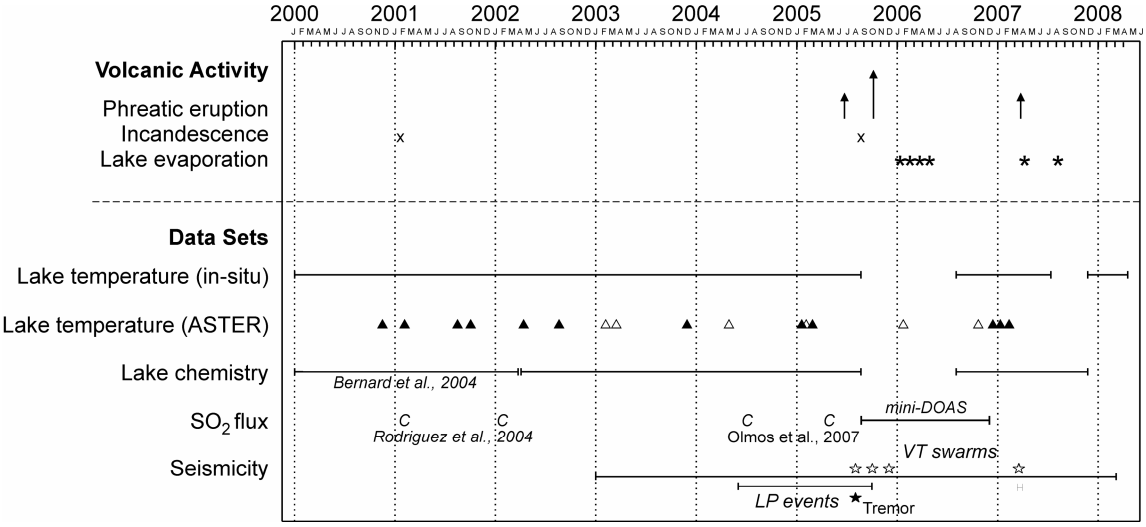

Figure 3.1: Timeline showing volcanic activity 2000-2008 and temporal coverage of datasets. Short arrows indicate minor phreatic eruptions on 16 June 2005 and 15 March 2007, and long arrow indicates phreatic eruption on 1 October 2005. Solid black triangles are daytime ASTER images and hollow black triangles are nighttime ASTER images. C indicates COSPEC measurement of SO2 flux.

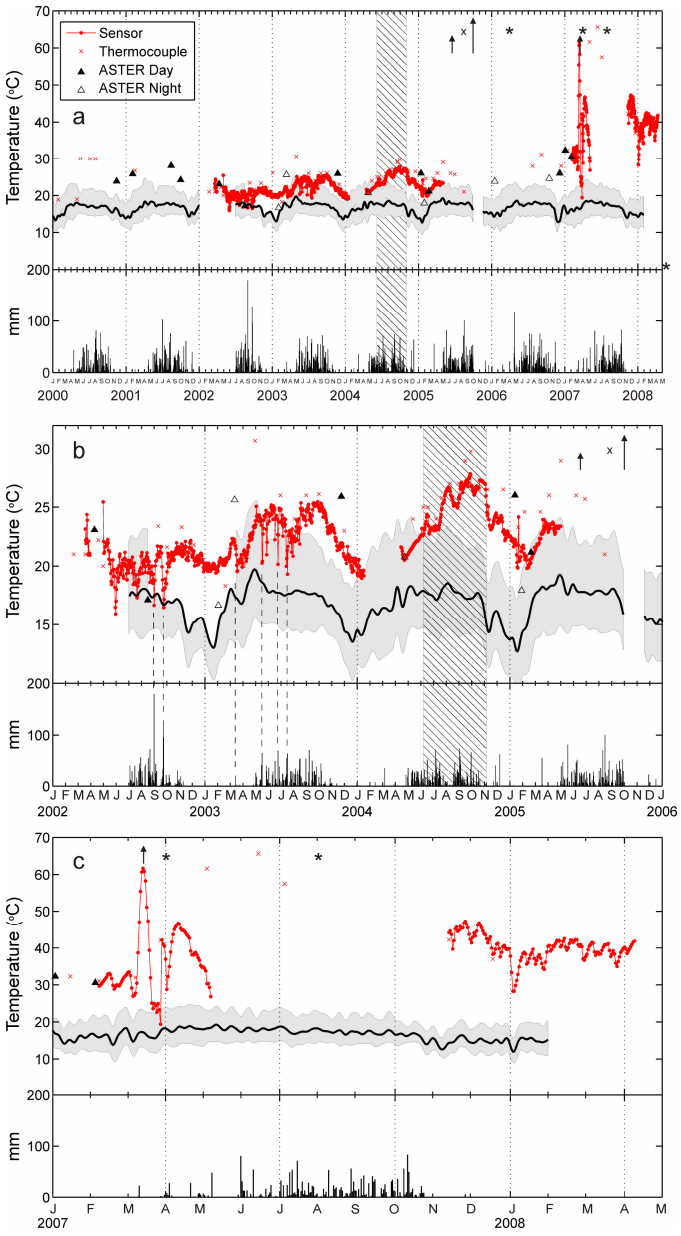

Figure 3.2: Crater lake temperatures and meteorological data. a: Comprehensive temperature time series from 2000 to 2008. b: Pre-eruptive period, 2002-2006. Dashed lines indicate cooling events in the lake caused by intense rainfall. c: Post-eruptive period, 2007-2008. For all plots, red circles are sensor temperatures, red crosses are thermocouple temperatures, solid black triangles are daytime ASTER temperatures and hollow black triangles are nighttime ASTER temperatures. Hatched area indicates heating event, arrows depict phreatic eruptions and asterisks specify evaporation. Air temperature and precipitation data are from Los Andes Meteorological Station (13.88N,-89.65E, 1770 m.a.s.l.), 4 km N of Santa Ana volcano. Gray shaded area is the range of daily atmospheric temperatures, with black line showing the average atmospheric temperature. Air temperatures have been smoothed with a Hanning window.

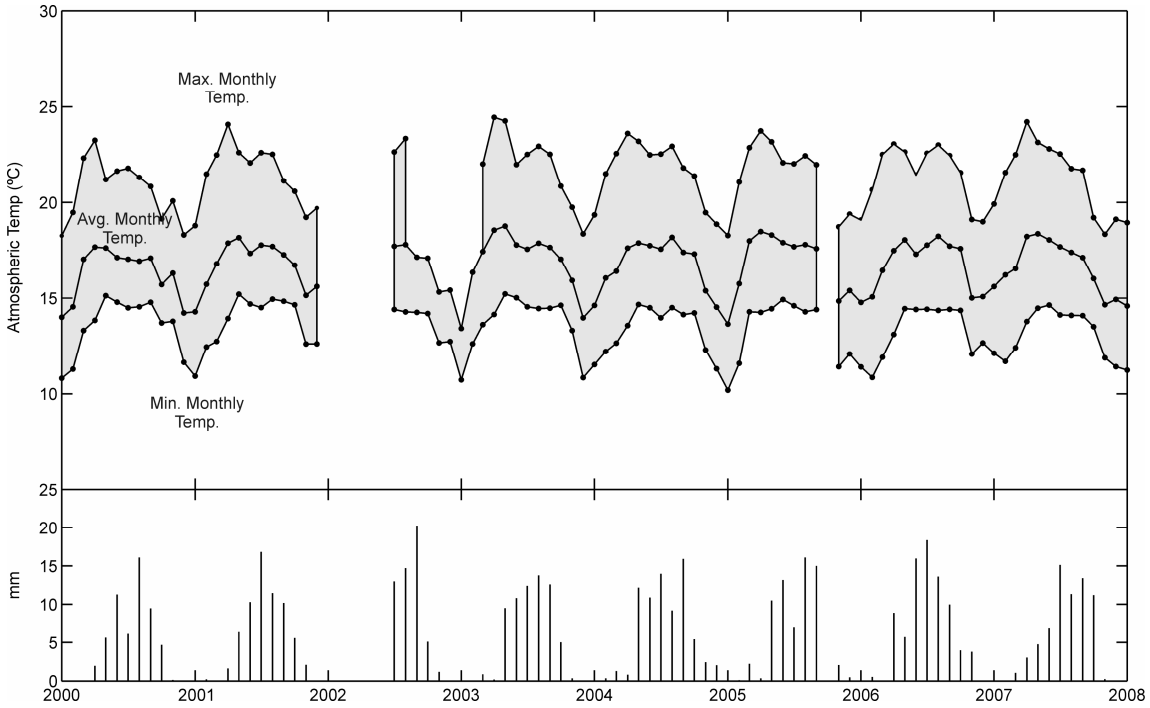

Figure 3.3: Monthly meteorological data. Monthly averages of minimum, maximum and average atmospheric temperature recorded at Los Andes meteorological station.

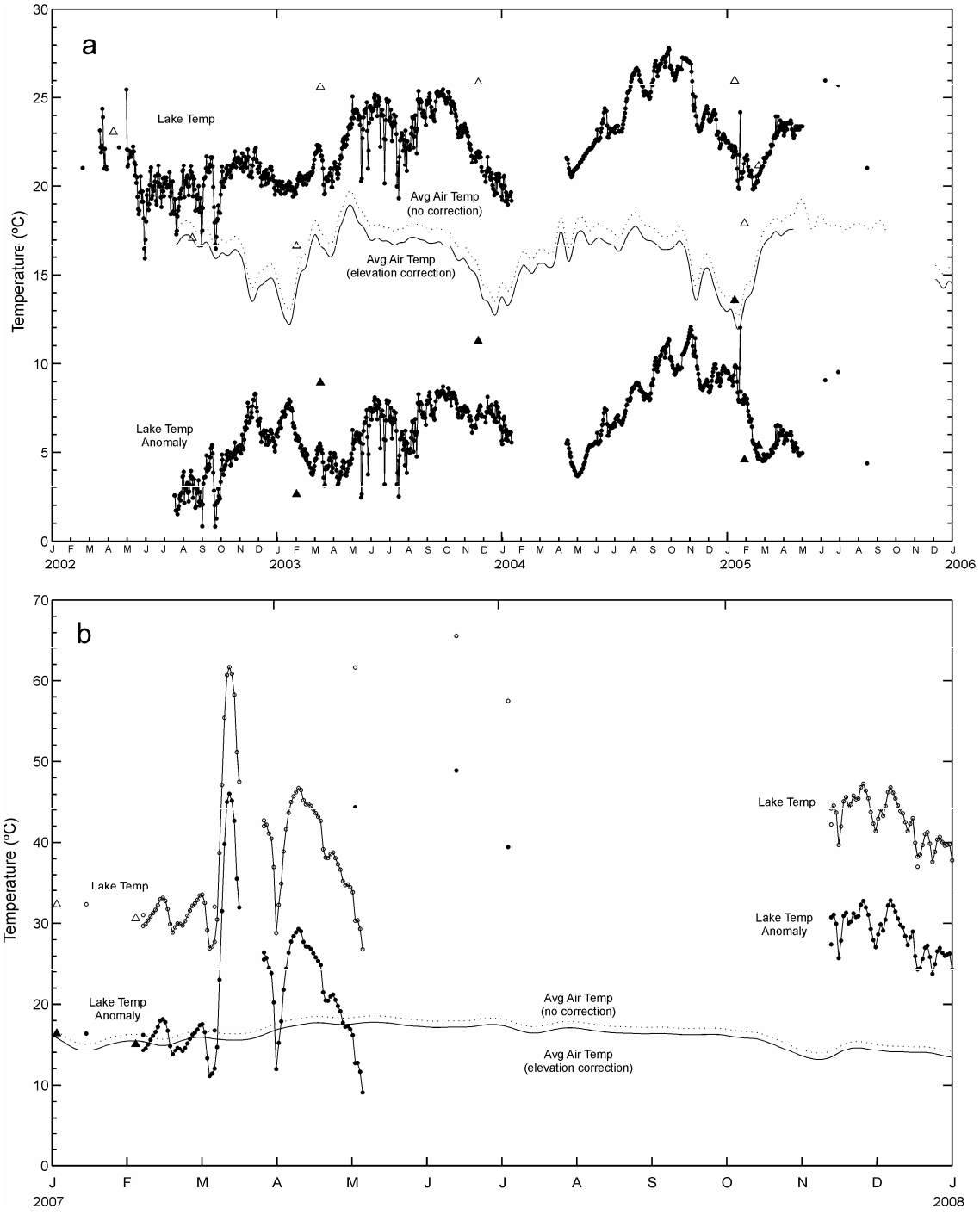

Figure 3.4: Lake temperature anomaly for a) 2002-2006 and b) 2007. The lake temperature anomaly (solid circles) is obtained from lake temperature (hollow circles) minus average atmospheric temperature. Atmospheric temperature was corrected for the decrease in temperature with increasing elevation and smoothed with a Hanning window (solid line).

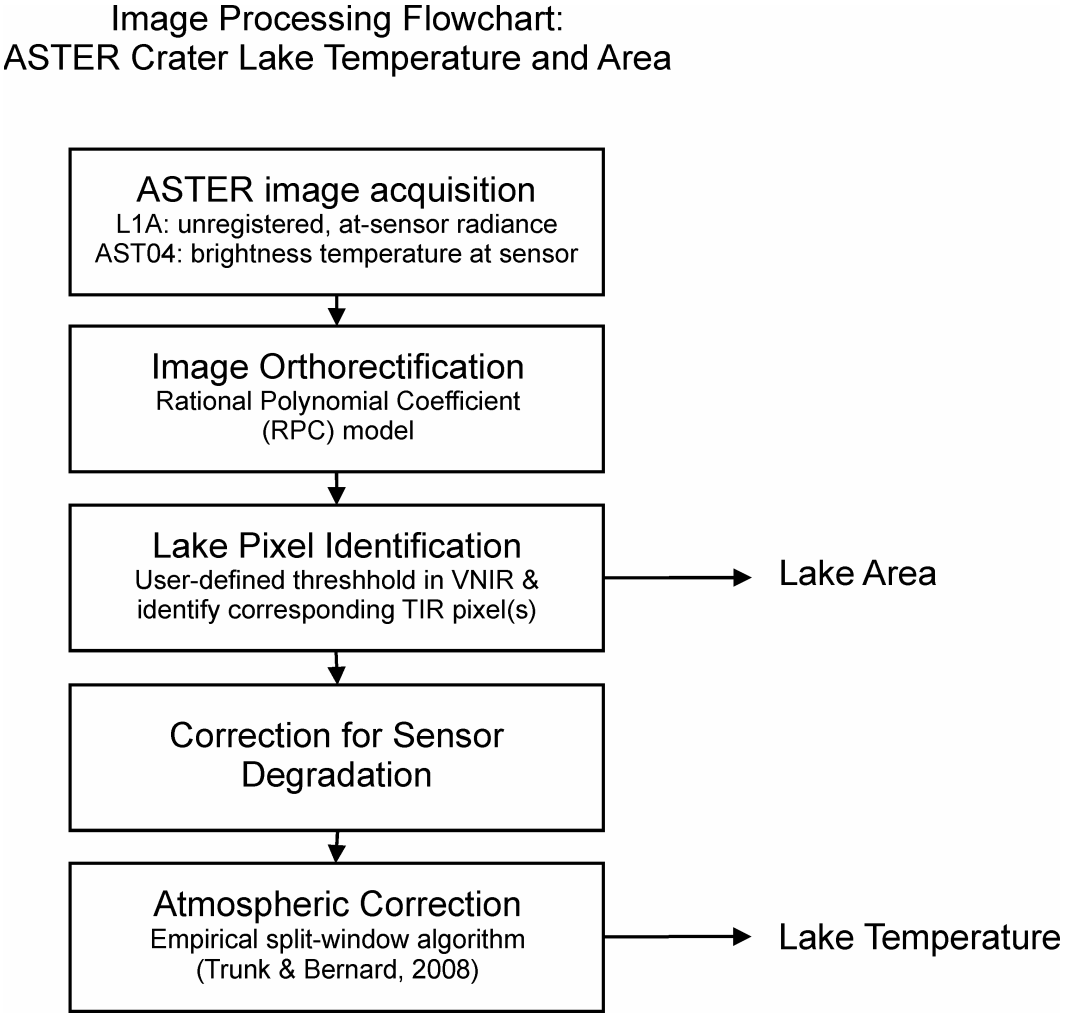

Figure 3.5: Flowchart of image processing methodology to retrieve crater lake areas and temperatures from ASTER images.

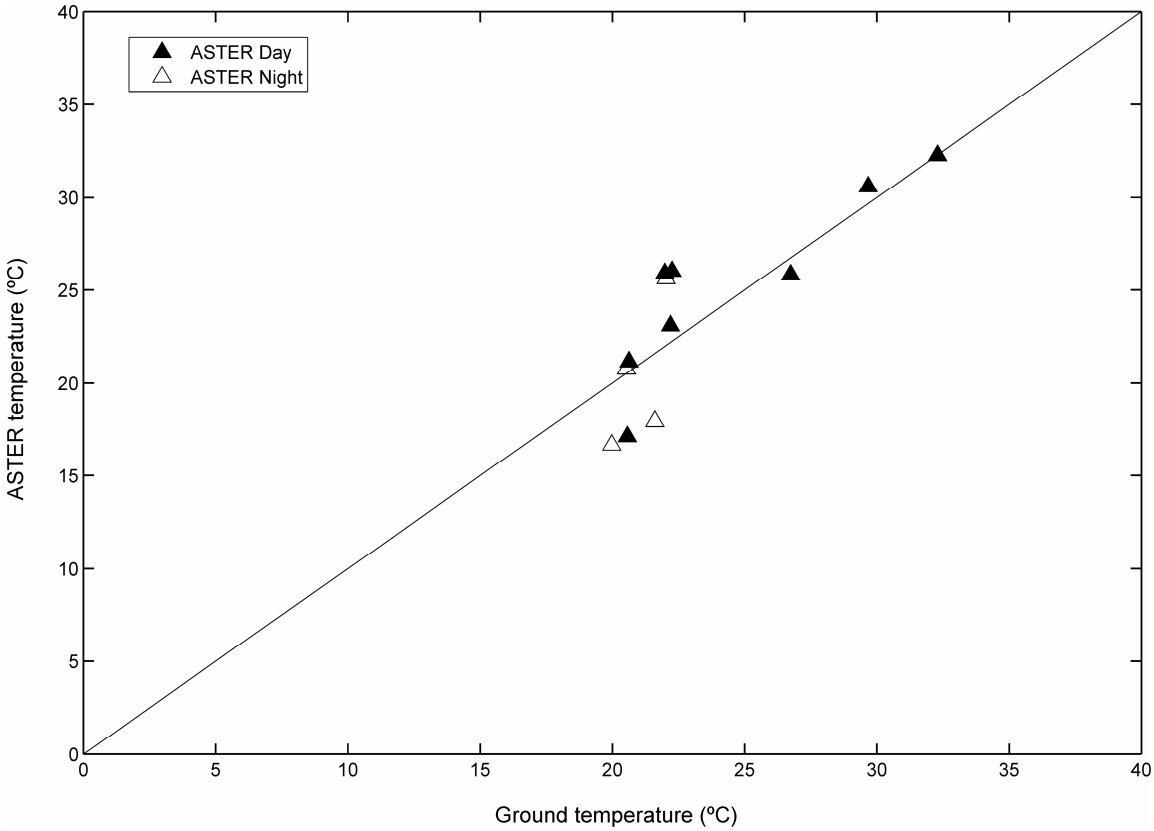

Figure 3.6: ASTER error assessment. Lake temperature obtained from ASTER imagery ground truthed with in-situ lake temperatures.

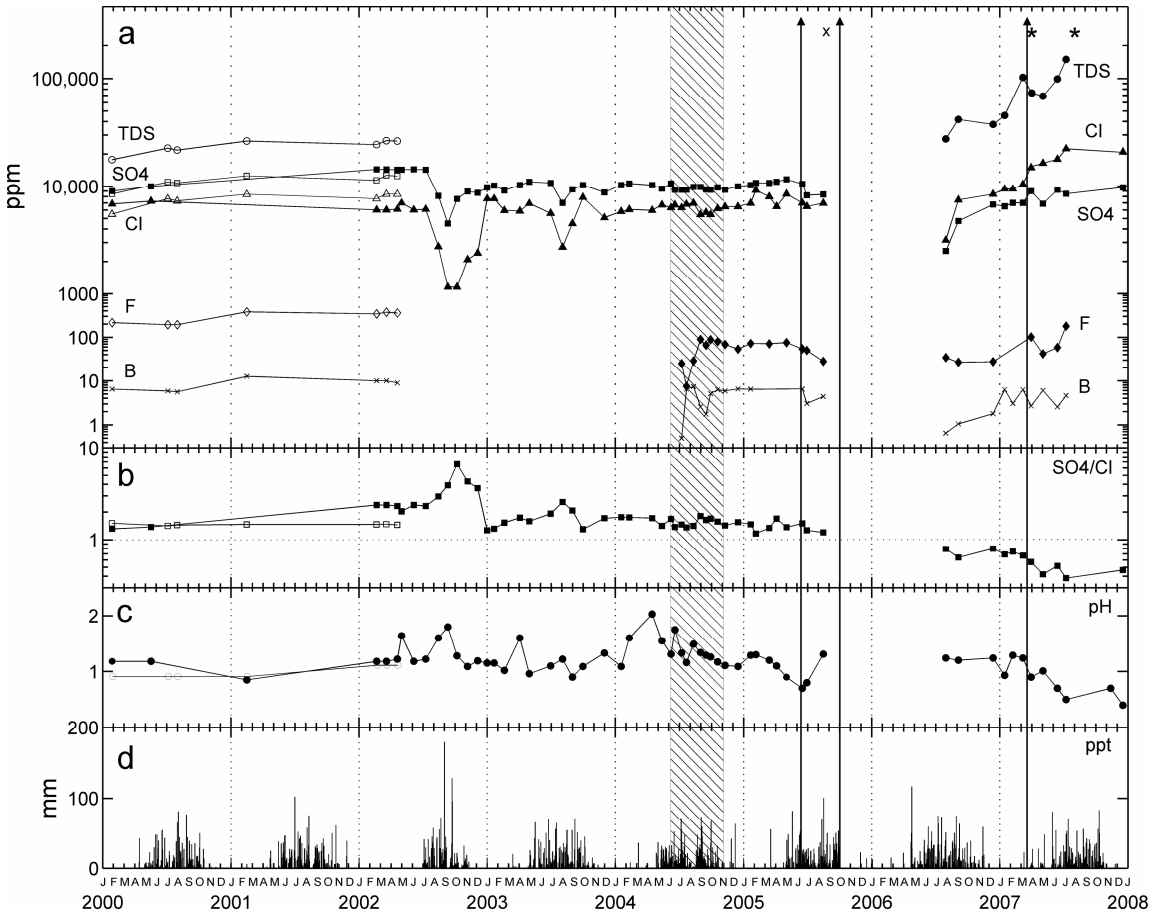

Figure 3.7: Time series of crater lake anions. a: Crater lake anion concentrations. Units are mg/kg. b: Sulfate over chloride ratio. c: pH over time. d: Daily averages of precipitation recorded at Los Andes Meteorological Station, 4 km N of Santa Ana volcano. Units are in mm. Hatched area indicates heating event, long arrows depict phreatic eruptions, cross indicates incandescence, and asterisks indicate evaporation. Hollow symbols for 2000-2002 are from *Bernard et al., 2004*.

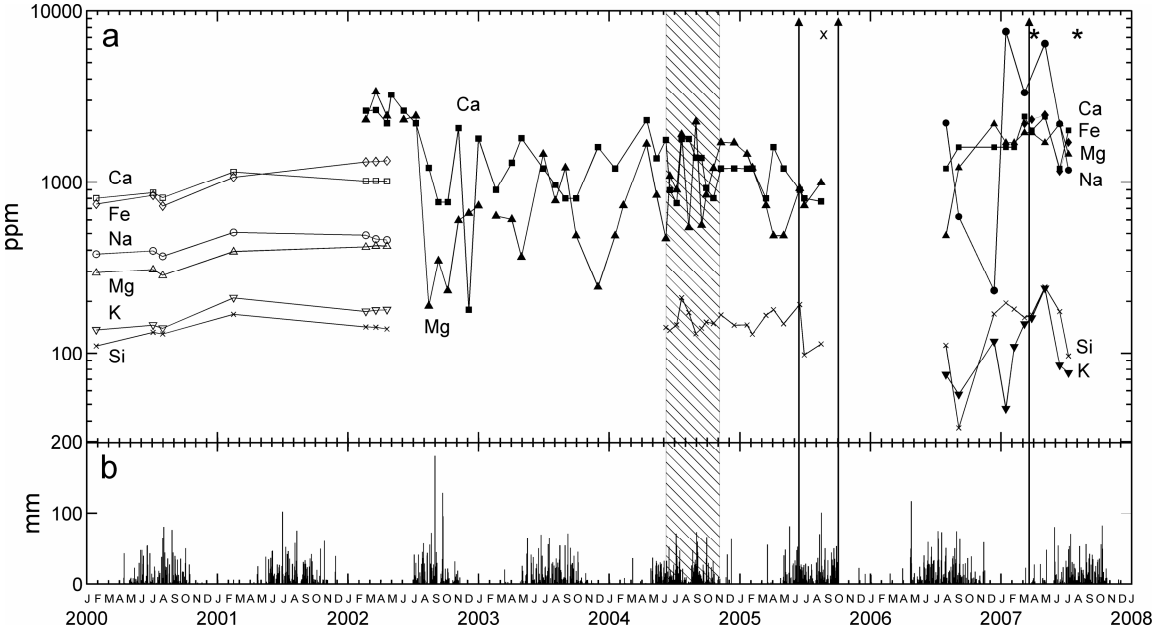

Figure 3.8: Time series of crater lake cations. a: Crater lake cation concentrations. Units are mg/kg. b: Daily averages of precipitation recorded at Los Andes Meteorological Station, 4 km N of Santa Ana volcano. Units are in mm. Hatched area indicates heating event, long arrows depict phreatic eruptions, cross indicates incandescence, and asterisks indicate evaporation.. Hollow symbols for 2000-2002 are from *Bernard et al., 2004*.

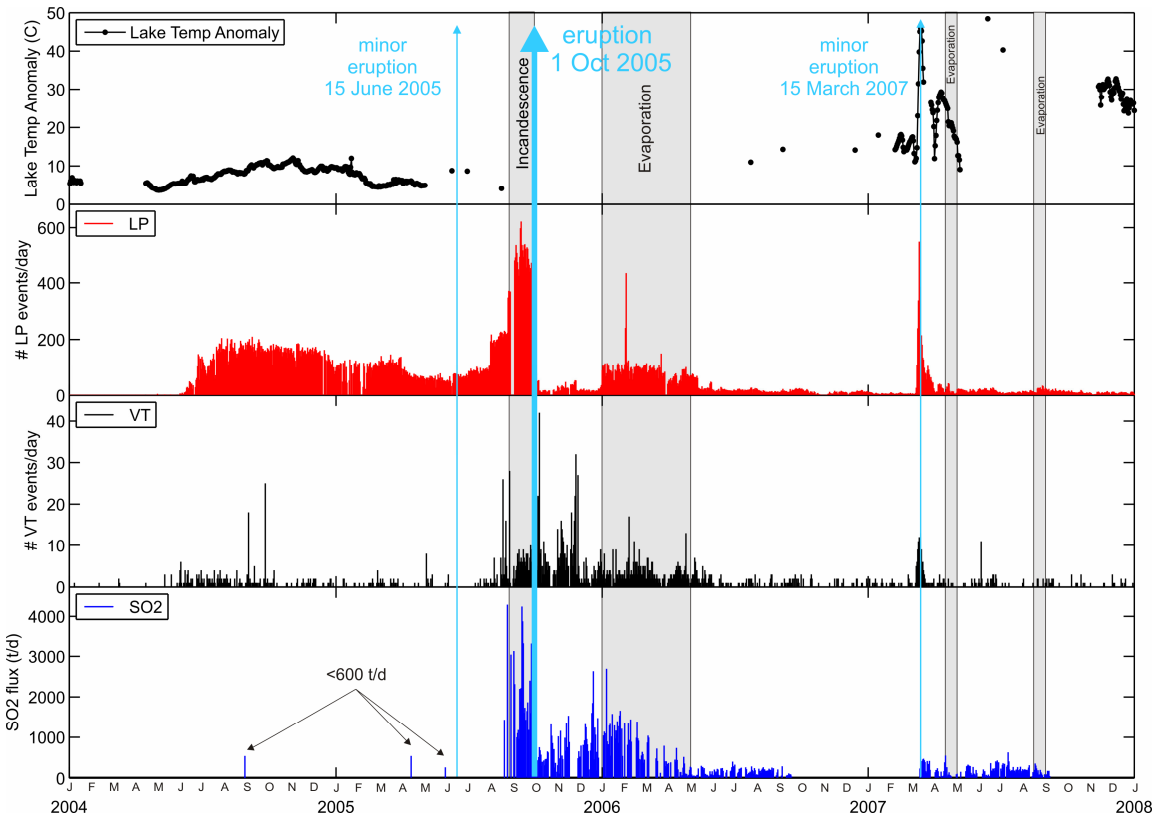

Figure 3.9a. Daily sulfur dioxide fluxes and seismicity for entire data set 2002 to 2006. SO_2 fluxes have units of tons per day. Seismicity is reported as number of counts per day of long-period (LP) or volcano-tectonic (VT) events. Lake temperature anomaly (ºC) is shown for comparison. Arrows denote phreatic eruptions. Gray boxes indicate periods of incandescence or evaporation.

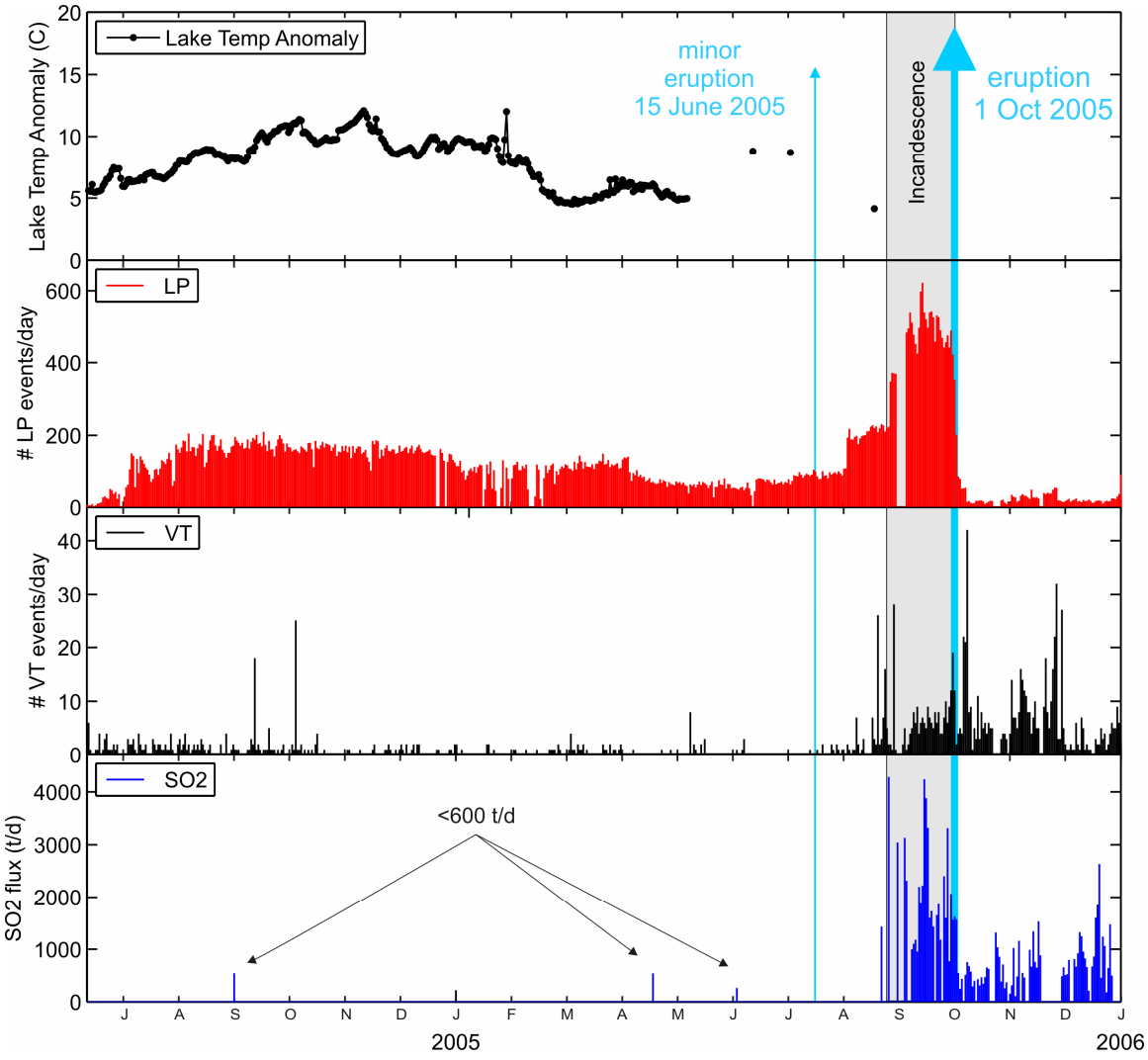

Figure 3.9b. Daily sulfur dioxide fluxes and seismicity 2004 & 2005. SO2 fluxes have units of tons per day. Seismicity is reported as number of counts per day of long-period (LP) or volcano-tectonic (VT) events. Lake temperature anomaly (ºC) is shown for comparison. Arrows denote phreatic eruptions. Gray boxes indicate periods of incandescence or evaporation.

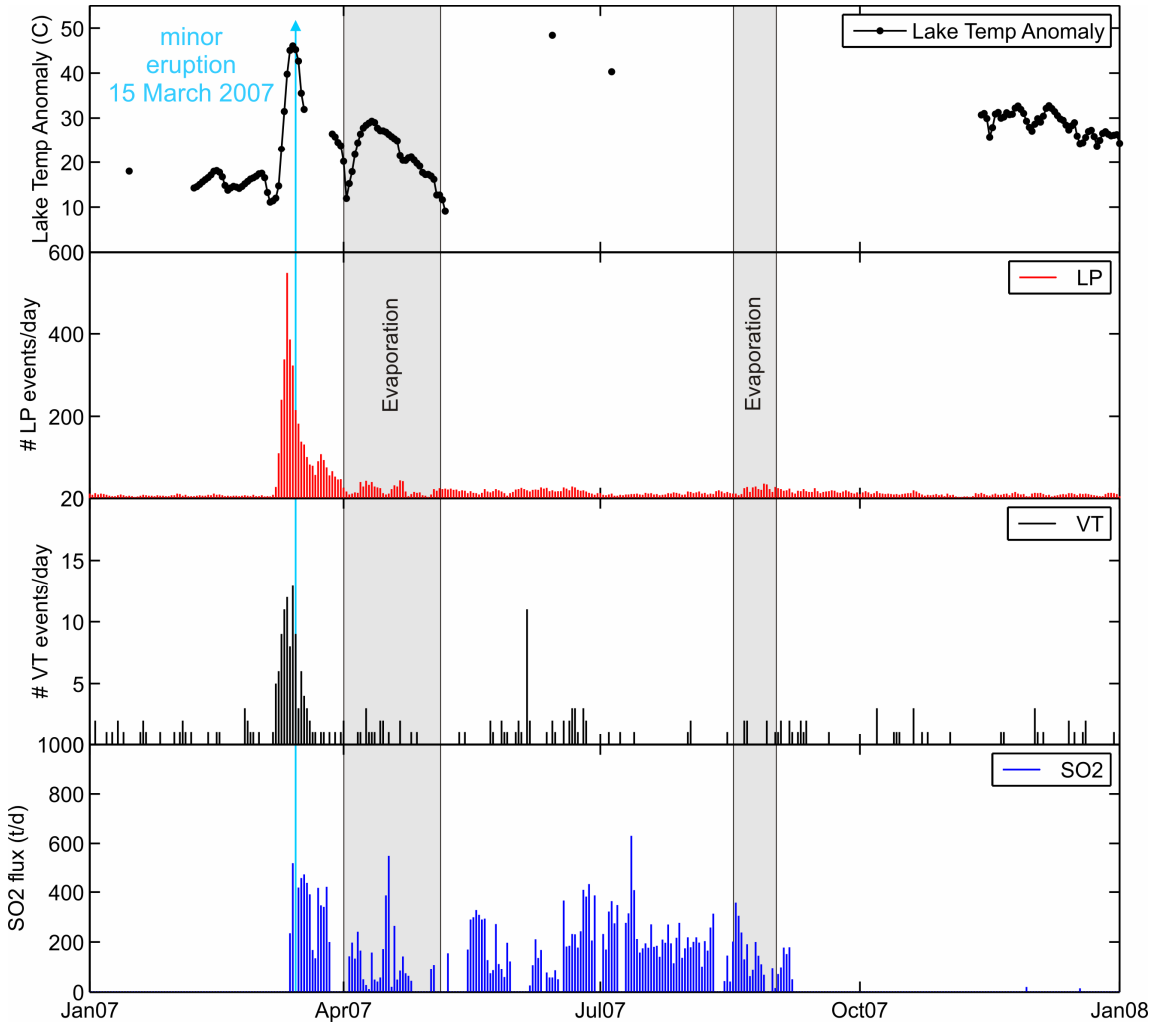

Figure 3.9c. Daily sulfur dioxide fluxes and seismicity for 2007. SO_2 fluxes have units of tons per day. Seismicity is reported as number of counts per day of long-period (LP) or volcano-tectonic (VT) events. Lake temperature anomaly (ºC) is shown for comparison. Arrows denote phreatic eruptions. Gray boxes indicate periods of incandescence or evaporation.

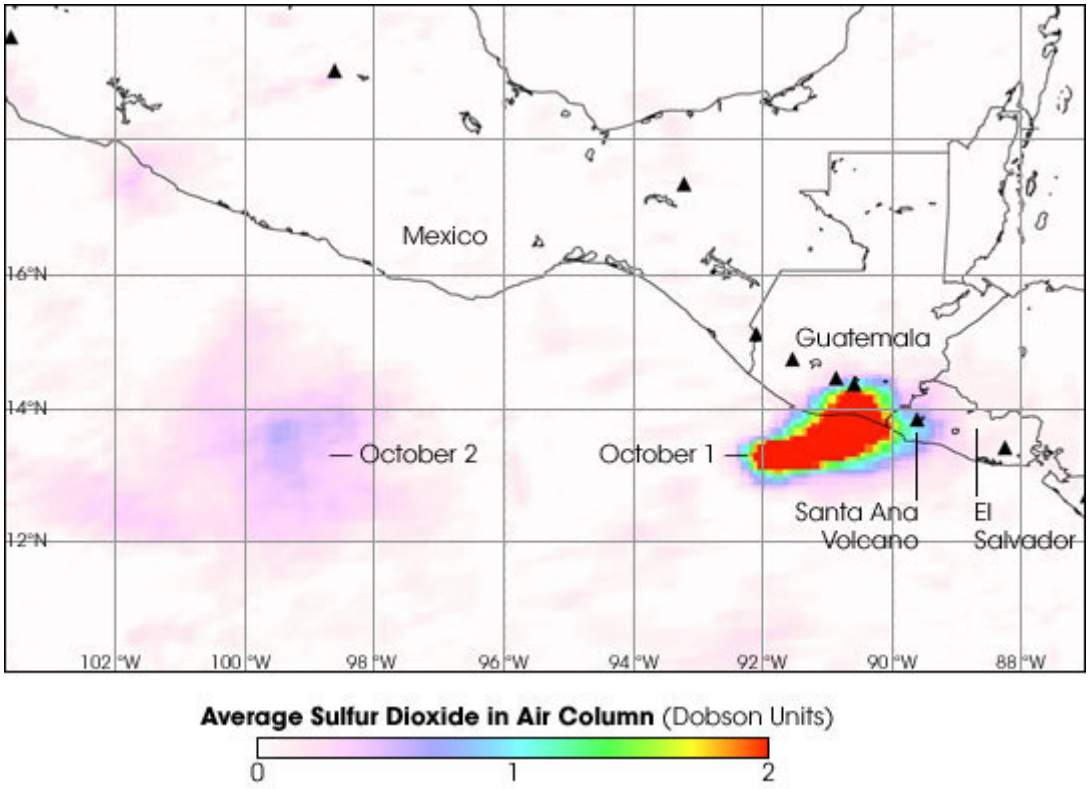

Figure 3.10. Eruptive sulfur dioxide emission imaged by the Ozone Monitoring Instrument (OMI) on October 1 and 2, 2005. Sulfur dioxide concentrations are color coded in Dobson units, with highest concentrations in red and lowest concentrations in pink. A Dobson Unit is the number of SO_2 molecules per square centimeter of atmosphere. One Dobson Unit equals 0.02848 grams of sulfur dioxide per square meter of vertical column of atmosphere. Black triangles indicate active volcanoes. NASA image courtesy Simon Carn, Joint Center for Earth Systems Technology (JCET), University of Maryland Baltimore County (UMBC).

Table 3.1: Annual rainfall statistics.

Year	Atmospheric Temperature			Precipitation		
	Maximum C	Minimum C	Average C	Total m/yr	Average mm/day	Maximum mm/day
2000	20.6	13.5	16.3	1.69	12.9	81.2
2001	21.4	13.7	16.7	1.98	15.2	102.2
2002*	23.0	14.3	17.8	1.67	17.1	179.3
2003	22.0	14.0	17.3	2.00	13.6	71.6
2004	21.6	13.3	16.7	2.28	15.6	74.0
2005^	21.4	13.3	16.9	2.00	15.2	100.6
2006	21.4	13.2	16.7	2.48	15.6	116.6
2007	21.4	13.2	16.7	2.05	13.5	83.1
7 year total	21.6	13.6	16.9	2.02	14.8	101.1

*Data gap January - June 2002.
^Data gap October 2005, omitting rainfall from Hurricane Stan (2-10 October 2005) immediately following the 1 October 2005 eruption.
All meteorological data collected at Los Andes Meteorological Station (13.88N, -89.65E, 1770 m.a.s.l).

Table 3.2: Monthly Averages of Meteorological Data.

Date	Air Temperature (ºC) max	Air Temperature (ºC) min	Air Temperature (ºC) avg	Precipitation (mm)
1-Jan-00	18.26	10.81	14.00	0.00
1-Feb-00	19.48	11.29	14.54	0.00
1-Mar-00	22.32	13.30	17.03	0.01
1-Apr-00	23.25	13.84	17.67	1.96
1-May-00	21.20	15.12	17.62	5.61
1-Jun-00	21.64	14.79	17.12	11.28
1-Jul-00	21.79	14.49	17.04	6.11
1-Aug-00	21.32	14.54	16.94	16.07
1-Sep-00	20.84	14.78	17.09	9.48
1-Oct -00	19.15	13.70	15.71	4.67
1-Nov-00	20.08	13.79	16.30	0.15
1-Dec-00	18.30	11.64	14.23	0.00
1-Jan-01	18.79	10.92	14.28	0.00
1-Feb-01	21.49	12.45	15.72	0.21
1-Mar-01	22.49	12.74	16.80	0.00
1-Apr-01	24.08	13.94	17.88	1.62
1-May-01	22.61	15.20	18.16	6.35
1-Jun-01	22.08	14.69	17.34	10.28
1-Jul-01	22.61	14.50	17.78	16.79
1-Aug-01	22.52	14.94	17.70	11.46
1-Sep-01	21.13	14.84	17.27	10.17
1-Oct-01	20.58	14.65	16.72	5.56
1-Nov-01	19.22	12.60	15.14	2.09
1-Dec-01	19.71	12.61	15.60	0.00
1-Jan-02	Data Gap			
1-Feb-02				
1-Mar-02				
1-Apr-02				
1-May-02				
1-Jun-02				
1-Jul-02	22.64	14.40	17.71	12.97
1-Aug-02	23.34	14.28	17.80	14.67
1-Sep-02	Data Gap	14.25	17.14	20.25
1-Oct-02		14.20	17.09	5.07
1-Nov-02		12.67	15.32	1.18
1-Dec-02		12.73	15.41	0.01
1-Jan-03		10.72	13.41	0.00
1-Feb-03		12.61	16.35	0.00
1-Mar-03	22.01	13.61	17.44	0.87
1-Apr-03	24.45	14.15	18.56	0.17
1-May-03	24.26	15.21	18.77	9.48
1-Jun-03	21.98	15.02	17.78	10.82
1-Jul-03	22.51	14.54	17.56	12.38

All meteorological data collected at Los Andes Meteorological Station (13.88N, -89.65E, 1770 m.a.s.l).

Table 3.2 con't .

Date	Air Temperature (ºC) max	Air Temperature (ºC) min	Air Temperature (ºC) avg	Precipitation (mm)
1-Aug-03	22.94	14.45	17.87	13.74
1-Sep-03	22.52	14.47	17.66	12.56
1-Oct-03	20.85	14.62	17.04	5.02
1-Nov-03	19.75	13.30	15.92	0.33
1-Dec-03	18.36	10.84	13.97	0.00
1-Jan-04	19.35	11.52	14.62	0.07
1-Feb-04	21.50	12.21	16.05	0.35
1-Mar-04	22.56	12.65	16.41	1.29
1-Apr-04	23.61	13.56	17.62	0.81
1-May-04	23.20	14.67	17.88	12.16
1-Jun-04	22.49	14.49	17.75	10.87
1-Jul-04	22.54	13.97	17.56	13.97
1-Aug-04	22.94	14.50	18.18	9.18
1-Sep-04	21.81	14.14	17.39	15.90
1-Oct-04	21.38	14.22	17.31	5.39
1-Nov-04	19.47	12.29	15.38	2.43
1-Dec-04	18.87	11.30	14.53	2.05
1-Jan-05	18.28	10.18	13.65	0.15
1-Feb-05	21.06	11.58	15.75	0.10
1-Mar-05	22.87	14.28	17.99	2.22
1-Apr-05	23.74	14.25	18.48	0.35
1-May-05	23.17	14.44	18.30	10.48
1-Jun-05	22.08	14.92	17.90	13.16
1-Jul-05	22.03	14.60	17.69	6.91
1-Aug-05	22.44	14.29	17.80	16.07
1-Sep-05	21.98	14.40	17.59	14.98
1-Oct-05	Data Gap			
1-Nov-05	18.73	11.41	14.85	2.05
1-Dec-05	19.39	12.08	15.40	0.47
1-Jan-06	19.08	11.40	14.77	0.47
1-Feb-06	20.66	10.85	15.07	0.52
1-Mar-06	22.51	11.90	16.45	0.00
1-Apr-06	23.06	13.10	17.49	8.87
1-May-06	22.64	14.45	18.04	5.68
1-Jun-06	21.44	14.41	17.30	15.95
1-Jul-06	22.58	14.42	17.77	18.35
1-Aug-06	23.00	14.35	18.23	13.59
1-Sep-06	22.45	14.41	17.72	9.97
1-Oct-06	21.56	14.36	17.59	3.98
1-Nov-06	19.11	12.07	15.01	3.78
1-Dec-06	18.99	12.66	15.08	0.02
1-Jan-07	19.92	12.12	15.60	0.02
1-Feb-07	21.56	11.69	16.21	0.00
1-Mar-07	22.50	12.41	16.54	1.05
1-Apr-07	24.21	13.78	18.22	3.02
1-May-07	23.14	14.47	18.37	4.75
1-Jun-07	22.80	14.64	18.05	6.80
1-Jul-07	22.54	14.12	17.69	15.11
1-Sep-07	21.69	14.08	17.12	13.39

Table 3.2 con't .

Date	Air Temperature (ºC) max	Air Temperature (ºC) min	Air Temperature (ºC) avg	Precipitation (mm)
1-Aug-07	21.77	14.10	17.39	11.34
1-Sep-07	21.69	14.08	17.12	13.39
1-Oct-07	19.21	13.50	16.02	11.19
1-Nov-07	18.34	11.87	14.65	0.24
1-Dec-07	19.12	11.41	14.93	0.01

Table 3.3: ASTER lake areas and lake temperatures compared to ground temperatures, 2000-2007.

Date	Day or Night	ASTER equivalent radius (m)	ASTER T (°C)	Ground T (°C)	Error (°C)	No. Pixels in Lake	Percent of Pixel in Lake
15-Nov-00	D	78.9	23.85	NA	NA	1	81.0
3-Feb-01	D	114.8	25.82	26.74	0.92	1	100
14-Aug-01	D	107.6	28.07	NA	NA	1	100
1-Oct-01	D	71.7	24.21	NA	NA	1	100
11-Apr-02	D	87.3	23.08	22.20	0.88	1	100
17-Aug-02	D	84.6	17.12	20.57	3.45	1	89.3
2-Feb-03	N	NA	16.66	19.98	3.32	4	97.2, 86.1, 80.6, 69.4
13-Mar-03	N	NA	25.62	22.03	3.59	1	100
24-Nov-03	D	99.1	25.90	21.98	3.93	1	100
25-Apr-04	N	NA	20.77	20.54	0.23	1	100
13-Jan-05	D	100.2	26.01	22.26	3.75	1	100
29-Jan-05	N	NA	17.94	21.61	3.67	4	94.5, 90.7, 85.9, 81.7
21-Feb-05	D	101.2	21.16	20.63	0.53	2	100, 100
16-Jan-06	N	NA	23.83	NA	NA	1	100
15-Oct-06	N	NA	24.62	NA	NA	2	80.7, 92.0
2-Dec-06	D	100.1	26.02	NA	NA	1	100
3-Jan-07	D	99.4	32.27	32.30	0.03	1	89.6
4-Feb-07	D	96.6	30.59	29.67	0.92	1	95.7

Table 3.4: Lake water chemistry of Santa Ana crater lake, 2000-2007.

Date	T (°C)	pH_m	Cl	SO_4	Mg	Ca	SiO_2	B	F	S^{-2}	K	Na	TDS	Fe total	Al	Mn	Ti
28-Jan-00[a]	18.9	0.9	5472	8417	294	799	235	6.6	215		136	378	17600	738	1143	16.0	1.4
5-Jul-00 [a]	30.0	0.9	7603	10907	307	862	282	6.0	194		145	395	22500	832	1214	17.0	1.0
1-Aug-00 [a]	30.0	0.9	7267	10661	283	805	276	5.7	194		139	367	21600	720	1161	16.0	1.3
15-Feb-01 [a]	26.0	0.9	8369	12464	392	1144	359	12.8	379		209	506	26200	1065	1654	20.0	2.8
20-Feb-02 [a]	20.6	1.1	7615	11318	417	1010	303	10.2	341		174	487	24300	1308	1717	21.0	3.1
20-Mar-02 [a]	21.0	1.1	8401	12598	423	1013	302	10.2	372		177	463	26400	1314	1743	23.2	3.2
20-Apr-02 [a]	21.0	1.1	8402	12378	422	1006	295	9.1	357		178	457	26200	1330	1741	23.3	3.1
2-May-02	25.4	1.6	7002	14250		3239											
6-Jun-02	19.0	1.2	6027	14375	2310	2608											
10-Jul-02	20.0	1.2	6115	14250	2432	2206											
15-Aug-02	21.1	1.6	2747	8125	188	1214											
11-Sep-02	21.0	1.8	1153	4500	347	762											
7-Oct-02	19.9	1.3	1152	7625	231	762											
6-Nov-02	21.9	1.1	2083	8937	596	2064											
5-Dec-02	21.3	1.2	2393	8688	656	179											
1-Jan-03	20.1	1.2	7665	9750	726	1796											
21-Jan-03	20.2	1.2	7665	10125													
19-Feb-03	19.5	1.0	5949	9125	632	898											
4-Apr-03	21.3	1.6	5889	10250	605	1297											
1-May-03	23.3	1.0	6921	11000	365	1805											
1-Jul-03	24.7	1.1	5591	10750	1458	1203											
4-Aug-03	22.5	1.2	2722	7000	777	961											
1-Sep-03	24.6	0.9	4497	9375	1214	801											
1-Oct-03	25.0	1.1	7876	10250	486	801											
1-Dec-03	23.0	1.3	5104	8750	243	1602											
18-Jan-04	21.5	1.1	5834	10250	486	1201											
10-Feb-04	25.1	1.6	6077	10625	729												
15-Apr-04	21.6	2.0	5965	10250	1672	2297											
13-May-04	21.7	1.6	6711	9500	836	1379											

a: Analyses from Bernard et al., 2004. b: Analyses by SGS, Canada. All other analyses by SNET. All units are in mg/L. pH_m is measured in-situ at lake temperature.

Table 3.4 con't.

Date	T (°C)	pH_m	Cl	SO_4	Mg	Ca	SiO_2	B	F	S^{-2}	K	Na	TDS	Fe total	Al	Mn	Ti
8-Jun-04	23.2	1.3	6314	10625	468	1764	302										
19-Jun-04	24.2	1.8	6711	9250	1084	894	290										
8-Jul-04	23.4	1.3	6314	9250	900	751	313	0.5	25								
22-Jul-04	24.9	1.2	6799	9250	1897	1788	450	6.5	8								
11-Aug-04	26.3	1.5	6959	9875	542	1788	368	7.4	29								
31-Aug-04	25.8	1.3	5468	9875	2249	1391	278	2.6	90								
16-Sep-04	27.0	1.3	5707	9375	559	1384	299	1.8	66								
29-Sep-04	27.7	1.3	5459	9250	839	923	324	5.1	89								
19-Oct-04	26.6	1.2	6204	9750	1206	802	318	6.3	80								
9-Nov-04	24.4	1.1	6452	9250	1703	1203	357	5.9	69								
16-Dec-04	22.9	1.1	6452	10000	1700	1203	312	6.5	54								
21-Jan-05	21.8	1.3	6959	10250	1457	1201	312	6.5	73								
5-Feb-05	20.9	1.3	9196	10750	1214	1201	276										
15-Mar-05	22.3	1.2	7985	10750	729	801	355		71								
5-Apr-05	23.4	1.1	6488	11000	486	1602	383										
3-May-05	23.4	0.9	8484	11625	486	1201	317		76								
17-Jun-05		0.7	6987	10525	913	897	410	6.5	55								
30-Jun-05	25.7	0.8	6488	8250	729	801	209	3.1	50								
16-Aug-05	21.0	1.3	6970	8375	991	769	242	4.4	28								
31-Jul-06		1.2	3158	2500	486	1201	238	0.7	34	0.12	75	2213	27500				
5-Sep-06		1.2	7453	4750	1214	1602	78	1.1	27	0.75	57	627	41750				
13-Dec-06	28.0	1.2	8446	6750	2186	1602	362	1.8	28	0.02	117	231	37600				
15-Jan-07	32.3	0.9	9440	6500	1700	1602	419	6.3		0.10	47	7575	45500				
15-Jan-07 [b]	32.3	0.9			1692	1074					89	892		1709	331	98	0.6
7-Feb-07	29.7	1.3	9440	7000	1700	1602	386	3.1		0.10	109						
8-Mar-07	32.0	1.2	10433	7000	1943	2409	344	6.3			148	3333	102500	2188			
8-Mar-07 [b]	32.0	1.2			1898	1184					121	1078		1840	362	112	0.6
28-Mar-07	42.0	0.9	15402	9000	1943	2002	359	2.9	103	0.06	160		74250	2315			
28-Mar-07 [b]	42.0	0.9			2104	1492					163	1271		2100	680	119	2.4
4-May-07	61.6	1.0	16396	6875	1700	2403	519	6.0	42	0.30	238	6450	68750	2461			
4-May-07 [b]	61.6	1.1			1841	1848					135	1165		2131	981	103	0.5

Table 3.4 con't.

Date	T (°C)	pH_m	Cl	SO_4	Mg	Ca	SiO_2	B	F	S^{-2}	K	Na	TDS	Fe total	Al	Mn	Ti
16-Jun-07	65.6	0.7	17873	9250	2186	1201	373	2.6	59	0.01	85	2190	99250	1159			
16-Jun-07 [b]	65.6	0.7			995	1531					117	663		1449	1329	47	3.8
9-Jul-07	57.5	0.5	22340	8500	1457	2002	206	4.6	180	0.01	76	1178	150250	1708			
9-Jul-07 [b]	57.5	0.5			818	1458					130	620		1428	1384	41	8.4
13-Nov-07	44.1	0.7															
18-Dec-07	38.3	0.4	20851	9750													
RSD (%)			NA	NA	5.1	4.2	NA	NA	NA	NA	8.1	6.0	NA	15.2	19.6	6.2	NA

Table 3.5: Summary of dataset trends in the crater lake and fumaroles from 2000 to 2007.

Dataset	Data Type	pre-eruption						post-eruption	
		1 January 2000-18 May 2000	18 May 2000-20 Feb 2002	20 Feb 2002-8 June 2004	8 June 2004-Nov 2004	Nov 2004-23 August 2005	23 August 2005-1 Oct 2005	1 Oct 2005-8 March 2007	8 March 2007-31 Dec 2007
		low level activity	hydrothermal activity	low level activity	long-range precursors	long-range precursors	mid-range precursors	hydrothermal activity	hydrothermal activity
Lake temperature	Temperature	19ºC	26-30ºC	16-25.5ºC	20-28ºC	21ºC (16 August 2005)	N.D.	25-35ºC	25-65ºC
	Temperature anomaly	1.5-4ºC	10-13ºC	0.5-8ºC	increasing to 12ºC	decreasing to 4.3ºC (16 August 2005)	N.D.	10-18ºC	10-50ºC
	Volcanic input (MW)	N.D.	21 MW	0.5-6.5 MW	4-15 MW	0.5-8 MW	N.D.	13-40 MW	80-830 MW
Lake chemistry	Anions	pH = 1, SO_4/Cl = 1, seasonal variation (rainy season dilution)	pH = 1, SO_4/Cl = 1, seasonal variation (rainy season dilution)	pH = 1.1, SO_4/Cl =1-1.5, seasonal variation (rainy season dilution)	pH decreasing, SO_4/Cl = 1.1, no rainy season dilution	pH decreasing, SO_4/Cl = 1.1, no rainy season dilution	N.D.	pH = 1, SO_4/Cl <1	pH < 1, SO_4/Cl < 1
	Cations	stable concentrations	stable concentrations	seasonal variation (rainy season dilution)	Mg increasing	Mg decreasing	N.D.		
	PRA	18%	25%	5-32%	<20%	10-40%	N.D.	35-10%	15-45%
	Dissolution mode	congruent dissolution	congruent dissolution	N.D.	N.D.	N.D.	N.D.	incongruent dissolution	incongruent dissolution
	Mineral saturation	alunite, jarosite, gibbsite, and diaspore saturation over 100-200ºC	higher saturation temperatures for alunite and diaspore	N.D.	N.D.	N.D.	N.D.	alunite, jarosite, gibbsite, and diaspore saturation over 100-200C	higher saturation temperatures for alunite and diaspore (28 March-4 May); no saturated phases at higher temperatures (16 June - 9 July)

Table 3.5 con't.

Dataset	Data Type	pre-eruption						post-eruption	
		1 January 2000-18 May 2000	18 May 2000-20 Feb 2002	20 Feb 2002-8 June 2004	8 June 2004-Nov 2004	Nov 2004-23 August 2005	23 August 2005-1 Oct 2005	1 Oct 2005-8 March 2007	8 March 2007-31 Dec 2007
		low level activity	hydrothermal activity	low level activity	long-range precursors	long-range precursors	mid-range precursors	hydrothermal activity	hydrothermal activity
SO_2	SO_2 flux	N.D	<400 t/d (Feb 2001)	30-80 t/d (2002)	<600 t/d	<600 t/d	>4000 t/d	decreasing from 2500 t/d in January 2006	<600 t/d
Seismicity	LP	none	yes	none	~200 events/day	decreasing from 200 to 80 events/day	<600 events/day	100 events/day during evaporation (Jan-May 2006)	jump to 550 events/day (8-12 March)
	VT	N.D	N.D.	few	few	swarms (18, 22, 27 August)	<10 events/day	cyclical peaks decreasing in magnitude from 40 to 10 events/day	jump to 13 events/day (8-16 March)
	Tremor	none	none	none	none	tremor (25 Jan, 3 May)	banded tremor (27 August)	banded tremor (20-23 March 2006)	banded tremor (1, 15, 24 April)

CHAPTER 4

4. Analysis of Results

4.1 Introduction

In this chapter I will use crater lake temperature and chemical data to evaluate sources of volcanogenic elements and rock forming elements, water-rock and water-gas interactions, saturation state of lake waters and energy budgets of the lake. This data analysis will contribute to evaluating the impact of the 2005 eruption on the crater lake. The crater time series data presented in Chapter 3 demonstrates that the chemistry of the lake was quite different after eruption than it was before. It is likely that these geochemical changes are attributable to new gas delivery from depth to the lake, subsequent water-gas and water-rock interactions occurring in the lake and near vent environment, and the fate of volcanic SO_2 in the hydrothermal system. The aim of this chapter is to ascertain how observed lake chemistry is influenced by changing volcanic and/or hydrothermal processes, and to clarify likely future scenarios.

4.2 Source of volcanogenic elements in the lake

Volcano-hosted hydrothermal systems are acidified by magmatic gases ascending from a shallowly degassing magma body. Condensing magmatic gases may form acidic fluids *in-situ* upon cooling which subsequently mix with groundwater or magmatic gases and then may be directly injected into the hydrothermal system or lake (e.g. Poas, *Rowe [1992]*, Kawah Ijen, *Demelle and Bernard, [1994])*. More soluble species, like SO_2 and HCl, are scrubbed into the hydrothermal system through hydrolysis reactions. SO_2 disproportionates into $H_2S + H_2SO_4$ or $S^0 + H_2SO_4$ at $pH < 2$, and SO_4 is the dominant

sulfur species in the crater lake environment. H_2S escapes to the surface while native S accumulates at the bottom of the lake or in the near vent environment. Cl is conservative and a good indicator of volcanic gas input to the lake. The relatively insoluble species, mainly CO_2 and H_2S, either pass through the hydrothermal system to the atmosphere along open pathways, or if confined, contribute substantially to overpressurization at depth.

Magnesium versus chloride concentration variation diagrams have been used to identify signatures of water-rock interaction and volcanic input (Figure 4.1a). Both Mg and Cl are conservative, and are only lost from the lake by seepage. In a global study on volcanic lakes (*Varekamp et al., 2000*), large gains in Mg relative to Cl, or dominance of water-rock interaction, were observed at Ruapehu crater lake, and the inverse, large gains in Cl relative to Mg, or dominance of volcanic gas component, were observed at Poas crater lake (*Varekamp et al., 2000*). At Santa Ana crater lake, both trends have been observed during pre- and post-eruptive periods, respectively. Figure 4.1a indicates that varying degrees of water-rock interaction dominated the hydrothermal system from 2000 to 2005 (constant Cl with varying Mg), whereas the lake showed a trend towards an increasing rate of volcanic input (constant Mg with increasing Cl) from late 2006 through 2007. In this figure, a dilution trend (equal depletions in Mg and Cl) is also apparent for some samples in 2002 and 2003.

Sulfate versus chloride concentration variation diagrams have been used to describe the composition of the volcanic input (Figure 4.1b). SO_4/Cl ratio is affected by the original composition of the volcanic gas (H_2S+SO_2/HCl) and by the fate of volcanic SO_2 in the hydrothermal system (*Varekamp et al., 2000). Varekamp et al. (2000)* found

that most crater lake data from Ruapehu, Poas, Yugama, and Keli Mutu lakes fell along a line representing a one to one relationship (SO_4/Cl~1). At Santa Ana, a similar type of relationship occurs for most data from 2000 to 2005, where relative abundances of sulfate and chloride are unchanging producing with roughly linear SO_4/Cl ratios > 1. However, after the 2005 eruption, SO_4/Cl ratios were < 1, becoming progressively enriched in chloride relative to sulfate. Until March 2007, Cl concentrations were at pre-2005 levels until March 2007, when Cl concentrations increased dramatically. SO_4/Cl ratios were as low as 0.38 in July 2007. One or several sources of Cl (e.g. Cl rich brine) or sinks for SO_4 (e.g. precipitation of native sulfur or sulfate minerals) must be invoked to explain SO_4/Cl ratios <1 and the post-2005 trends in sulfate versus chloride abundances.

4.3 Source of rock forming elements in lake water

Acidic crater lake waters primarily derive rock forming elements (RFE) from dissolution of wall rocks during water-rock interaction, and from precipitation and redissolution of secondary minerals, with minor contributions from volatile metal chlorides from high temperature volcanic gases (*Symonds et al., 1994*) or concentrated volcanic brines in some cases, e.g. El Chichón (*Rouwet et al., 2004*). The main elements leached from a silicate framework during water rock interaction are Mg, Na, K, Ca, Fe and Al. Mg and Na are most easily leached first, followed by K and Ca, and Fe and Al are last. Mg and Mn are highly leachable but not incorporated into secondary minerals under acid conditions, and are considered to be conservative. Precipitation of saturated silica phases significantly lowers Si concentration in lake waters.

Concentrations of RFE relative to average Santa Ana andesite (Figure 4.2) and element transfer ratios (ETR) (Figure 4.3) are used evaluate rock dissolution processes (*Pasternack & Varekamp, 1994)*. ETR differentiate between congruent and incongruent rock dissolution, while isopleths on the RFE concentrations versus average Santa Ana andesite graph indicate the amount of rock dissolution. Element transfer rations are observed RFE concentrations in fluid divided by compositions predicted from congruent dissolution:

$$\text{ETR} = \frac{\text{Observed RFE concentration in lake water}}{\text{Predicted RFE concentration in lake water}}$$

where

$$\text{Predicted RFE concentration} = \frac{\text{Mg concentration in water}}{\text{Mg concentration in rock}} * \text{RFE concentration in rock}$$

ETR = 1 indicates congruent dissolution, ETR > 1 indicates incongruent dissolution and/or redissolution of previously precipitated mineral phases, and ETR < 1 indicates incongruent dissolution and/or mineral precipitation. Complete cation chemical analyses for 2000-2002 and 2007 samples allowed comparison of these two time periods. Lack of many major element cation analyses during 2002-2006 precluded ETR analysis.

Congruent dissolution has been proposed as the dominant mode of rock-water interaction during 2000 to 2002 (*Bernard et al., 2004*). This interpretation is supported by ETR = 1, very closely corresponding concentrations of RFE in lake waters and average andesite, equivalent to dissolution of 12 to 18 gr andesite per kg of lake water (Figure 4.2), and the general lack of saturated secondary minerals. This amount of rock dissolution is within the range of dissolution reported at other crater lakes, (e.g. 12-30 gr rock per kg water at Copahue, *Ouimette [2000]),* but fairly low compared to other crater

lakes worldwide (e.g. 60 gr rock per kg water at Kawah Ijen, *Demelle and Bernard [1994]).*

In contrast, congruent dissolution was not the dominant mode of water-rock interaction during 2007. ETR < 1 and highly disparate concentrations of RFE in lake waters relative to those in average andesite, suggest that incongruent dissolution and/or mineral precipitation were the dominant modes of rock dissolution. The amount of rock dissolution was much higher in 2007 than in 2000-2002, corresponding to dissolution of ~70-90 gr andesite per kg of water in January to May and ~30-40 gr andesite per kg water in June-July 2007 (Figure 4.2). ETR values trend back towards unity over time, though unity was not achieved by January -July 2007.

Incongruent dissolution, caused by differences in rates of leachability of selective elements or in kinetics of dissolution of primary magmatic minerals, was probably the source of water-rock discrepancies. Incongruent dissolution is sometimes observed in crater lakes when there is an intrusion of fresh magma (*Varekamp et al., 2000*).Saturation state modeling shows that 2007 lake waters were only saturated in Si phases (cristobalite and amorphous silica), pyrite, barite and close to saturation in sulfur, anhydrite, gypsum. Thus precipitation of secondary minerals is probably only minimal in 2007.

4.4 Water-rock and water-gas interactions in the lake

The chemical composition of volcanic lake waters is a product of several processes occurring in and below the lake: acidification of hydrothermal waters by hydrolysis of readily soluble volcanic gases; dissolution of andesite wallrock or fresh magmatic intrusion by water-rock interaction; precipitation and dissolution of secondary

minerals; dilution by meteoric and volcanic water; and evaporation. Few minerals tend to be saturated in acid lake waters, and usually lake chemistry is mainly controlled by acidification by volcanic gas counterbalanced by neutralization by water-rock interaction with overprints of dilution and evaporation.

Degree of neutralization (DON) and its inverse, percent residual acidity (PRA), are semi-empirical parameters that describe the effectiveness of neutralization relative to acidification (*Varekamp et al., 2000*). DON is the amount of H^+ consumed during water-rock interaction and PRA is the amount of residual H^+ left behind after water-rock interaction. DON and PRA, which are independent of dilution or evaporation, are used in this study to evaluate the relative roles of water-rock interaction and water-gas interaction.

PRA is calculated from a graph of the total sum of anions versus pH (Figure 4.4) as follows: From *Varekamp et al. (2000)*, PRA is defined as:

$$\frac{100\%\{(\text{pure acid } H^+ \text{ level}) - (\text{amount of } H^+ \text{ consumed})\}}{(\text{pure acid } H^+ \text{ level})}$$

The 'pure acid H^+ level' is the value on the pure acid boundary expressed as H^+ ($H^+=10^{-pH}$), where the pure acid boundary is an empirically derived line of maximum acidity that represents acidity of a volcanic fluid that has not undergone water-rock interaction. The pure acid boundary was determined using a global dataset of crater lake chemistry which included all available data from crater lakes in Central America, New Zealand, Indonesia, and Japan. The 'amount of H^+ consumed' is the vertical distance between the pure acid boundary and a data point on the graph.

To recreate the pure acid boundary in this study, the slope and intercept of pure acid boundary was estimated from Figure 6 in *Varekamp et al. (2000)* as

pure acid pH level =-0.4342944819* LN(ΣAnions(Cl+SO_4)) +3

Pure acid pH level was then converted to pure acid H^+ level. This term is used to calculate the amount of H^+ consumed:

amount of H^+ consumed = (pure acid H^+ level) – (H^+)

It should be noted that a shortcoming of the DON and PRA parameters is the use of calculated H^+ concentrations from the anion analyses versus H^+ activities from the pH measurement (*Varekamp et al., 2000)*.This only has a significant impact at pH values below pH = 0.5. Fortunately, all samples in this study have pH ≥ 0.5.

PRA calculations versus for sum of anions for Santa Ana data are presented in Figure 4.5. *Varekamp et al. (2000)* define two regions on this graph, a rock-dominated region and a gas-dominated region. In the rock-dominated region, the rate of neutralization exceeds the rate of acidification and PRA is less than 50%. Conversely, in the gas-dominated region, the rate of acidification exceeds the rate of acidification and PRA is greater than 50%. According to *Varekamp et al. (2000),* "lake waters will plot high on the right side of the diagram when the magnitude of the volcanic gas input is large (and evaporation has an impact as well) and low on the right side when the rate of neutralization is small and dilution occurs. Hydrothermal systems with already strongly altered rocks and a lack of easily leached cations may display such low rates of neutralization. Data on the left side of the diagram come from lakes with either small volcanic gas inputs and/or a very reactive rock matrix (e.g. hot, freshly erupted magma)."

Most Santa Ana lake water samples are 50 – 90 % neutralized (between 50% and 10% H+ left; Figure 4.4) with PRA < 50% (Figure 4.5). All samples fall in the rock-dominated region of Figure 4.5, indicating the rate of neutralization exceeds the rate of

acidification. Low PRA (<50%) for all lake water samples imply that varying degrees of water-rock interaction and water-rock ratios dominate the Santa Ana magmatic-hydrothermal system, especially pre-2005.

The 2000-2003 rainy season samples consistently lie below ~ 250 μmoles/gr SO_4 + Cl and dry season samples consistently lie above ~ 300 μmoles/gr SO_4 + Cl. 2004 data are well constrained within 250-300 μmoles/gr SO_4 + Cl, indicating a constant rate of volcanic input. Neither dilution nor evaporation is apparent in 2004, as previously shown in anion temporal trends (Figure 3.6). High degrees of neutralization (i.e. lower % H+ left) were observed in 2004 in contrast to previous years (Figure 4.4). PRA in 2004 never exceeded 20% (Figure 4.5), dropping to a record low of 2% in mid April 2004 and increasing somewhat linearly to 18% in mid Dec 2004.

After 2005, PRA remained < 50%, indicating that the rate of neutralization continued to exceed the rate of acidification. However, 2006 and 2007 samples exhibited a new trend. Anions increased to ~700 μmoles/gr SO4 + Cl as PRA concurrently increased to 45% residual acidity, suggesting an increasing rate of volcanic input that was progressively less effectively neutralized.

Temporal evolution of PRA during the study period presented in Figure 4.6 shows that PRA follows temperature trends fairly closely. However, PRA remains high after each of the three phreatic eruptions,: in June 2005, July 2006, and June-July 2007. The high PRA recorded on July 2006 occurs on a longer timescale than the other two minor phreatic eruptions due to data gap limitations. In fact, PRA and temperature show reverse trends in late 2007, and PRA continues to increase even though the lake cools from 65ºC to 40ºC. Phreatic eruptions temporarily increase permeability in the vent region,

enhancing acid fluid flow to the lake which raises the lake temperature. However, already depleted country rock in the lake basin and sublimnic vent region have low buffering capacity to neutralize the newly arriving fluids. This results in excess acidity (relatively high PRA values) immediately following eruptions.

4.5 Saturation state of lake waters

Saturation state modeling was carried out for six samples with complete cation analyses January 2007 to July 2007 to predict mineral assemblages in the crater lake and sublimnic environment. Modeling was performed with an aqueous ion-association speciation program, PHREEQC version 2 (*Parkhurst and Appelo, 1999*), using the WATEQ4F thermodynamic database (*Ball and Nordstrom, 1991*). The model is available from the USGS Water Resources Group website at http://wwwbrr.cr.usgs.gov/projects/GWC_coupled/phreeqc/.

The model requires inputs of concentrations of aqueous species, pe or a redox couple to calculate distribution of redox elements among their valence states, and temperature. Aluminum is a significant constituent of the Santa Ana crater lake (300-1300 kg/L), and the lack of aluminum analyses for 2002-2005 samples precluded saturation state modeling for this part of the time series. Based on the inputs, the model calculates equilibrium pH, mineral saturation indices, and distribution of aqueous species for the specified temperature by simultaneously solving nonlinear thermodynamic activities and mass-action equations with a modified Newton-Raphson method (*Parkhurst and Appelo, 1999*). Activity coefficients of aqueous species are defined with the Davies equation or an extended Debye-Hückel equation, which are valid for ionic

strengths < 2.0 molal (*Parkhurst and Appelo, 1999*). All water samples from 2007 have ionic strengths of < 1.5 molal.

Using the lake water compositions given in Table 3, saturation indices (SI) were calculated over a range of temperatures (25ºC to 250ºC) to simulate conditions in and below the lake (Figure 4.7). Positive SI indicates supersaturation and precipitation, and negative SI indicates undersaturation. Modeling shows that for all samples at observed surface temperatures (32-65ºC) pyrite, silica phases (amorphous silica, cristobalite, and chalcedony), barite, gypsum, and native sulfur are supersaturated or close to saturation. Gypsum crystals were identified in the filtered suspension for all six samples.

The six samples give disparate results for saturation at depth, and may be split into three groups representing progressive acidification with time. The first group, 15 January 2007 (VSA1) and 8 March 2007 (VSA2), strongly resemble typical saturation of lake waters (ANA21) during 2000-2002 (*Bernard et al., 2004*). VSA2 was sampled one week prior to a minor phreatic eruption on 15 March 2007. Modeling shows that the first group is supersaturated with alunite, jarosite, gibbsite, and diaspore over the temperature range of 100-200ºC. This assemblage compares well with minerals identified in lake bottom ejecta from the October 2005 eruption: cristobalite, gypsum, alunite, natroalunite, native sulfur, and iron sulfides. Cristobalite and anhydrite were found in ash samples <4 phi from the same eruption.

The second group, 28 March 2007 (VSA3) and 4 May 2007 (VSA4), strongly resemble waters from late 2000 (SAN1) which have been proposed to reflect dilution by acid fluids (*Bernard et al., 2004*). VSA3 was sampled on 28 March 2007, two weeks following the phreatic eruption. The second group is supersaturated with alunite and

diaspore, but at higher temperatures than the first group. Alunite equilibrium temperatures are pushed back from ~100ºC to 125-150ºC and diaspore equilibrium temperatures are pushed back from 140ºC to 165-190ºC.

The third group, 16 June 2007 (VSA5) and 9 July 2007 (VSA6), do not share similarities with any previous chemical analyses. The third group is not in equilibrium with any previously supersaturated phases, and only anhydrite is saturated at 135-165ºC. This degree of acidification was not observed during 2000-2002.

Modeling indicates that native sulfur is very close to saturation at observed lake temperatures for the first (VSA1, VSA2) and second (VSA3, VSA4) groups. Sulfur saturation could be achieved by doubling or tripling the analytically determined H_2S concentration. For the third group (VSA5, VSA6), however, H_2S concentration would have to be increased 30 to 80 times to achieve sulfur saturation.

Figure 4.8 shows mineral saturation temperatures, for quiet lake periods (low level activity), active lake periods (pre-eruptive hydrothermal activity), and very active lake periods (post-eruptive hydrothermal activity). Mineral saturation temperatures are defined as where the saturation index for each mineral is equal to zero (see Figure 4.7). For many minerals saturated at depth during quiet lake periods, namely gibbsite, kaolinite, diaspore, alunite and anhydrite, saturation temperatures increase to higher temperatures, sometimes greater than 250ºC during active and very active lake periods (Figure 4.8a). Silica phases (cristobalite and amorphous silica) and pyrite, on the other hand, saturate at lower temperatures during very active lake periods (Figure 4.8b). These model data suggest that the composition of volcanic fluids entering the lake change during periods of

enhanced hydrothermal activity, and that their composition changed even more after the 15 March 2007 phreatic event.

4.6 Energy budget modeling of the lake

Energy and mass budget modeling is used to evaluate the volcanic input into the crater lake during the study period. The modeling will contribute to determining the influence of the 2005 eruptions on the volcanic flux rate. Many energy budget models have been applied to crater lakes in the last 20 years (*Taran & Rouwet, 2008*; *Pasternack & Varekamp, 1997*; *Oppenheimer, 1996*; *Ohba et al., 1991;, Brantly et al., 1993; Rowe et al., 1992; Hurst et al., 1991*). The hydrologic steady state box model of *Pasternack & Varekamp (1997)* was selected to use at Santa Ana crater lake. An advantage of this model over other models is it has been previously applied to 14 crater lakes worldwide (*Pasternack & Varekamp, 1997*), facilitating comparison between Santa Ana and other lakes. An additional significant advantage of this model is that it accounts for the long-wave radiative input from the atmosphere with an empirical relationship (*Linacre, 1992*). The model is written in Mathematica software, and I have tailored the code to suit Santa Ana crater lake. Annotated coding is provided in Appendix B. Annotations are in italics following the "%" sign.

The energy and mass balances for a steady-state volcanic lake are given by:

$$E_{VolcCond} + E_{Volc} + E_{SunRad} + E_{AtmRad} = E_{Evap} + E_{Meteoric} + E_{LakeRad} + E_{LakeCond} \quad \text{(Eq. 1)}$$

$$W_{Volc} + W_{Meteoric} = W_{Evap} + W_{Outflow} + W_{Seepage} \quad \text{(Eq. 2)}$$

Energy inputs are the conductive heat from shallow magma ($E_{VolcCond}$), enthalpy of volcanic gas/brine flux (E_{Volc}), short-wave solar flux (E_{SunRad}), and long-wave radiative

input from the atmosphere (E_{AtmRad}). Energy outputs are evaporation (E_{Evap}), heating of meteoric water ($E_{Meteoric}$), long-wave radiation ($E_{LakeRad}$), and conduction ($E_{LakeCond}$). Mass inputs are volcanic (W_{Volc}) and meteoric water fluxes ($W_{Meteoric}$), and mass outputs are fluxes owing to evaporation (W_{Evap}), outflow ($W_{Outflow}$) and seepage ($W_{Seepage}$). Evaporation is the most important process controlling lake temperature, especially at high temperatures, and thereby lake persistence.

The model simultaneously solves energy balance and state mass balance equations. The model determines the volcanic input in MW necessary to produce measured lake temperatures ranging from ~18ºC to 65.6ºC during the study period from 2000-2007. The volcanic flux can alternatively be expressed in tons of SO_2 per day.

Several assumptions are inherent to the model. The model assumes steady state conditions, meaning energy inputs equal energy outputs. Non-steady state conditions, e.g. extreme rainfall events or extreme evaporation events, cannot be replicated with this model. The model does not take into account the volume of the lake (only uses area) and assumes that the lake is thermally homogenous. Santa Ana crater lake is probably well mixed, as subaqueous hotsprings in the lake drive convection, but the lake may be locally hotter on the surface at hotsprings locations. Heat supplied by conduction from the shallow magma body is not considered in the model because it is negligible for magma body depths > 1 km (*Pasternack & Varekamp, 1997).* Santa Ana's crater lake has no observed outlets, and so the outflow term is ignored in the mass balance. Seepage is also excluded from the mass balance because it cannot be adequately constrained, and most likely represents a small energy flux (*Pasternack & Varekamp, 1997*).

The model is expressed in terms of lake temperature, basin geometry, meteorological and magmatic parameters. Systematic sensitivity tests were performed over the range of measured lake temperatures on the primary model input parameters—equivalent lake radius (m) (elsewhere called effective radius), windspeed (m/s), atmospheric temperature (ºC), precipitation (m/yr), gas temperature (ºC), and gas ratio (H_2O:CO_2:SO_2)—to determine appropriate input parameters values (Figure 4.9). Sensitivity tests show that the model is most sensitive to lake radius and windspeed, moderately sensitive to atmospheric temperature and precipitation, and relatively insensitive to magmatic gas temperature and magmatic gas ratio. Sensitivity increases at higher temperatures. The majority of energy input derives from the conversion of steam to liquid water (enthalpy of condensation), so magmatic gas temperature and magmatic gas ratio are not critical parameters (*Pasternack & Varekamp, 1997*). Based on sensitivity tests, a set of representative input parameters for the study period was chosen:

Input Parameter	**Representative Value**
Equivalent radius	100 m
Windspeed	2.5 m/s
Air temperature	16.12ºC
Precipitation	5.4 m/yr
Magmatic gas temperature	800ºC
Magmatic gas ratio (H_2O:CO_2:SO_2)	93:05:02

Table 4.1: Representative input parameters for energy budget modeling. See text for further discussion.

Equivalent radius, windspeed, magmatic gas temperature, and magmatic gas ratio are treated as constants in the model, whereas air temperature and precipitation are treated as variables based on meteorological data recorded daily at the Los Andes Meteorological Station. Average, maximum, and minimum values of air temperature (with elevation

correction) and precipitation found in Table 3.1 were tested in the model. Average values of climactic parameters were selected for comparison to real climactic data.

Magmatic gas temperatures and gas ratios produce negligible changes in lake temperature and are assumed to not vary over the study time period. Gas temperatures of 1000ºC, 900ºC and 800ºC produce temperature variations on the 1/10,000 of a degree scale. Molar gas ratios from Poas and Momotombo volcanoes produce temperature variations on a similarly small scale. No direct fumarole measurements are available for Santa Ana, so gas compositions of Poas and Momotombo, which have similar compositions (basalt to basaltic andesite) and in a similar tectonic setting (convergent plate), were compared to common arc values. A common volcanic arc magma temperature of 800ºC and an average molar gas ratio of 93% H_2O, 5% CO_2, and 2% SO_2 (*Symonds et al., 1994*) were selected following *Pasternack & Varekamp (1997*).

Lake radius and windspeed produce the most variable changes in lake temperatures and are the least constrained input parameters (Figure 4.9). Variability of lake radius and windspeed at 30ºC and 60ºC are presented in Figure 4.10. Colored lines represent isopleths—lines of equal volcanic input—required to produce a lake of 30ºC (Figure 4.10a and Figure 4.10b) or 60ºC (Figure 4.10c and Figure 4.10d). The magnitude of volcanic input increases with increasing lake size and windspeed, but changing lake area at lower temperatures, e.g. 30ºC, has more of an impact than at higher temperatures, e.g. 60ºC. Likely limits of equivalent radii and windspeeds are denoted by the boxes in Figure 4.10. An equivalent radius of 100 m was chosen as a representative value based on: 1) lake radii determined from orthorectified ASTER satellite images (Table 3.3); 2) the bathymetric survey of *Bernard et al. (2004)*; and 3) oblique digital photographs of the

lake. During the rainy season, the lake may have grown to ~110% its normal area, but during post-2005 evaporation episodes the lake shrank considerably. A reduction in size to 30% of normal area during evaporation periods was estimated from digital photographs. Using an equivalent lake radius of 100 m therefore represents a minimum value of volcanic input. Windspeed was arbitrarily set to 2.5 m/s. The lake lies in the bottom of a 100 m deep steep walled crater, and windspeeds will likely be close to zero though the variability of windspeeds at the crater floor is not constrained.

Based on the modeling, the upper limit of lake level occurs at 56ºC = 735 SO_2 t/d or 385 MW. For representative input parameters, the lake begins losing mass at temperatures and volcanic inputs higher than this upper limit.

Energy and mass balance modeling was carried out for representative Santa Ana lake data during 2002-2005 and 2007 (Figure 4.11a and Figure 4.11b). Daily measurements of atmospheric temperature and precipitation were used for these input parameters and representative values were used for all other input parameters. The results using daily meteorological data (solid and hollow symbols) are compared to results obtained using average values for all parameters (solid line). Varying meteorological input parameters does not have a significant effect on results, except perhaps at low lake temperatures. Modeling shows that during 2002-2005 energy inputs of 0.3-15 MW, or an equivalent SO_2 flux of 0.5-28 t/d, were required to produce observed lake temperatures. During this period, energy input reached a maximum of 15 MW (SO_2 flux of 28 t/d) November 2004 when the lake temperature anomaly was largest. Required volcanic input post-2005 was much higher in 2007, at 8-830 MW, or an equivalent SO_2 flux of 16-1600 t/d. A large peak of 620 MW (SO_2 flux of 1195 t/d) was observed on 14 March 2007 one

day prior to the phreatic eruption on 15 March 2007, and volcanic input reached its maximum of 830 MW (1600 t/d SO_2) in June 2007.

Volcanic input phrased in tons of SO_2 per day is compared to volcanic degassing measured by UV spectrometry (Figure 4.12 and Figure 4.13). During 2002-2005, it is likely that most sulfur dioxide was scrubbed into the hydrothermal system and little sulfur dioxide escaped through the lake to the atmosphere, whereas sulfur dioxide emitted from the fumarole field was largely unaffected on its ascent to the surface. Therefore, it is reasonable that during 2002-2005, COSPEC or DOAS measurements that predominantly reflect subaerial degassing. During this time, volcanic input to the lake was relatively low (0.5-28 t/d SO_2) (Figure 4.12). In fact, the volcanic input to the lake was less than volcanic degassing measured by COSPEC/DOAS during all periods of observed activity (low level, hydrothermal, and fumarolic). Even when volcanic degassing reached a maximum of > 4000 t/d SO_2 in late August 2005, lake inputs never rose above 28 t/d SO_2, confirming that the majority of degassing prior to the eruption occurred along dry pathways via the fumaroles.

Following the 2005 events, however, volcanic input to the lake increased substantially to 16-1600 t/d SO_2 in 2007 (Figure 4.13). During this time, observations of sulfur spherules provide evidence of vapor phase volcanic gas being injected directly into the lake via the central subaqueous fumarole. It is likely that some sulfur dioxide would be scrubbed into the hydrothermal system on its ascent through the drowned fumarole, but sulfur spherules indicated that nevertheless some gas phase volatiles reached the lake. Intense degassing and a strong sulfur smell in the crater suggest that some rapidly traveling gas may reach the lake surface without being scrubbed due to a kinetic effect.

The gas reaching the surface is likely composed of hydrogen sulfide (low solubility) but may also contain sulfur dioxide. DOAS measurements during this time likely reflect degassing from subaerial fumaroles and from the lake, seeing as the weak, low temperature (<100ºC) subaerial fumaroles were much diminished from their previous intensity.

Most volcanic input values to the lake in 2007 were higher than pre-2005 values, and many were in the range of 200-400 t/d SO_2, but several were extremely high in March, June and July 2007 at 800-1600 t/d SO_2. Degassing measured by DOAS during March to September 2007 yield fluxes < 600 t/d SO_2, which is significantly less than volcanic inputs to the lake. This suggests that volcanic inputs to the lake were greater than volcanic degassing, which represents a significant change post-2005.

4.7 Crater Lake Evolution

A summary of crater lake evolution based on data results and data analysis is provided below and in Table 3.5. As shown in Chapter 3, Santa Ana crater lake chemistry was similar from 2002 until the 2005 events, with most of the characteristics described by *Bernard et al. (2004)*. During this period, varying degrees of water-rock interaction (Figure 4.1a) dominated the hydrothermal system. During periods of low level activity (January 2000, February 2002-June 2004), congruent rock dissolution (ETR=1) (Figure 4.3) was the dominant mode of rock dissolution, with an average of 12-18 gr of rock dissolved per kg of water (Figures 4.2). Dilution by meteoric rainwater during the rainy season was quite evident during low level activity, especially in anion concentrations during 2002 and 2003, perhaps because the rate of volcanic input was constant (~250

μmoles/gr SO_4 + Cl) and relative low (Figure 4.5). Energy budget modeling determined that magnitude of the volcanic input into the lake was 0.3-15 MW, or an equivalent SO_2 flux of 0.5-28 t/d (Figure 4.11). The magmatic flux reaching the lake was small compared to the amount of SO_2 degassed subaerially through the adjacent fumaroles (30-80 t/d SO_2 during low level activity, <600 t/d SO_2 during hydrothermal activity, <4000 t/d SO_2 during fumarolic activity), indicating that the majority of degassing prior to the eruption occurred along dry pathways via the fumaroles (Figure 4.12).

During 2006 and 2007, the lake chemistry began to change (max. temp=65ºC, max. Cl=22,000 ppm, SO_4/Cl <1). The magmatic flux reaching the lake was large (16-1600 t/d SO_2) compared to volcanic degassing (<600 t/d SO_2) (Figure 4.13), and the lake nearly completely evaporated on several occasions. Physical changes in the lake were evident and are likely attributable to changing sources of volcanic input from depth to the lake, subsequent water-gas and water-rock interactions occurring in the lake and near vent environment, and the fate of volcanic SO_2 in the hydrothermal system.

The lake struggled to acidify but was effectively neutralized by water-rock interaction in the hydrothermal system (PRA < 50%) (Figure 4.5), suggesting that the lake was acidified mostly by brines entering the lake from hot springs and partially by gas directly injected into the lake at subaqueous vents. Incongruent rock dissolution (ETR<1) (Figure 4.3) was the dominant mode of rock dissolution, with a maximum of 90 gr of rock dissolved per kg of water (Figure 4.2), and mineral precipitation probably played a minor role. Indeed, the lake was only saturated or close to saturation in silica phases, pyrite, elemental sulfur, barite, anhydrite, and gypsum at lake and subliminic temperatures (<250ºC) (Figure 4.7). Post-2005 geochemical changes were likely caused

by both an increase in the rate of the volcanic input to the lake (Figure 4.1a, Figure 4.11), and a change in composition of the volcanic input to the lake (Figure 4.1b, Figure 4.5, Figure 4.7, Figure 4.8), including direct inject of volatiles to the lake at underwater vents (sulfur spherules), and by sulfate disproportionation in the lake (elemental sulfur bottom layer, modeled sulfur saturation).

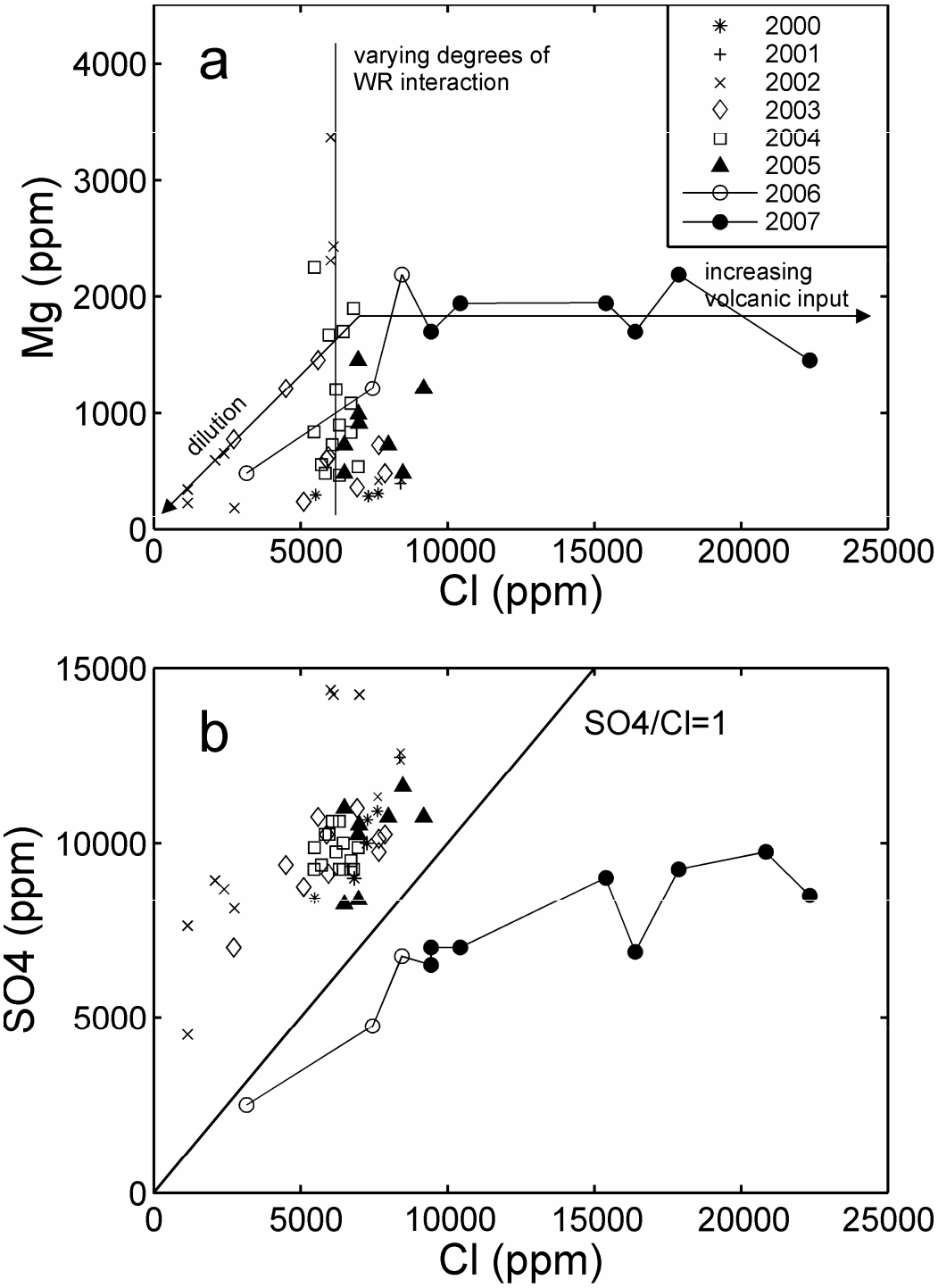

Figure 4.1: Water-rock interaction and water-gas interaction. a: Varying degrees of water rock interaction before the October 2005 eruption (Mg varying, Cl constant) replaced by increasing volcanic input after the eruption (Mg constant, Cl increasing); b: Changing SO_4 versus Cl concentrations in the volcanic input after the October 2005 eruption. Units in ppm.

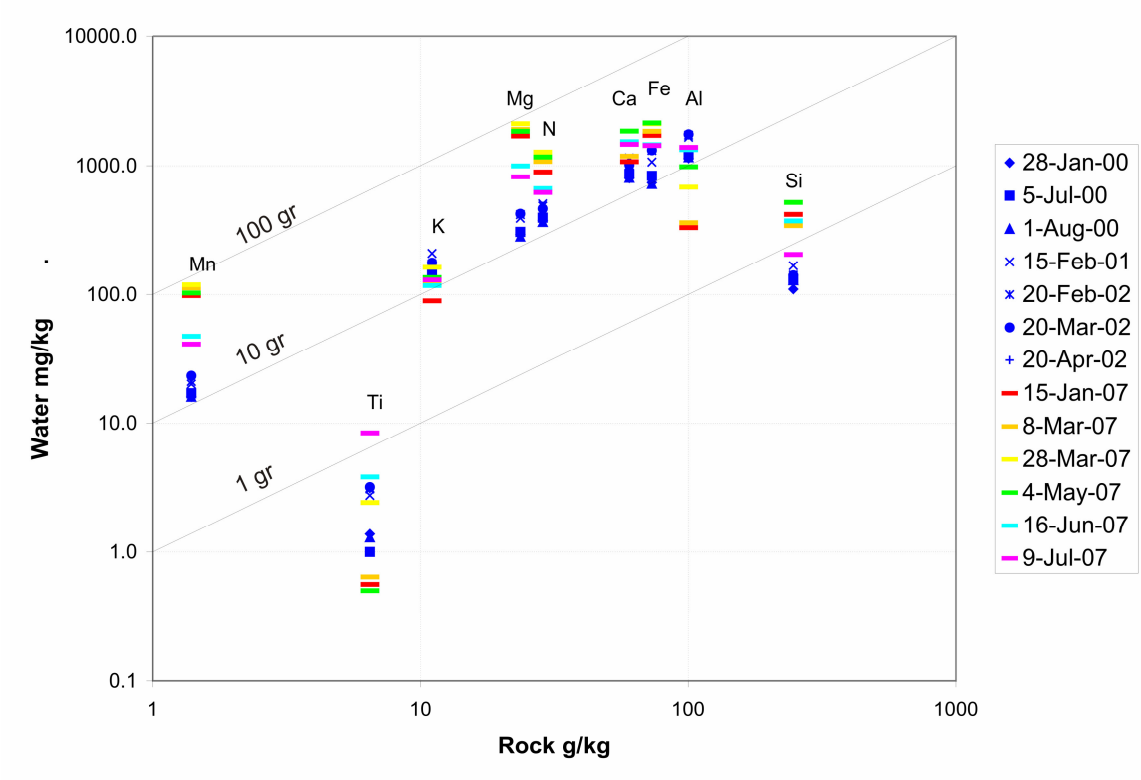

Figure 4.2: Concentrations of RFE relative to average Santa Ana andesite. One, 10, and 100 gr isopleths indicate amount of rock dissolution. 2007 samples from this study are shown in rainbow colors. Representative samples for 2000-2002 from *Bernard et al. (2004)* are shown in blue for comparison.

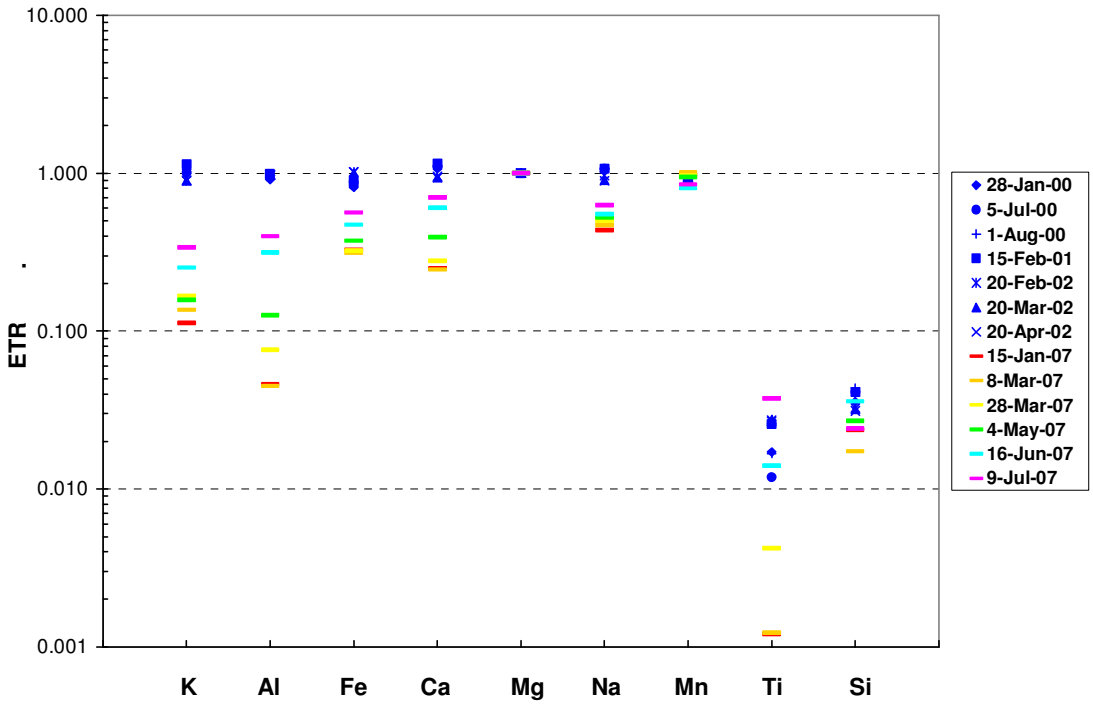

Figure 4.3: Element transfer ratios (ETR): Mg normalized concentrations of rock forming elements (RFE) relative to Mg normalized average Santa Ana andesite. Depletions of RFE relative to average andesite are caused by incongruent dissolution or precipitation of mineral phases. Average andesite composition is an average value of 9 olivine basalts and basaltic andesites recalculated from *Pullinger (1988)* by *Bernard et al. (2004)*.

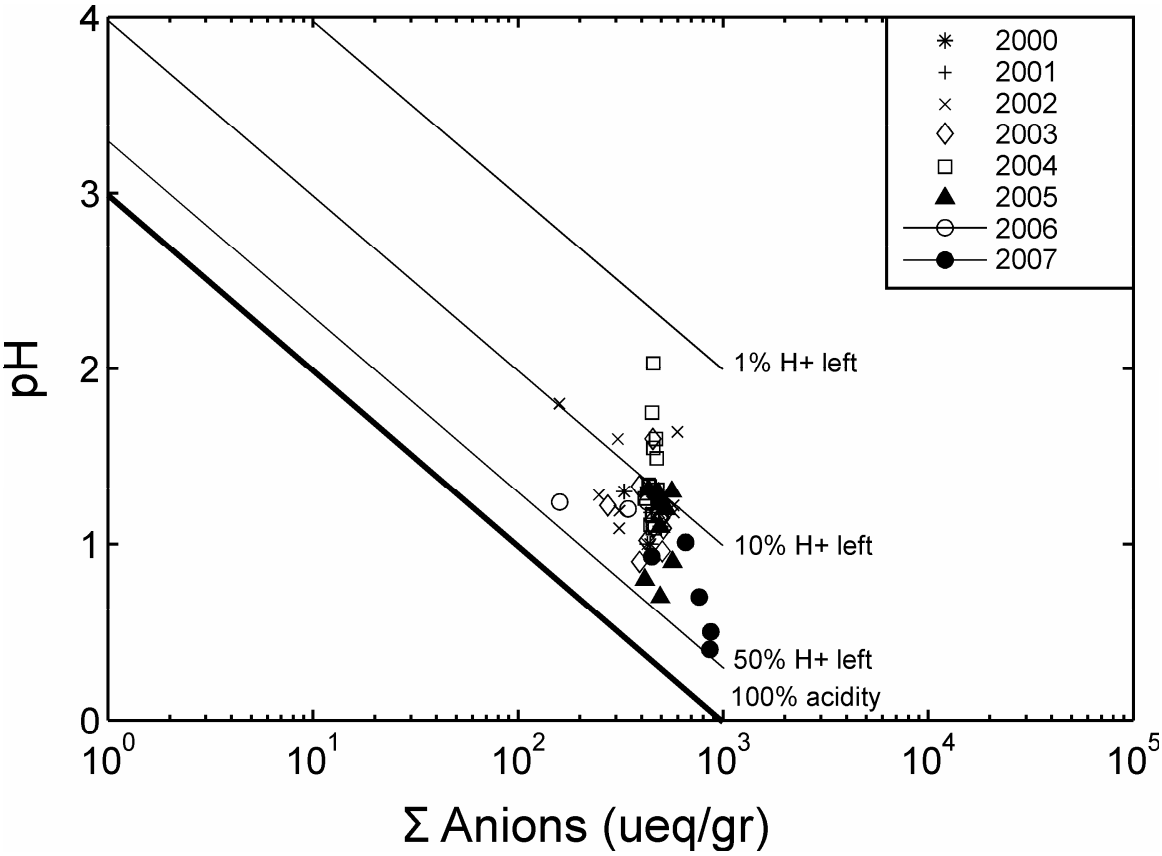

Figure 4.4: Degree of neutralization (DON). Thick solid line indicates 100% pure acid with no neutralization and thin solid lines indicate amount of H+ left (PRA) after neutralization. The line indicating 50% H + left in this diagram is the same as the line indicating 50% PRA in Figure 4.5. Values between the 100% H+ left line and the 50% H+ left line indicate gas-dominated systems, and values less than 50% H + left indicate rock-dominated systems. After *Varekamp et al., 2000*.

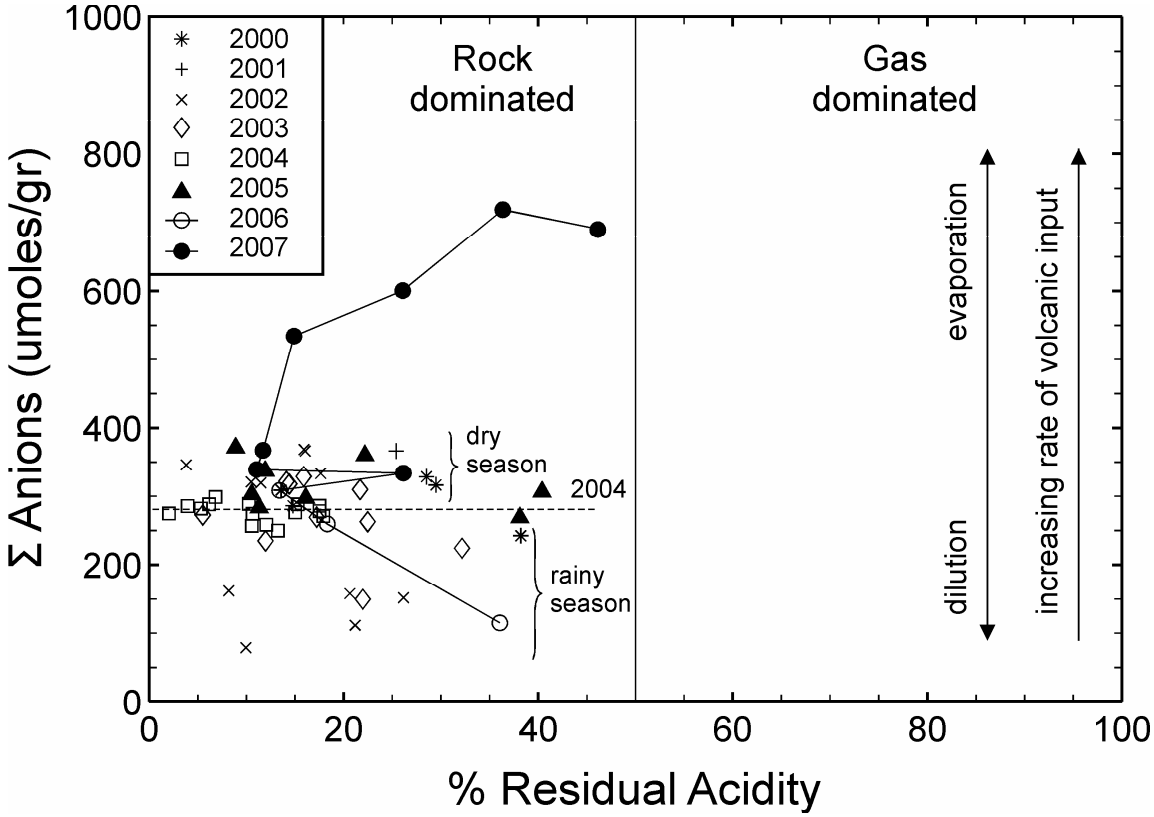

Figure 4.5: Rock- and gas-dominated lake systems distinguished by percent residual acidity (PRA). Vertical axis represents increasing rate of volcanic input and horizontal axis represents decreasing host rock reactivity. PRA is insensitive to dilution or evaporation, whereas dilution and evaporation are also represented on the vertical axis. The dotted lined at ~250 μmoles/gram divides rainy season samples from dry season samples. Symbols given in Figure 4.4. After *Varekamp et al., 2000.*

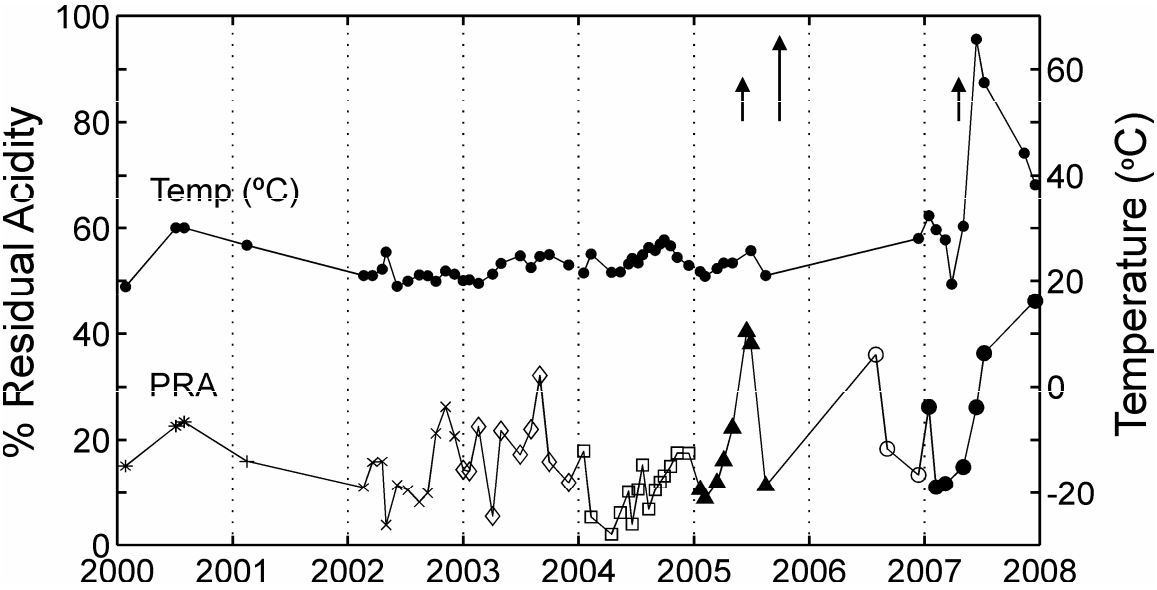

Figure 4.6: Coupling and decoupling of percent residual acidity (PRA) and temperature through time. PRA is given by the left hand vertical axis and temperature is given by the right hand vertical axis. Symbols given in Figure 4.4. Arrows denote phreatic eruptions.

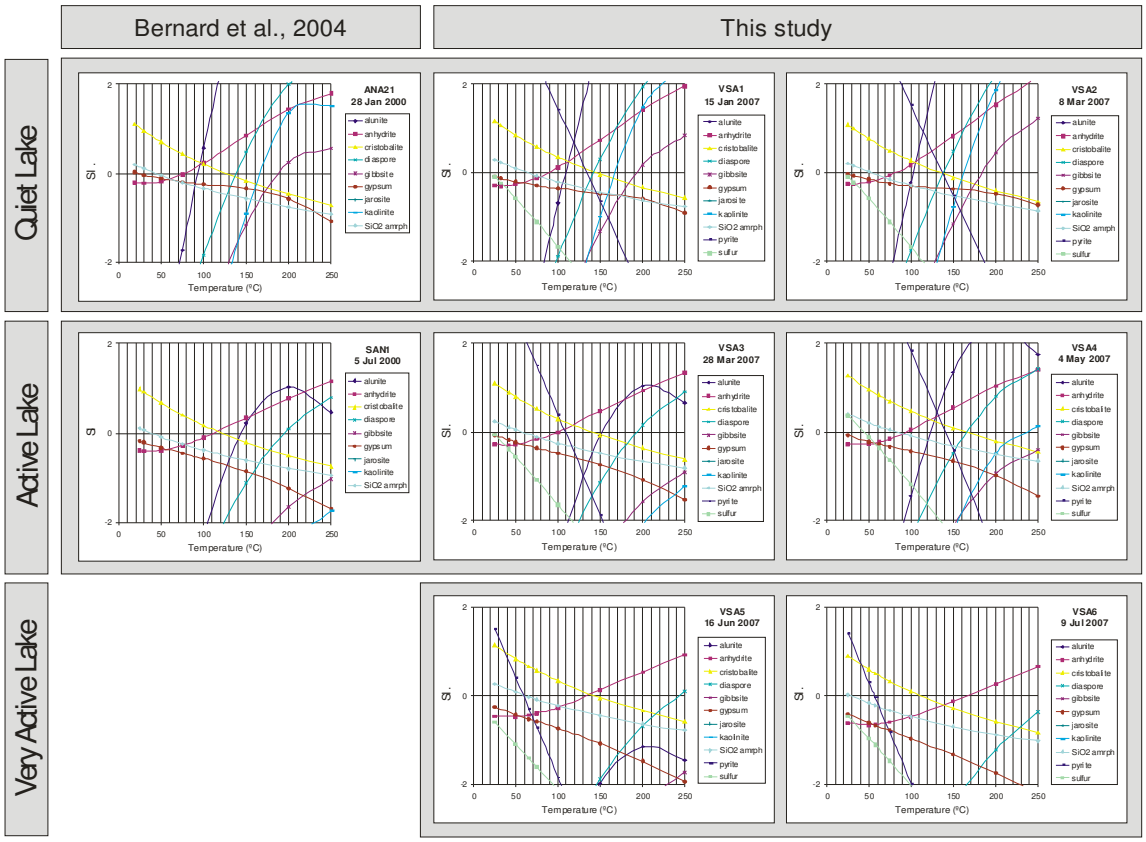

Figure 4.7: Saturation indices of 2007 lake waters. Saturation indices (SI) are given by log Q/K, where Q is the ion activity coefficient and K is the solubility constant. Positive SI values indicate supersaturation and negative SI values indicate undersaturation or precipitation.

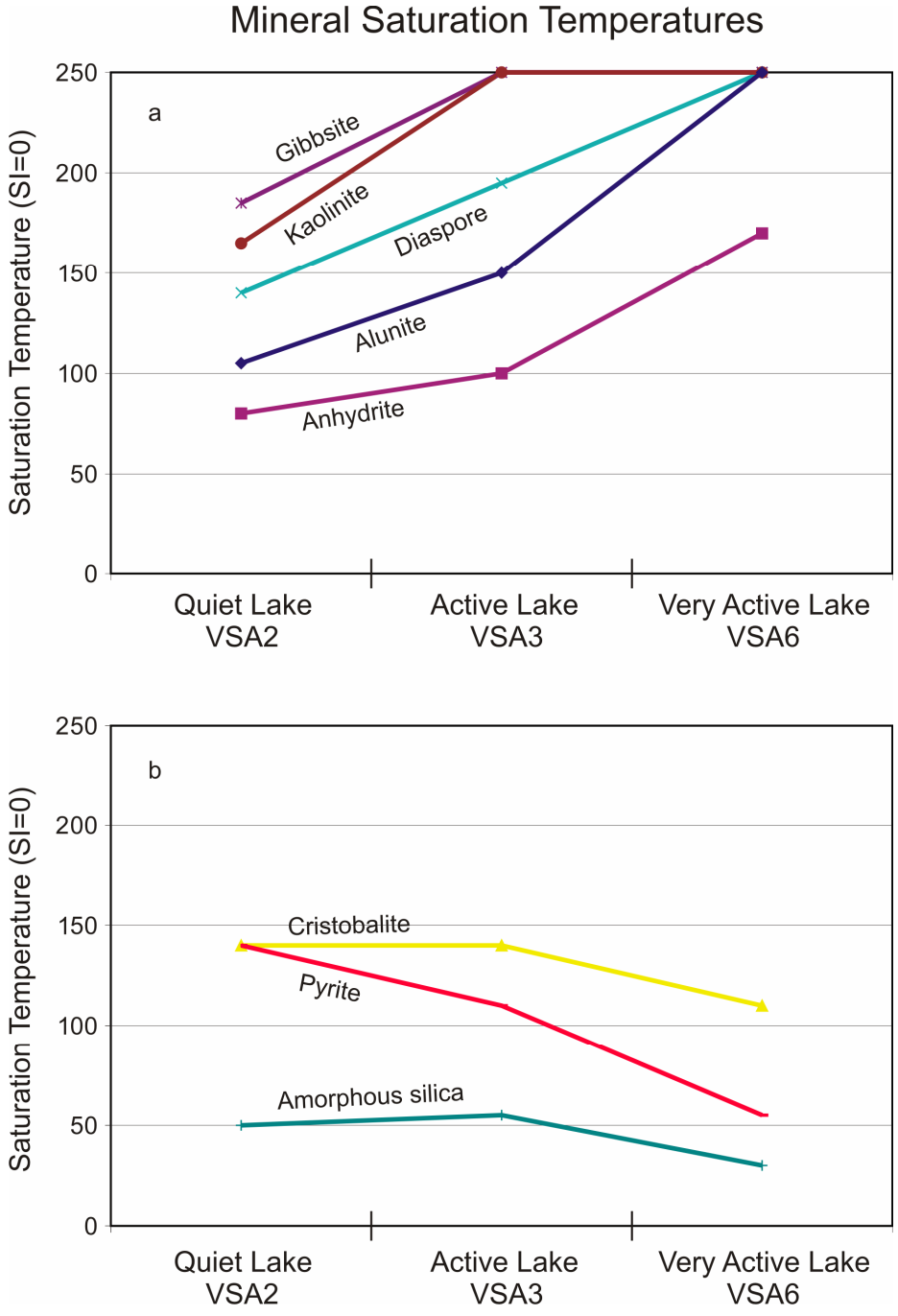

Figure 4.8: Representative saturation temperatures of minerals for quiet lake, active, and very active lake periods. Saturation temperatures are obtained from Figure 4.7 where mineral saturation lines cross SI=0. 4.8a: Minerals which saturate at higher temperatures with increasing activity levels. 4.8b: Minerals which saturate at lower temperatures with increasing activity levels. Sulfur, gypsum, and jarosite do not appear on the graph because these minerals are undersaturated or slightly undersaturated over 25-250ºC.

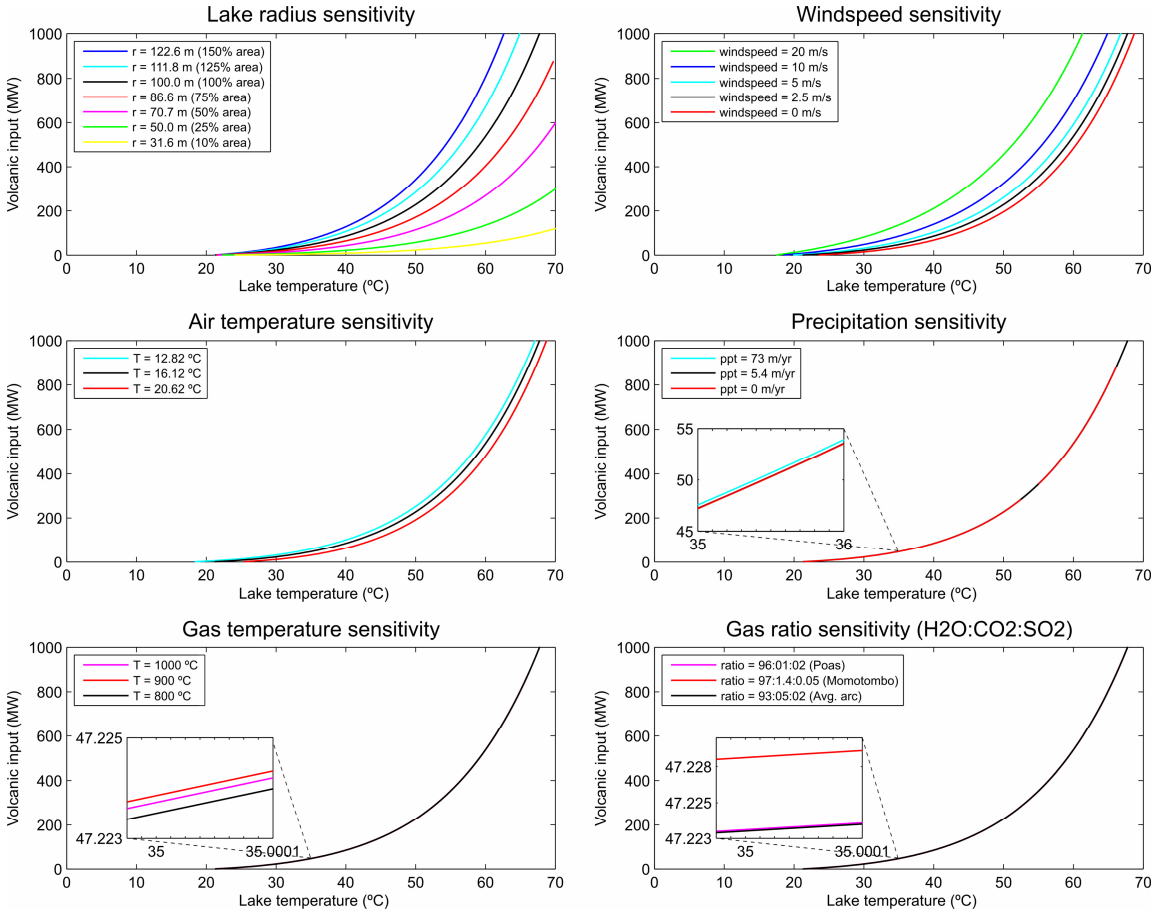

Figure 4.9: Energy budget modeling sensitivity tests for effective lake radius, windspeed, gas temperature, precipitation and atmospheric temperature.

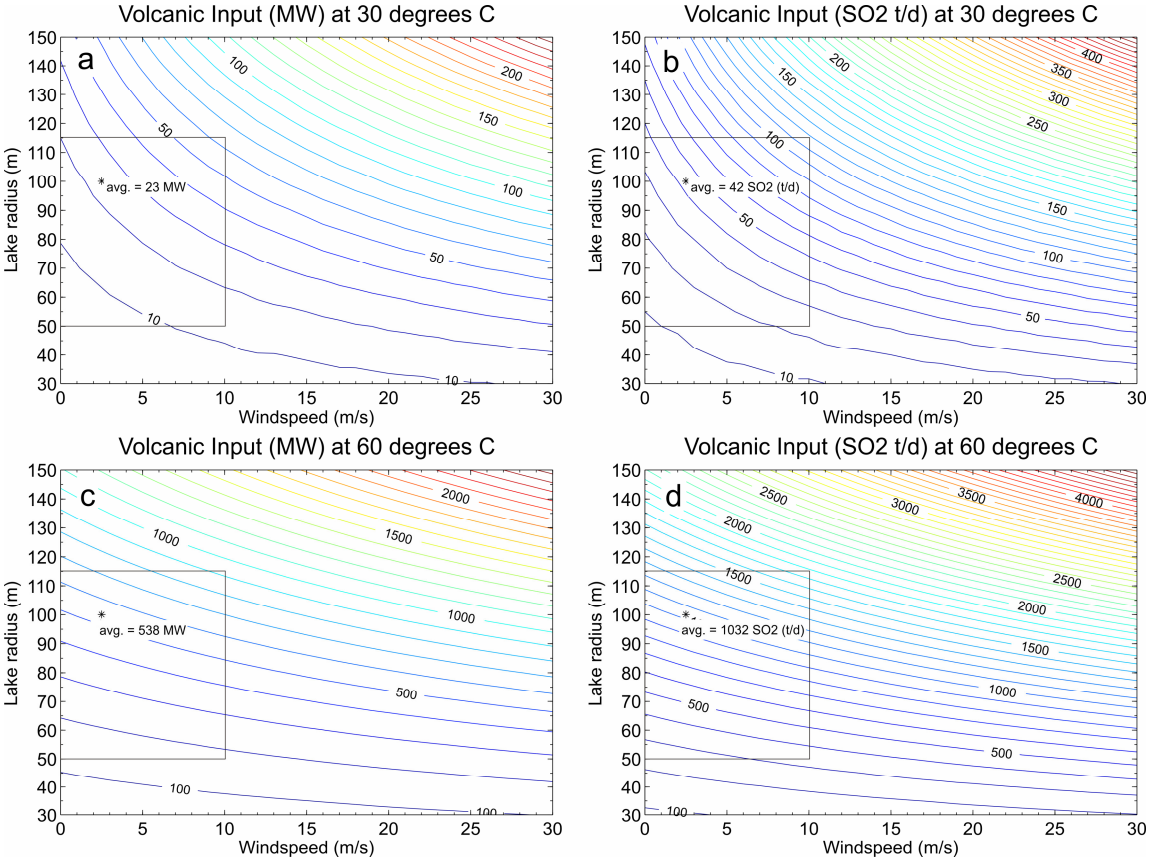

Figure 4.10: Variability in volcanic input as a function of lake radius and windspeed at 30ºC (4.10 a and 4.10 b) and 60ºC (4.10 c and 4.10 d). Colored lines represent lines of equal volcanic input. Boxes denote likely limits of lake radius and windspeeds.

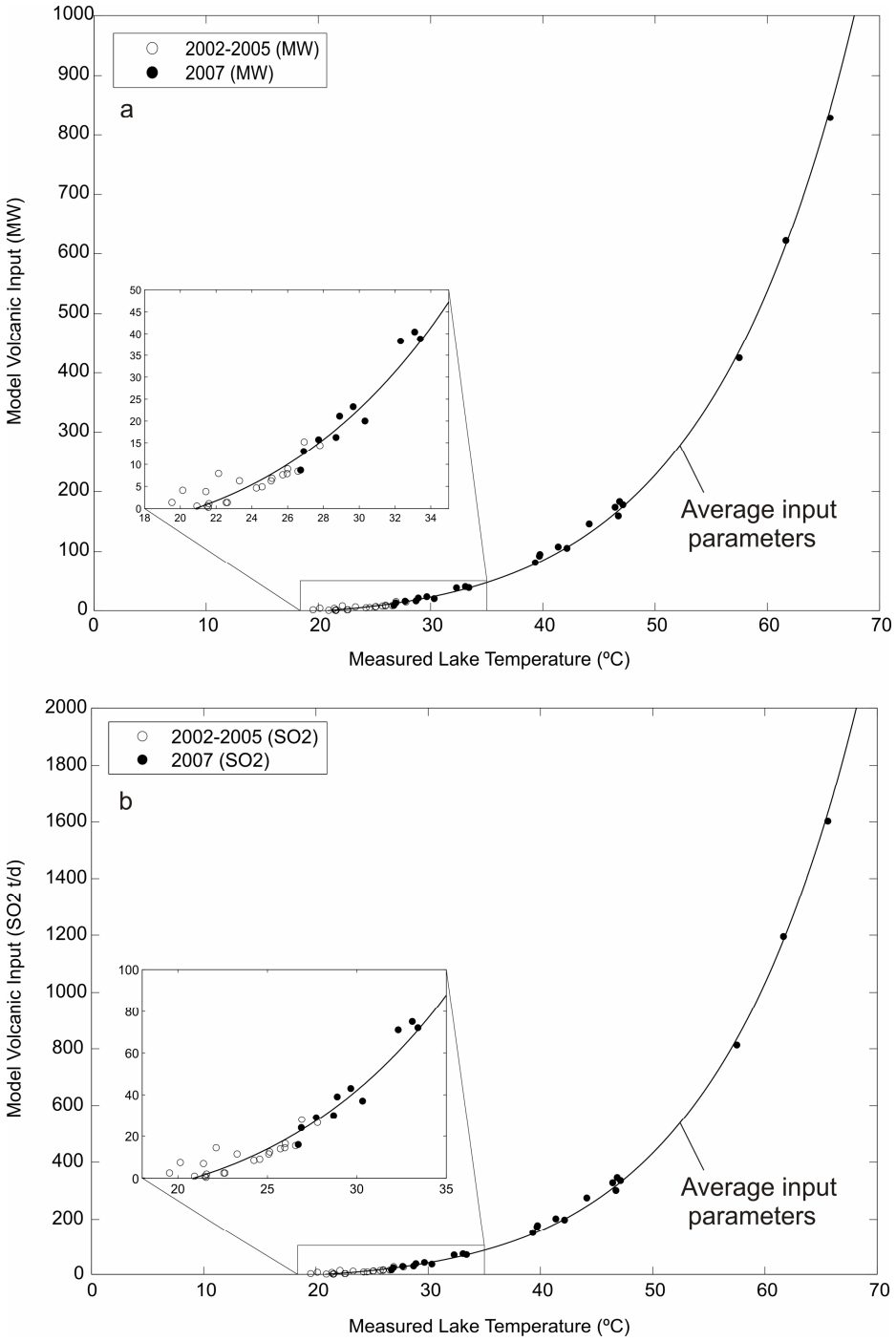

Figure 4.11: Energy budget modeling results. Volcanic input needed to achieve observed lake temperatures. 4.11a: Volcanic input is expressed in MW. 4.11b: volcanic input expressed in SO2 in tons per day. Solid line denotes volcanic inputs over observed lake temperatures obtained using average values for all input parameters, whereas circles use real data for air temperature and precipitation, and averages for all other input parameters. Hollow circles are for 2002-2005, and solid circles are for 2007.

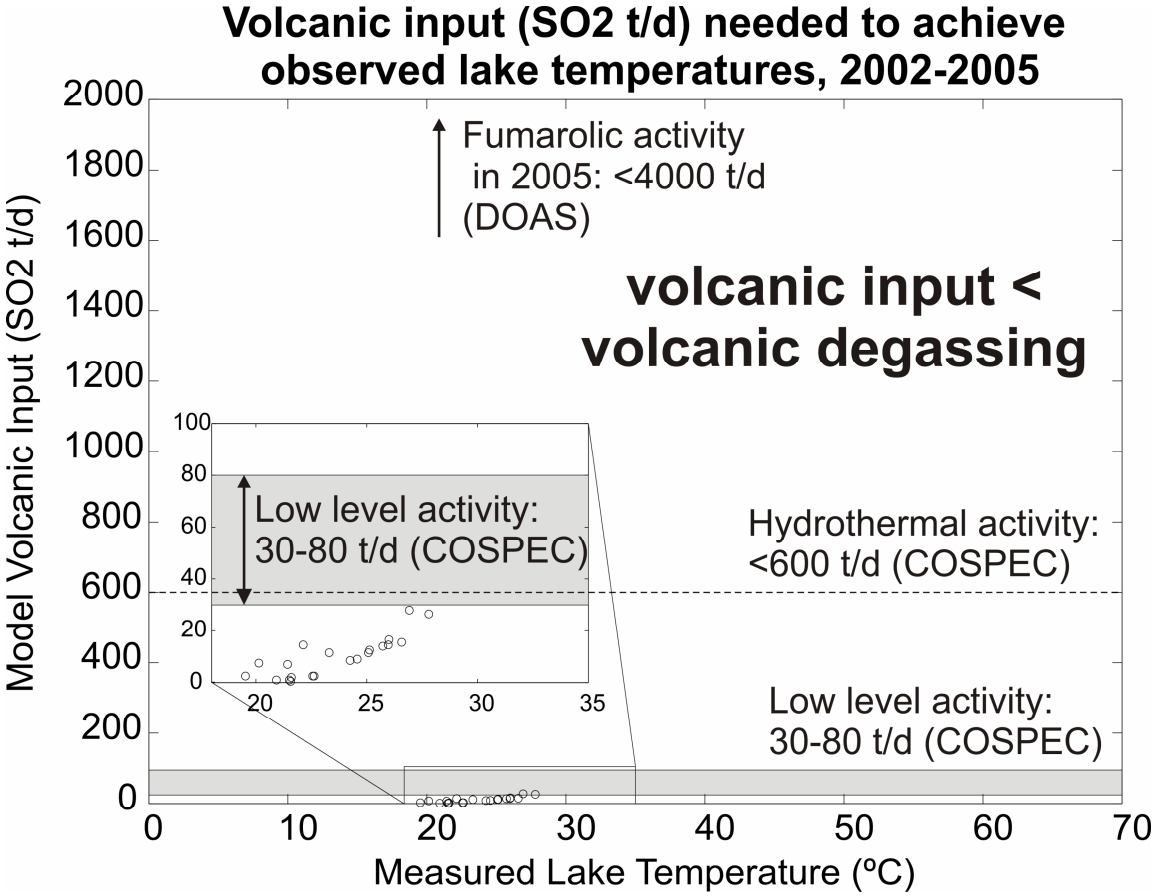

Figure 4.12: Comparison of volcanic inputs to the lake (energy budget model results) with volcanic degassing (measured by UV spectrometry) during 2002-2005.

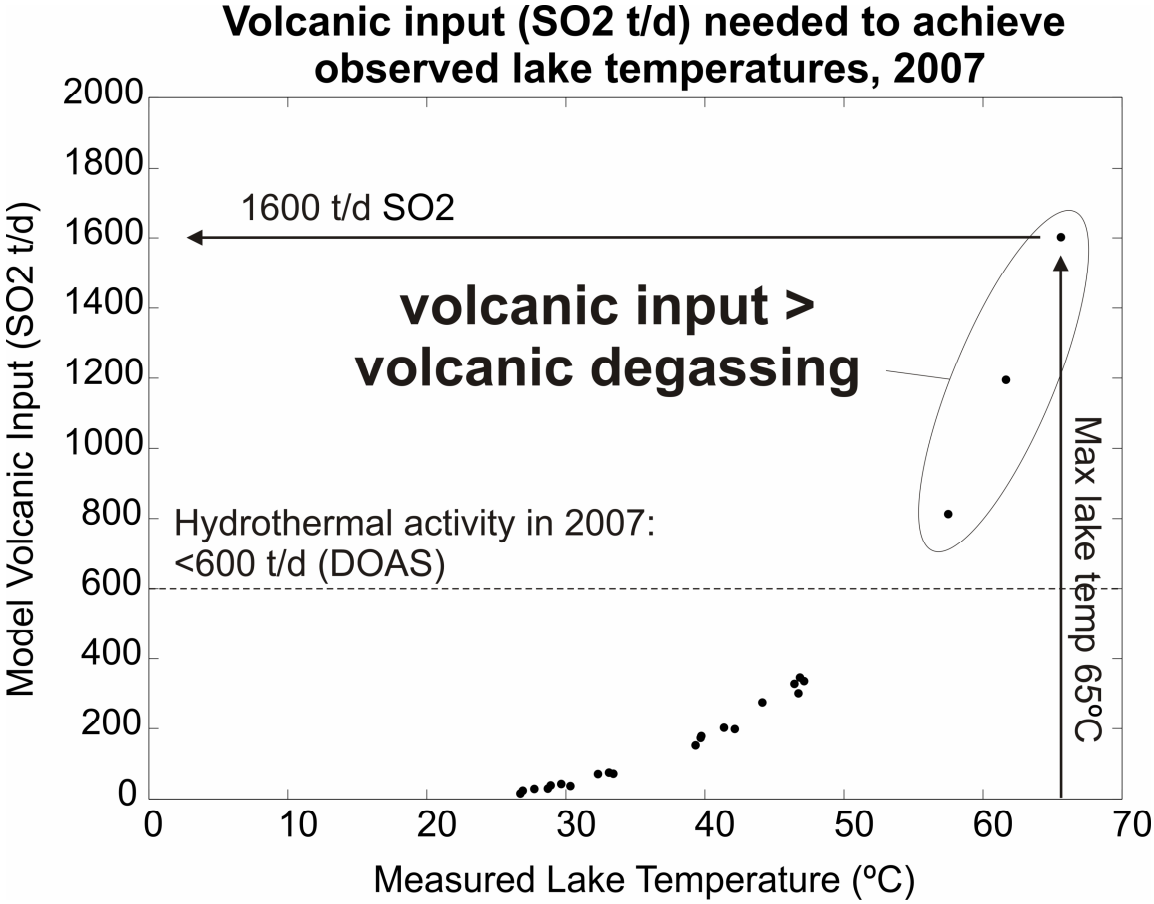

Figure 4.13: Comparison of volcanic inputs to the lake (energy budget model results) with volcanic degassing (measured by UV spectrometry) during 2007.

CHAPTER 5: Discussion

5.1 Introduction

In this section, I will synthesize the main findings of the data results (Chapter 3) and data analysis (Chapter 4) to achieve the following goals: 1) propose a physical model; 2) identify eruption precursors; 3) interpret possible eruption triggering mechanisms; 4) assess the impact of the 2005 eruption in order to identify potential eruption hazards; 5) recognize possible hazard scenarios.

The physical model will provide a framework within which to link observed events/dataset trends with plausible physical processes. This physical model will provide a context to identify eruption precursors, potential eruption triggering mechanisms, and changes to the magmatic and hydrothermal systems post-2005. Classifying the lake during pre-eruptive, and post-eruptive periods using the physiochemical classification scheme of *Pasternack & Varekamp (1997)* will facilitate identification of potential hazards for the prevailing magmatic-hydrothermal conditions.

5.2 Physical model of the Santa Ana magmatic – hydrothermal systems

The study is divided into six periods based on observed activity levels: 1) low level activity (January 2000); 2) hydrothermal activity (May 2000-February 2002); 3) low level activity (February 2002-June 2004); 4) hydrothermal activity (June 2004-August 2005); 5) fumarolic activity (August 2005-October 2005); and 6) hydrothermal activity (October 2005-December 2007). A schematic conceptual model has been developed for each stage of activity (low level activity, pre-2005 hydrothermal activity, fumarolic activity, post-2005 hydrothermal activity) to relate observations on the surface

to processes at depth (Figure 5.1). This model is based on other models of hydrothermal and geothermal systems, e.g. *Delmelle & Bernard, 2000*, *Pasternack & Varekamp (1997), Christenson & Wood (1993)*, *Christenson (2000), Giggenbach et al. (1990)*, *Ingebritson & Sorey (1988),* and contains similar features as these other models.

Low level activity and hydrothermal activity occurring during 2000-2002 were previously reported on by *Bernard et al. (2004)*, and serve as a basis for comparison for subsequent periods of similar low level and hydrothermal activity in 2002-2005. Unprecedented fumarolic activity occurred in late August and September 2005, leading up to the eruption on October 1st 2005. Long-range and short-range precursors were identified during these respective periods of hydrothermal and fumarolic activity periods. The final period encompasses all post-2005 behavior, lasting from the eruption until the end of 2007. Hydrothermal activity was observed in the lake during this time, but the eruption produced significant changes in the hydrothermal system and this activity was markedly different from previous periods of hydrothermal activity.

5.2.1 Low level activity: January 2000 and February 2002 to June 2004

Santa Ana crater lake existed in a state of low level activity during early 2000 and in February 2002-June 2004. In early 2000, the lake was observed to contain cool acid-sulfate-chloride waters (T=19ºC, LTA=1.5-4ºC (several degrees above ambient temperature), pH ~ 1, SO_4 = 11,000 mg/kg, Cl = 7000 mg/kg, SO_4/Cl ~ 1.5, and TDS = 23,000 [*Bernard et al., 2004]*), and from February 2002 to June 2004, the lake possessed similar characteristics (T=16ºC to 25ºC, LTA= 0.5 to 8ºC, SO_4=10,000 mg/kg, Cl=6000 mg/kg, SO_4/Cl~1.5, pH~1). During low level activity, volatiles ascending from a

degassing magma body at depth acidified the overlying groundwater in a two phase gas + liquid region, whose surface expression was an acid lake in the summit crater (Figure 5.1a). Likely sources of the volcanic fluid input to the lake are condensing magmatic gases which formed acidic fluids in-situ upon cooling and subsequently mix with groundwater, and/or gas scrubbed at depth in the hydrothermal system.

Volcanic brines in the two phase region migrated upwards, perhaps preferentially along pre-existing fractures, and enter the lake at hotsprings along the lakeshore. These hotsprings (T~80ºC [*Bernard et al., 2004*]) supply the lake with heat and acidity. Energy budget modeling for 2000-2005 determined that the supply rate of volcanic input to the lake was relatively low (0.3-15 MW, equivalent SO_2 flux of 0.5-28 t/d) (Figure 4.10). A low volcanic input is consistent with low calculated PRA < 50%, indicating that varying degrees of water-rock interaction dominated the Santa Ana hydrothermal system. The major element cations were derived from isochemical dissolution (ETR=1) (Figure 4.3) of andesite host rock at ~100ºC, with an average of 12-18 gr of rock dissolved per kg of water (Figure 4.2), indicating slow movement of volcanic fluids through the edifice (*Bernard et al., 2004*). Dilution by meteoric rainwater during the rainy season was quite evident during low level activity, especially in anion concentrations during 2002 and 2003 (Figure 3.7), perhaps because the rate of volcanic input was constant (~250 µmoles/gr SO_4 + Cl) and relatively low (Figure 4.5).

Gas that was not scrubbed by the hydrothermal system would have ascended along vapor phase conduits, which could be either physical conduits or ascent paths followed by less soluble volatiles like H_2S or CO_2. This can be considered open system degassing, where volatiles ascend independent of host magmas. Gas escaped directly to

the atmosphere at high temperature subaerial fumaroles (max. T=875ºC, June 2002 [*Bernard et al., 2004*]) adjacent to the lake on the western crater wall. No data is available on the composition of the fumarolic gases.

The presence of high temperature subaerial fumaroles and acid-sulfate hot springs indicate the existence of a single vapor phase zone at depth below the hydrothermal system (*Bernard et al., 2004; Ingebritson & Sorey, 1988*). Volcanic gases ascending through the hydrothermal condensate zone via "dry pathways" in vapor dominated conduits (*Oppenheimer, 1996*) and reach the surface largely unaffected by condensation or interaction with the subsurface hydrothermal system (*Bernard et al., 2004*). Single phase vapor-dominated regions are common features in geothermal areas, e.g. The Geysers, California; Larderello, Italy; Kamojang, Indonesia; and Matsukawa, Japan (*Ingebritson & Sorey, 1988*), and are most likely also present in other magmatic-hydrothermal systems (*Giggenbach, 1996*), e.g. Ruapehu (*Christenson & Wood, 1993*); Nevado del Ruiz (*Giggenbach et al., 1999*).

A low permeability sealing mineral cap likely occurs at the interface between the vapor dominated zone and adjacent overlying groundwater. Several processes contribute to the formation of a self-sealing mineral horizon: deposition of silica (*Fournier, 1985*), conversion of wallrock minerals to secondary hydrothermal alteration products (alunite, anhydrite, clays, sulfur), and evaporation of volcanic brines. This type of feature has been proposed at Nevado del Ruiz (*Giggenbach, 1999*), and serves to further confine the vapor phase region.

The lack of appreciable seismic activity during low level activity periods suggests that no subsurface magma movement occurs during these intervals of relative quiescence.

5.2.2 Hydrothermal activity: May 2000 to February 2002 and June 2004 to August 2005

During periods of hydrothermal activity in May 2000-February 2002 and June 2004-August 2005, enhanced degassing observed from the fumaroles, hot springs and lake was likely a result of increased heat and mass flow through the hydrothermal system (Figure 5.1b). The characteristics of both periods are quite similar, and are likely a result of the same processes. The changes observed during May 2000-February 2002 have been previously interpreted as venting of the hydrothermal system (*BVGN 26:04*), and the same mechanism is proposed here to account for hydrothermal activity in June 2004-August 2005.

During these periods, elevated SO_2 fluxes were measured at <400 t/d in 2001 and <600t/d in 2004, which are high values for a quiescent volcano when compared to gas emissions during low level activity. Such high SO_2 emission rates without eruptive or effusive activity require further explanation. One likely scenario is that gas flow may be enhanced by increasing permeability of the mineral cap. Magmatic gas in a vapor-dominated zone accumulates beneath this authigenic mineral cap, and leaking or cracking of this mineral cap can produce high gas emission rates. This mechanism has been invoked at other volcanoes, e.g. Nevado del Ruiz (*Giggenbach et al., 1990*), and has also been proposed for Santa Ana during May 2000-February 2002 (*Rodriguez et al., 2004; BVGN 26:04*). However, cracking the already "leaky" cap is not absolutely necessary to achieve higher gas emission rates.

Another mechanism sometimes invoked to account for high SO_2 emission rates at volcanoes is the remobilization of previously deposited hydrothermal sulfur by

combustion (e.g. *Oppenheimer, 1996; Symonds et al., 2001; Christenson, 2000*). Hydrothermal sulfur is abundant in the volcanic edifice as it precipitates in pore spaces and along pre-existing fractures. However, remobilization of hydrothermal sulfur requires combustion and high heat conditions which are probably only feasible during eruptions. Combustion requires available oxygen and probably takes place in an eruption plume rather than in the edifice (*Oppenheimer, 1996).*

As subaerial degassing increased during these periods, the hydrothermal system scrubbed more volcanic gas and the lake subsequently acidified and warmed (max. T=30ºC, max. LTA=13ºC in 2001; max. T=28ºC, max. LTA=12ºC in 2004). Seasonal dilution, which had been a prominent process during low level activity, was not observed and anion concentrations remained remarkably constant with $SO_4/Cl = 1.1$. These results indicate that rate of volcanic input was higher but the composition of the volcanic input was unchanged. This could be attributable to increased heat and mass flow through the hydrothermal system and/or boiling of fluids in the near vent region which may have created concentrated brines and acidified the crater lake. Additionally, observations of sulfur spherules in the lake in February 2001 and floating sulfur rafts in the lake in December 2004 and April 2005, also support enhanced degassing into the lake and indicate that at least some volcanic gas was being directly injecting into the lake.

In addition to increasing subaerial degassing and heating and acidifying the lake, increased heat and mass flow through the hydrothermal system generated LP seismicity in June 2004-2005. Elevated sulfur dioxide gas emissions to <600 t/d were accompanied by concurrent long-period seismicity (~ 200 events/day). Synchronized observations determined that large gas pulses corresponded with seismic signals, and LP seismicity

was interpreted by SNET to be associated with degassing of the hydrothermal system. The crater lake warmed simultaneously, reaching 28ºC (LTA=12ºC). Trends in the number of LP events per day were mirrored by LTA trends (Figure 3.9b), suggesting that upward fluid movement in the hydrothermal system subsequently led to crater lake warming.

Long period seismicity without volcano-tectonic seismicity during these periods suggest that hydrothermal activity was not driven by a magmatic intrusion and that LP seismicity was likely sourced in the hydrothermal system.

5.2.3 Fumarolic activity: August 2005 to October 2005 & eruption triggering mechanisms

In August and September 2005, enhanced fumarolic activity was observed leading up to the phreatic eruption on 1 October 2005. As detailed in Section 3.2g, incandescent fumaroles, large SO_2 emissions <~4000 t/d, and LP seismicity, VT swarms, banded tremor occurred during this period prior to the eruption. Two end-member scenarios which explain observed fumarolic activity and eruption triggering mechanisms are discussed below.

In 1st scenario (Figure 5.1c), all observed seismicity is attributed to hydrothermal processes, and the phreatic eruption occurs without being triggered by magma movement. Raised pore pressures allow slip on cracks by reducing the "effective" normal stress. The high SO_2 flux derives from accumulation of gas in magma chamber, and also possibly from single phase vapor zone. Cooling of a crystallizing magma body over time, on the order of 50-100 years, leads to gas accumulation and overpressurization, until critical

overpressures are reached and a phreatic eruption ensues (*Tait et al., 1989)*. In this situation, the phreatic eruption is ultimately triggered by crystallization of magma at depth without magma movement.

In the 2nd scenario (Figure 5.1d), a new batch of gas rich basaltic magma intrudes the existing magmatic system. Deep dike intrusion may possibly lead to further dike propagation at shallower levels. The unusually high SO_2 flux measured on the surface is derived from arrival of this new magma and VT seismicity is also associated with dike propagation and cooling.

In this situation, movement of magma at depth in late August 2005 caused shear fracture of surrounding wall rock generating VT swarms. Magma migration may have initiated in late August 2005, when three high frequency volcano-tectonic (VT) swarms were recorded on 18, 22, and 27 August 2005. VT events are commonly recorded prior to and during eruptions and have been identified as one of the earliest detectable precursors to volcanic activity (*Lahr et al., 1994*, *Roman & Cashman, 2006).*

Enhanced heat and gas fluxes along fumarole conduits, as well as gas and fluid movement in the two phase region of the hydrothermal system followed magma migration. Incandescence in the main fumarole field was observed beginning on 23 August, accompanied by rapid increases in SO_2 flux on 24 August (~ 4000 t/d) and LP seismicity on 25 August (from 200 to 350 events/day).

A conclusive juvenile component was not identified among the erupted tephra (Chapter 3.2h), implying that the intrusion must have stalled at depth. A stalled intrusion would have induced overpressures in the hydrothermal system, which in turn ultimately triggered the phreatic eruption. During September 2005, SO_2 flux and LP seismicity

remained at very high levels, while VT events were minimal, suggesting that the intrusion ceased moving but continued degassing through the hydrothermal system.

The stalled intrusion probably did not reach the hydrothermal system. There is no unambiguous evidence in the tephras that show magma in direct contact with water. Moreover, several lines of geochemical evidence support the lack of a fresh magmatic intrusion in the hydrothermal system. First, if magma had intruded into the hydrothermal system, enhanced water-rock interaction would likely occur as acid waters attacked fresh material. Cation concentrations would be expected to rise, as would the Mg/Cl ratio. However, neither of these trends is observed in the data prior to or following the eruption, suggesting if there was a magmatic intrusion, the intrusion stalled below the mineral cap precluding interaction between fresh magma and hydrothermal waters. Second, the lack of clay minerals and significant hydrothermal sulfur in the erupted tephra suggest that the eruption only tapped shallow depths in the hydrothermal system. The authigenic mineral cap presumably contains both clay minerals and hydrothermal sulfur, and was likely deeper than the source of the eruption.

Immediately following the 1 October eruption, the system would have been depressurized, and SO_2 and LP seismicity did in fact decrease substantially. A VT swarm occurred shortly after the eruption on 7 October, possibly resulting from cooling of the carapace of the dike intrusion. Brittle fracture formation in the region surrounding molten magma resulted in the release of magmatic volatiles to the overlying hydrothermal system (*Sparks, 1977*). Gas emissions remained high post-eruption, but decreased over time, with SO_2 fluxes decreasing from 2500 t/d in January 2006 to below detection in October 2006.This mechanism has been invoked at Poas, Costa Rica (*Brown et al., 1989*).

5.2.4 Post-2005 hydrothermal activity: October 2005 to December 2007

The eruption had a significant effect on the geometry of the crater lake and fumaroles and may have increased permeability in the hydrothermal system. The October 2005 eruption destroyed the main fumarole area and the post-2005 lake drowned the area where the fumarole field previously existed. After the 2005 events, the single vapor phase conduits were compromised by the hydrothermal system, and heat and gases were injected directly into the lake via a central subaqueous fumarole (Figure 5.1e). The lake continued to be acidified by hotsprings following the 2005 eruption, but volatiles ascending along vapor phase conduits also provided a direct gas input into the lake at the subaqueous fumarole. Increased volcanic heat input (8-830 MW, equivalent SO_2 flux of 16-1600 t/d) led to more evaporation. The lake proved to be a sensitive calorimeter, and on several occasions the lake evaporated up to 30% its "normal" size of 200 m diameter. Each evaporation episode was accompanied by LP events merging into banded tremor. If Scenario #2 is invoked, volcanic input could be sourced from the cooling of the stalled shallow dike intrusions and repeated lake evaporations could indicate that the dike intrusion may be ongoing.

Changes in the rate and composition of volcanic input into the lake produced unprecedented changes in lake chemistry. The lake became more acidic (pH < 1) and chloride concentrations rose to maximum levels (~22,000 mg/kg), but surprisingly, sulfate concentrations did not rise concomitantly and SO_4/Cl ratios dropped below 1. To account for these changes, either a chloride rich source needs to be added to the lake, e.g. more scrubbing of HCl by hydrolysis (*Symonds et al., 2001*) and/or mixing with a deep seated neutral sodium chloride brine, and sulfate must be removed from the lake via

sulfur scrubbing by precipitation of native sulfur in the two phase gas+liquid subliminic region (*Symonds et al., 2001*) and/or a molten sulfur bottom layer in the lake (*Takano et al., 1994*).

Several lines of evidence support that sulfur scrubbing by precipitation of native sulfur and sulfate minerals, like anhydrite or gypsum, likely occurred in the lake. I adopt the broad definition of sulfur scrubbing used by *Symonds et al. (2001*): "any process that reduces emissions during reactions between magmatic gas, water, and sometimes rock; hence, scrubbing includes dissolution into the aqueous phase (e.g. hydrolysis) and formation of precipitates (e.g. sulfur, sulfides, fluorides, and sulfates) from gas-water or gas-rock interactions."

A bottom layer of molten sulfur is inferred to have accumulated subsequent to the 15 March 2007 phreatic eruption. This inference is based on observations of a wet native sulfur horizon observed along the lakeshore, observations of sulfur spherules in suspension and along the shorelines from May 2007 to July 2007, and sulfur saturation state modeling (Figure 2.9). In many crater lakes, elemental sulfur, with a specific gravity of ~2.0, accumulates on the lake bottom (e.g. Ruapehu, *Giggenbach [1974]*, Lake Yugama, *Takano et al., [1994]*). The elemental sulfur acts as a thermal barrier, and a layer of molten liquid sulfur rapidly forms. This process requires fumarolic temperatures > 119ºC, which is the melting point of orthorhombic sulfur (*Takano et al., 1994).* Sulfur spherules form as gas percolates through the molten sulfur layer on the bottom of the lake. The molten sulfur coats the rising gas bubbles to form hollow sulfur spherules which float on the surface. Convection currents in the lake and wind carry the spherules from their origin in the lake to the lakeshore. Observations supporting the existence of

elemental sulfur in the lake are consistent with saturation state modeling which demonstrated that sulfur was saturated or close to saturation at observed lake temperatures during January to July 2007.

Elemental sulfur can be produced by three inorganic reactions: disproportionation of SO_2, oxidation of H_2S (*Delmelle et al., 2000; Casadevall et al., 1984*), sulfitolysis of S_xO_6 (*Takano and Watanuki, 1990*). Magmatic SO_2 reacts with water in hydrolysis reactions involving disproportionations with cooling below 400ºC (*Symonds et al., 2001*):

$$3SO_{2(g)} + 2H_2O_{(aq)} \rightarrow S^0_{(s,l)} + 2H_2SO_{4(aq)} \quad (5.1)$$

At this time, the temperature/depth at which sulfur dioxide disproportionation occurs is unknown. If this reaction takes place at lake temperature, it would contribute to accumulation of native sulfur in the lake. However, if this process occurs deep in the hydrothermal system rather than in the lake, it would contribute only to hydrothermal sulfur deposition in the edifice.

Hydrogen sulfide may be abundant in the original gas stream entering the lake, and may be produced by oxidation of sulfuric acid by reduced iron supplied from frequent rockfall material:

$$6Fe_3O_4 + H_2SO_4 \rightarrow 9Fe_2O_3 + H_2S_{(g)} + 1/2O_2 \quad (5.2)$$

Oxidation of $H_2S_{(g)}$ by sulfur dioxide (Eq. 5.3), sulfuric acid (Eq. 5.4), sulfurous acid (Eq. 5.5), by ferric iron (Eq. 5.6), or atmospheric oxygen (Eq. 5.7) could produce elemental sulfur:

$$SO_2 + H_2S \rightarrow 3S^0 + 2H_2O \quad (5.3)$$

$$H_2SO_4 + 3H_2S \rightarrow 4S^0 + 4H_2O \quad (5.4)$$

$$H_2SO_3 + 2H_2S \rightarrow 3S^0 + 3H_2O \quad (5.5)$$

$$Fe^{3+} + H_2S \rightarrow S^0 + Fe^{2+} + 2H+ \quad (5.6)$$

$$O_2 + 2H_2S \rightarrow 2S^0 + 2H_2O \quad (5.7)$$

Consumption of sulfuric acid by Eq. 5.2 and/or Eq. 5.4 are potential reactions which would account for relatively low SO_4 concentrations in the lake.

Finally, elemental sulfur generation by sulfitolysis of polythionates can potentially produce significant amounts, but this process is unconstrained for Santa Ana due to lack of polythionate analyses.

5.3 Eruption precursors

The appearance of long period seismicity, constant net anion concentrations, and crater lake warming are interpreted here as long-range eruptive precursors during June 2004 - August 2005, months prior to the eruption. LP seismicity and crater lake warming were identified as precursory activity during the unrest event, but constant net anion concentrations were previously overlooked. Constancy of net anion concentrations may give the illusion of quiescence, i.e. no change over time, but in this case constancy of anion concentrations, the lack of rainy season dilution, and lake acidification represent important changes in geochemical behavior with respect to typical low level activity.

Vivid incandescence in the fumarole field, high gas emission, VT swarms, and banded tremor are interpreted here as short-range eruptive precursors during August and September 2005, on the order of weeks prior to the eruption. All of these events were recognized during the crisis to signify that major changes to the magmatic and hydrothermal systems were underway, though the root causes of the changes (i.e. a possible magmatic intrusion) were not (and perhaps still are not) completely clear.

The occurrence of banded tremor prior to the eruption on 27 August 2005 is highly significant, and was also poorly understood at the time. Banded tremor has been documented to precede phreatic events, and review of the literature reveals that it is fairly widespread. Banded tremor has observed at Nevado de Ruiz in Colombia (*Martinelli et al., 1990; Giggenbach et al., 1990*); Izu-Oshima in Japan (*Watanabe, 1987*); Etna in Italy (*Gresta et al., 1996)*; Karkar in Papua New Guinea (*McKee et al., 1981*); Pavlof in Alaska, Suwanose-jima in Japan, Ulawun in Papua New Guinea, Klyuchevskoy in Kamchatka, Russia (*McNutt, 1989*); Anatahan in the Mariana Islands (*Trusdell et al., 2001*); Guagua Pichincha in Ecuador (*Garcia-Aristizabal, 2004);* Pagan in the Mariana Islands (*BGVN 19:02*); Mt. Spurr in Alaska (*BVGN 17:09*); Nyiragongo, Democratic Republic of the Congo, (*BVGN31:01);* Pu'uO'o, Kilauea, Hawaii (*Barker et al., 2003*); and Soufriere, Monserrat, (*Baptie & Thomson, 2003*).

Banded tremor may be associated with a variety of volcanic activity, e.g. at Pu'uO'o, Kilauea, banded tremor is associated with drain-back of the lava lake (*Barker et al., 2003)*; at Montserrat, banded tremor is related to lava dome instability (*Batie & Thomson, 2003)*, but here I am interested in banded tremor associated with explosive volcanism. Notable examples of where banded tremor has preceded explosive eruptions include Nevado del Ruiz, Karkar, and Etna (*Martinelli et al., 1985, McKee et al., 1981, Montalto, 1995).* At Mt. Spurr and Anatahan, banded tremor has a strong correlation with observed eruptive activity (*BVGN 17:09, Trusdell et al., 2001).*

Banded tremor is a cyclic seismic signal related to periodic intervals of continuous energy release, causing the signal to appear on the seismograph in "bands" of high amplitude tremor separated by intervals of low amplitude tremor (*Montalto, 1995,*

McKee et al., 1981). "Banded tremor" observed at volcanoes has also been called "cyclic tremor" (*Martinelli, 1990*) or "intermittent volcanic tremor" (*Gresta et al., 1996*), and is often compared to similar cyclic seismicity observed at geysers, e.g. Old Faithful Geyser in Yellowstone *(Kieffer, 1984),* where hot water periodically flashes to steam when the supply of heat exceeds the heat-absorbing capacity of water (*McKee et al., 1981).Martinelli (1990)* observe that at Nevado del Ruiz, the frequency content of each cycle of banded tremor is the same, indicating that the same process is probably responsible for the seismic activity of every cycle. Furthermore, the banded tremor has a different frequency content than any other data collected at the same station at Nevado del Ruiz, indicating that the banded tremor are due to source characteristics rather than path effects. This source is postulated to be a rather shallow source, due to the absence of shear waves, and observed energy content in horizontal component one order of magnitude larger than the vertical component (*Martinelli, 1990).*

Several sources have been put forth to explain the intermittent nature of this type of volcanic tremor. In all models, magma must be present to passively supply heat and gases to shallow groundwater. *Leet (1988)* has proposed a source model to explain shallow, noneruptive tremor that has an emergent onset where sustained groundwater vibrations by steam bubble growth/collapse (hydrothermal boiling). "Saturated" hydrothermal boiling occurs if the fluid vibration is caused by steam bubble growth, whereas "subcooled" hydrothermal boiling occurs if the fluid vibration is caused by steam bubble collapse (subcooled boiling is 10^2 to 10^4 times more efficient than saturated boiling to convert thermal energy to seismic energy) (*Leet, 1988*). In this model, an aquifer is gradually heated until hydrothermal boiling is achieved and thermal energy is

converted to mechanical energy, accounting for emergent onset of tremor. The aquifer acts like a "pressure-cooker" (*Montalto, 1995*) and this process is self-limiting, eventually causing boiling to stop, and accounting for rapid cessation of tremor. *Montalto (1995*) proposes a similar source mechanism in his hazard assessment of Vulcano, whereby banded tremor is caused by intermittent hydrothermal boiling accompanying hydraulic fracturing of rocks at the top of a pressurized aquifer. Hydraulic fracturing instantaneously enhances vertical permeability, and re-establishes conditions necessary for hydrothermal boiling (*Montalto, 1995*). Alternatively, *McKee et al. (1981)* attribute banded tremor at Karkar to opening and closing of cracks by pulses of high-pressure steam and hot water. *Garcia-Aristizabal (2004)* invoke a similar mechanism of repetitive releases of hot gases generated from hydrothermal water-magma interaction to explain noneruptive banded tremor at Guagua Pichincha, Ecuador.

Hydrothermal boiling seems to be a reasonable mechanism to explain banded tremor at Santa Ana, given the existence of a shallow aquifer. *Montalto (1995)* notes that the disappearance of banded tremor can be associated with quick overpressurization of aquifer and higher phreatic eruption hazard. However, the phreatic blast will only proceed if the steam pressure reaches a value higher than the overburden at the top of the reservoir. Banded tremor observed at Santa Ana ceased one month prior to the eruption, could have perhaps been a sign that critical overpressures had been reached and that a phreatic eruption was imminent. Further investigation into banded tremor phenomena is required to attribute a source mechanism with a higher degree of confidence. Furthermore, it is unknown as to whether banded tremor observed prior to the October 2005 eruption can be attributed to the same source as banded tremor observed during evaporation

episodes. Detailed analysis of amplitude and frequency content of tremor would begin to address these issues.

5.4 Impact of the 2005 eruption and potential eruption hazards

Classification of Santa Ana crater lake and comparison to other similar crater lakes aids in assessing potential future activity and identifying associated hazards from a crater lake perspective (Table 5.1). The classification system used here is the physiochemical lake classification scheme of *Pasternack & Varekamp (1997)* introduced in Chapter 1.3. This approach quantitatively delineates lake classes based on three criteria: absolute energy, hydrodynamic mixing regimes, and chemistry. Key classification parameters identified by *Pasternack & Varekamp (1997)* include its eruption history, lake temperature, pH, and total dissolved solids (TDS). Additional important parameters of lake size, depth, power output, Cl and SO_4 concentration are also included in the summary table. Santa Ana is compared to several lakes on the basis of similarity in size, chemistry, and/or activity. Lakes chosen for comparison include: Laguna Caliente at Poas, Costa Rica; Lake Yugama at Kusatsu Shirane, Japan; Crater Lake at Ruapehu, New Zealand; Copahue crater lake in Argentina; Kawah Ijen at Merapi, Indonesia; and the Keli Mutu lakes TiN and TAP in Indonesia.

Prior to 2005, the Santa Ana lake can be classified as a high activity lake containing a cool acid-sulfate brine (T= 16-30C, pH = 0.7 to 2, TDS = 1.8-2.7%) with power output = 0.5-20 MW, Cl concentration = 1100-9200 ppm, and SO_4 concentration = 4500-14,000 ppm (Table 5.1). High activity lakes maintain their mass, are thermally stable, and are perfectly mixed (*Pasternack and Varekamp, 1997)*. Other cool acid-sulfate

brine high activity lakes include Yugama, Ruapehu, Copahue, Keli Mutu TiN. Santa Ana during this pre-2005 period closely resembles Yugama in temperature, pH, TDS, lake size, and power output and Ruapehu in lake chemistry, including pH and TDS.

The Santa Ana crater lake no longer existed as a cool acid-sulfate brine lake following the October 2005 eruption. The long existent cool acid-sulfate-chloride lake re-emerged post-2005 as a hotter, more acidic, chloride-rich lake. A central subaqueous fumarole replaced the subaerial fumarole field, contributing significantly in heat and mass transfer to the lake and affecting the fate of SO_2 in the lake and hydrothermal system. Sulfur scrubbing by precipitation of sulfur was likely an important process in the lake post-2005.

The post-2005 lake can be classified as a high activity lake evolving to peak activity/variable mass containing a hot acid brine (T=25-65ºC, pH = 0.4 to 1.2, TDS = 2.7-15%) with power output = 13-830 MW, Cl concentration = 3100-22,000 ppm, and SO_4 concentration = 2500-9700 ppm (Table 5.1). The post-2005 Santa Ana crater lake now most closely resembles Laguna Caliente at Poas, though Laguna Caliente is hotter (T<96ºC) and more concentrated (TDS<36%) with higher concentrations of Cl and SO_4 owing to evaporation. Laguna Caliente's power output (150-550 MW) is on the same order of magnitude as Santa Ana (13-380 MW), though the lower heat flux at Laguna Caliente despite higher temperatures may be due to variations in the energy budget codes, specifically in the expression of the long-wave radiative input from the atmosphere. Similar to Santa Ana, Laguna Caliente has experienced dessication episodes in 1953 and 1989. In 1953, complete lake evaporation coincided with the first eruption of juvenile material, and in 1989 lake disappearance was followed by several phreatic eruptions

(*Rowe et al., 1992*). At Santa Ana, complete lake dessication should be closely monitored, as lake dessications have been closely associated with phreatic and phreatomagmatic activity at Laguna Caliente.

Following the classification scheme, "high activity" lakes carry hazards of seepage of toxic fluids and evolution to peak activity, neither of which was observed leading up to the 2005 eruption at Santa Ana (Figure 1.2). However, "peak activity" and "variable mass" lakes carry more severe hazards of volcanic (magmatic/phreatomagmatic) and/or phreatic eruptions, lahars, and seepage of toxic fluids. A minor phreatic eruption was in fact observed at Santa Ana in March 2007. Slope instability and sector collapse are not identified as potential hazards by *Pasternack and Varekamp (1997),* but these are low frequency, high hazard events that are likely to occur at edifices where extensive hydrothermal alteration and faulting occur. *Pasternack and Varekamp (1997)* have noted that passively degassing volcanoes commonly do not emit more than 600 tons SO_2/day (*Andres et al., 1992*), and argue that a volcanic lake cannot exist as a peak-activity lake unless it is evolving towards an eruption. Degassing of <600 t/d SO_2 measured during Santa Ana's post-2005 places it at this upper limit of passively degassing volcanoes.

Given that the post-2005 "variable mass" Santa Ana lake exhibited increased variability in behavior, the unstable, highly variable nature of the post-eruption lake begs the question: does increased crater lake variability imply increased eruption hazard? From a crater lake point of view, the evolution to a "variable mass" lake does indeed imply that eruption hazards are increased. Lake conditions suggest that phreatic eruptions hazard is most certainly increased, and likelihood of magmatic/phreatomagmatic eruption

remains to be determined. On one hand, as in Scenario #1, the system is depressurized, and it might take another 50-100 years to reach critical overpressures, so hazard is lessened. The eruptive frequency of 1-2 eruptions per 100 years derived from the Smithsonian Eruptive History supports this argument. However, on the other hand, as in Scenario #2, magma may still reside at shallow levels and the magmatic intrusion could be ongoing. A stalled magmatic intrusion at some depth below the hydrothermal system is consistent with the very high heat fluxes needed to achieve high measured lake temperatures. Heat flux data suggests a continuous heat source, albeit perhaps passive, is needed. The possibility of a phreatomagmatic eruption occurring in the future is higher in scenario #2 than in scenario #1.

Based on the available data, I conclude that it is impossible to definitively rule out either end member scenario discussed here. Further data collection and research is required to more fully address hazard issues. Suggestions for further research are as follows:

- Geophysical techniques, including continued seismic monitoring with more stations and/or 3 component stations to better locate events, and deformation from GPS or tiltmeters to capture inflation/deflation episodes.
- Continued aqueous geochemical monitoring of the lake, with analyses of all RFE including aluminum.
- Sulfur isotopes on hydrothermal sulfur to determine temperature/depth at which disporportionation of sulfur dioxide takes place.
- Stable isotopes of lake waters to further constrain the effects of evaporation.

- Further investigation into seismicity, with focus on “banded” tremor and LP events associated with lake evaporation.
- Determination of composition of subaerial fumaroles.
- A hydrological study, including searching for springs lower on edifice, to constrain dimensions and zonation of hydrothermal system, like studies carried out at Zunil, Guatemala (*Walker et al., 2006*), or Poas (*Rowe et al., 1995*).

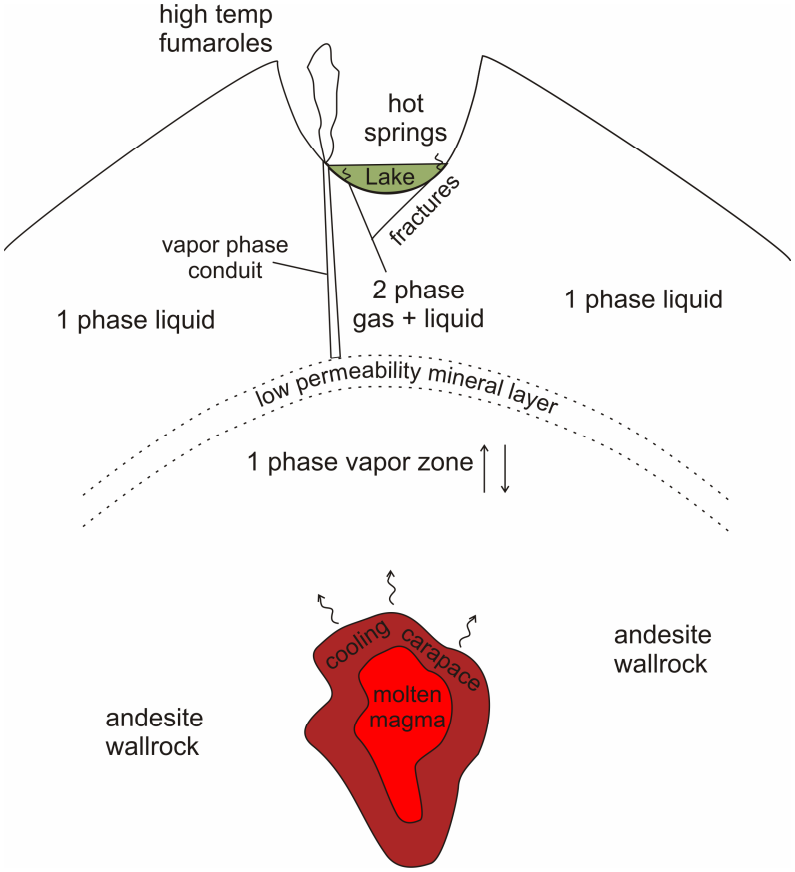

Figure 5.1a: Schematic model of the Santa Ana magmatic-hydrothermal system: pre-eruptive low level activity observed during early 2000 and February 2002-June 2004.

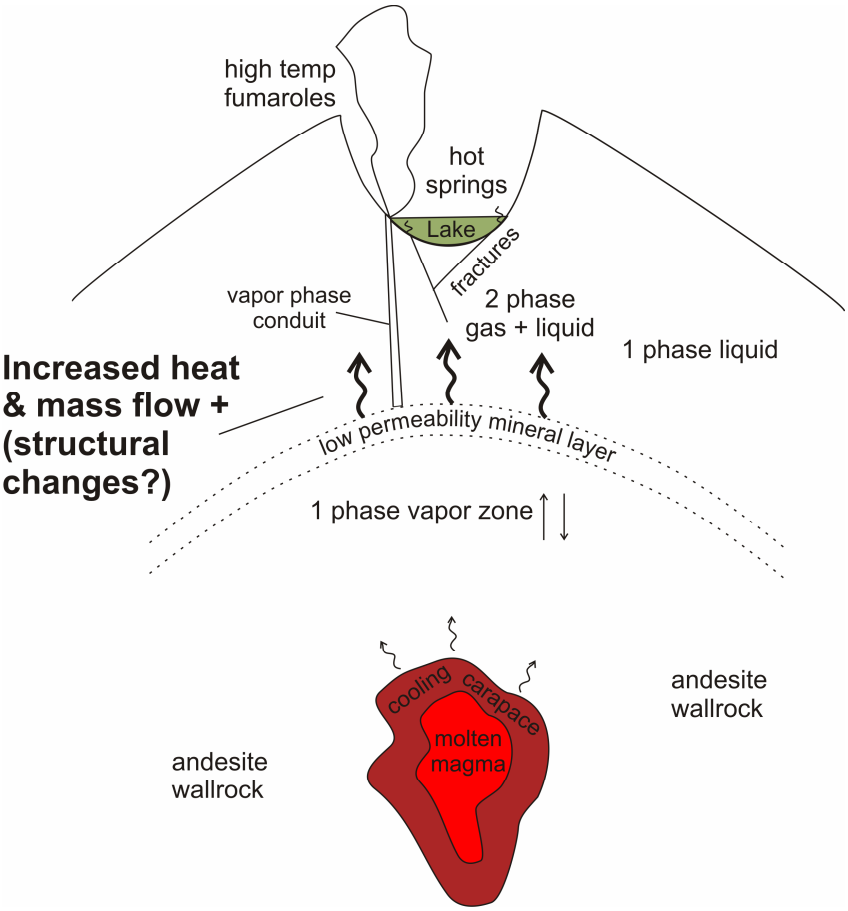

Figure 5.1b: Schematic model of the Santa Ana magmatic-hydrothermal system: pre-eruptive hydrothermal activity observed during May 2000-February 2002 and June 2004-August 2005.

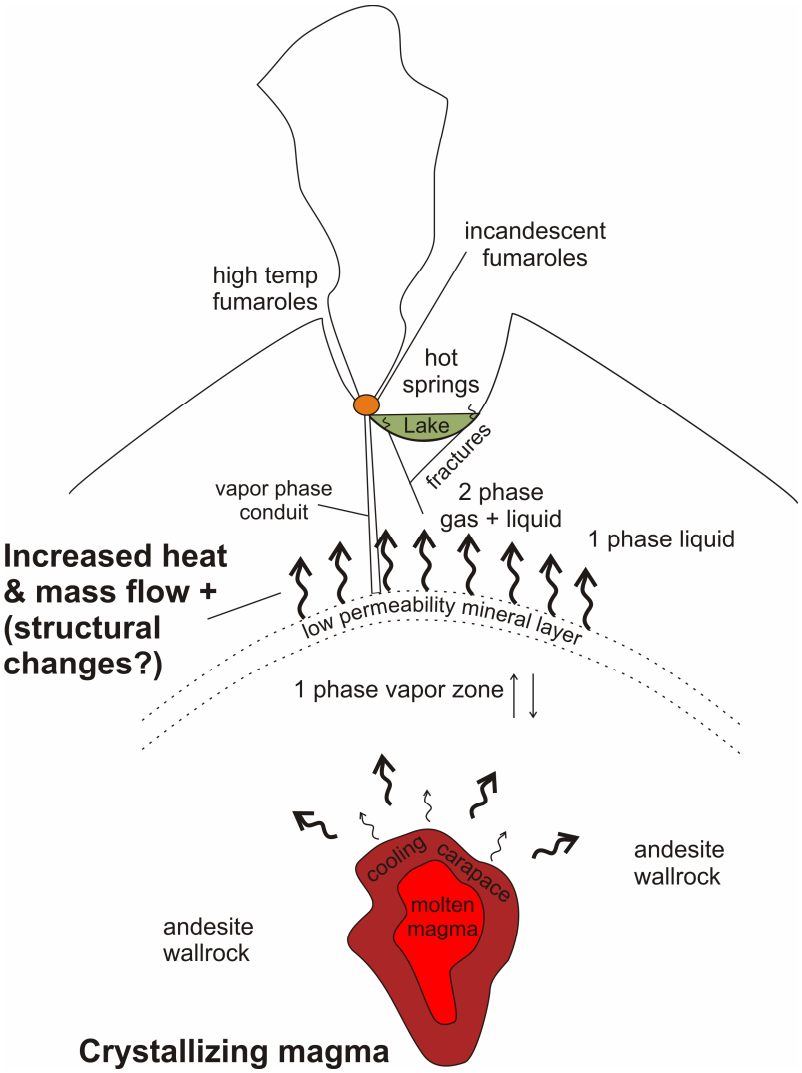

Figure 5.1c: Schematic model of the Santa Ana magmatic-hydrothermal system: Scenario #1 for fumarolic activity observed in August and September 2005.

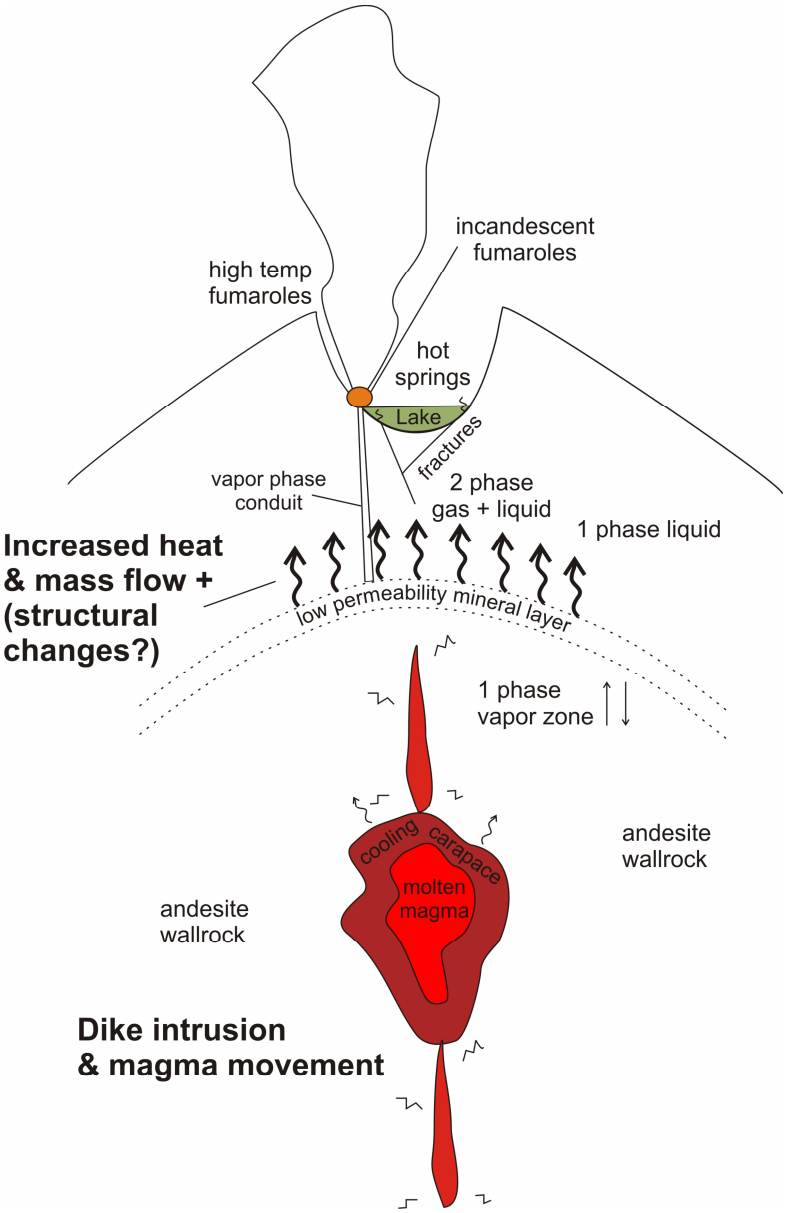

Figure 5.1d: Schematic model of the Santa Ana magmatic-hydrothermal system: Scenario #2 for fumarolic activity observed in August and September 2005.

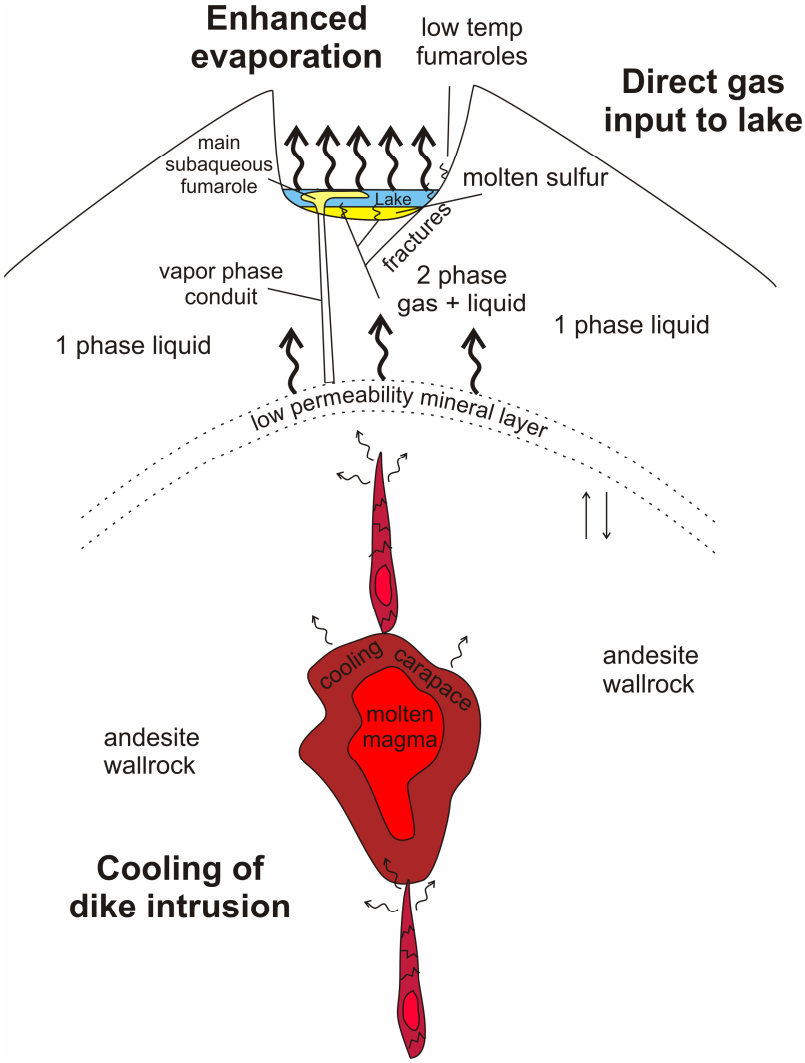

Figure 5.1e: Schematic model of the Santa Ana magmatic-hydrothermal system: post-eruptive hydrothermal activity observed in late 2006 and 2007.

Table 5.1 Comparison of Santa Ana to other crater lakes for hazard assessment.

Lake Name	Lake Type	Lake Subtype	Representative Values			Other parameters					Time Period	Eruption History	References
			Temp.	pH	TDS	Size (equivalent radius)	Depth (max.)	Power output	Cl	SO_4			
Santa Ana pre-2005	high activity	cool acid brine	16-30ºC	0.7 to 2	1.8-2.7%	100 m	27 m	0.5-20 MW	1100-9200 ppm	4500-14,000 ppm	2000-2005	Phreatic eruption October 2005.	Bernard et al., 2004; this study.
Santa Ana post-2005	high activity evolving to peak activity/ variable mass	hot acid brine	25-65ºC	0.4 to 1.2	2.7-15 %	<100 m	n.m.	13-830 MW	3100-22,000 ppm	2500-9700 ppm	2006-2007	Upwelling, several lake evaporations & minor phreatic eruption.	This study.
Laguna Caliente, Poas	peak activity/ variable mass	hot acid-hyperbrine	38-96ºC	-0.87 to 0.26	6-36 %	140 m	4-50 m	150-550 MW	16,500-129,000 ppm	37,000-230,000 ppm	1984-1990	Phreatic activity, lake disappears in April 1989 and liquid sulfur pools form.	Rowe et al., 1992.
Yugama, Kusatsu Shirane	high activity	cool acid brine	8-33ºC	1 to 1.8	0.4-1.2%	135 m	24 m	3-25 MW	1700-3500 ppm	2000 ppm	1988-1993	Phreatic eruptions; cool between eruption, hot before and after eruptions.	Ohba et al., 1994, Takano et al., 1994, Takano et al., 2007.
Crater Lake, Ruapehu	high activity	cool/hot acid brine	10-60ºC	0.6-1.8	1.9-3.7%	250 m	80-300 m	385 MW	5000-14,000 ppm	5200-20,000 ppm	1971-1991	Phreatomagmatic (1971, 1995-6) & phreatic eruptions (1988); heating cycles; lahars, e.g. 2007.	Christenson & Wood, 1993; Delmelle & Bernard, 2000; Christenson et al., 2000.
Copahue, Argentina	high activity	cool acid brine	21-54ºC	0.18-0.3	9%	150 m	40 m	173 MW	4300-14,000 ppm	20,000-64,000 ppm	1997-2004	Lake disappeared following phreatomagmatic eruption in July 2000.	Varekamp et al., 2001; Pasternack & Varekamp, 1997.
Kawah Ijen, Merapi	high activity	hot acid brine	33-44ºC	<0.3	10.50%	500 m	170 m	244 MW	19,000-25,000 ppm	59,000-77,000 ppm	1990-1996	Phreatic eruptions, relatively stable for last 50 yrs; similar to Keli Mutu TiN.	Delmelle & Bernard, 1994; Delmelle & Bernard, 2000.
Keli Mutu TiN	high activity	cool acid brine	28-33ºC	0.3-0.4	9.00%	150-215 m	127 m	54 MW	25,000 ppm	47,000-49,000 ppm	1989-1992	Upwelling, no eruptive activity since "hydrothermal blasts" in 1938 and 1965; similar to Kawah Ijen.	Pasternack & Varekamp, 1994; Pasternack & Varekamp, 1997.
Keli Mutu TAP	medium activity	seasonally fluctuates between reduced in dry season (dark green) and oxidized in wet season (blood red)	20-23ºC	1.75-1.8	1.4-1.7%	165-200 m	64 m	N.A.	2600 ppm	8600-9800 ppm	1989-1992	Upwelling, no eruptive activity.	Pasternack & Varekamp, 1994; Pasternack & Varekamp, 1997.

CHAPTER 6: Conclusions

This research has allowed investigation into crater lake evolution at Santa Ana crater lake from 2000 to 2007, encompassing a period of volcanic unrest from June 2004 to October 2005. For much of the study period, Santa Ana crater lake exhibited periods of relative quiescence interrupted by episodes of heightened hydrothermal activity. One such episode in June 2004 progressed into a volcanic crisis in late August 2005, marked by profound degassing and seismicity. This crisis ultimately developed into a moderately sized phreatic eruption (VEI 3) on 1 October 2005.

Delineation of crater lake evolution and integration with sulfur dioxide emission and seismic data has allowed for identification of eruption precursors and an interpretation of eruption triggering mechanisms. Long range precursors occurring months before the eruption during June 2004 to August 2005 were crater lake warming, LP seismicity, geochemical constancy. Short range precursors occurring weeks before the eruption during August and September 2005 include fumarole incandescence, high gas emissions, VT swarms, banded tremor.

Anomalous degassing to ~4000 tonnes SO_2/day and VT seismicity in August 2005 could be interpreted to signify an arrival of new magma prior to the October 2005 eruption, but lack of a conclusive magmatic component among eruptive products and lack of geochemical evidence of water-magma interaction suggest that new magma was not involved or that a batch of new magma stalled at depth below the hydrothermal system. Two possible end-member eruption triggering mechanisms have been proposed to explain the October 2005 phreatic eruption. In scenario #1, a crystallizing magma body

induces overpressurization in the hydrothermal system, which leads to a phreatic eruption. In scenario #2, a magmatic intrusion does not reach surface, but induces overpressurization in the hydrothermal system and triggers the phreatic eruption. In this scenario, the intrusion may be on-going and may yet trigger a magmatic eruption. Based on the available data, however, it is not possible to definitively rule out either end member scenario.

The 2005 eruption had a substantial impact on the thermal and chemical character of the crater lake owing to the appearance of a central subaqueous fumarole in the lake and the disappearance of high temperature subaerial fumaroles. Degassing directly into (and through) the lake caused increasing variability (evaporations) and acidity in the lake. The highly variable post 2005 crater lake presents increased eruption hazards and a challenge to monitoring until the system returns to equilibrium.

References

Aguado, E. and Burt, J.E., 2007, *Understand weather and climate*: Prentice Hall, New Jersey, 588p.

Andres, R.J., Barquero, J., Rose, W.I., 1992, New measurements of SO_2 flux at Poás Volcano, Costa Rica. J Volcanol Geotherm Res, 49, 175–177.

Ball, J.W. and Nordstrom,D.K., 1991, User's manual for WATERQ4F with revised thermodynamic data base and test cases for calculating speciation of minor, trace and redox elements in natural waters, U.S. Geological Survey Open File Report, 91–183.

Baptie, B., and Thomson, G., 2003, Post-collapse banded tremor at the Soufriere Hills volcano, Monterrat, West Indies, European Geophysical Society Geophysical Research Abstracts, v. 5, n.13276.

Barberi, F., Bertagnini, A., Landi, P., and Principe, C., 1992, A review on phreatic eruptions and their precursors, Journal of Volcanology and Geothermal Research, 52, 231-246.

Barker, S.R., Sherrod, D.R., Lisowski, M., Heliker, C., and Nakata, J.S., 2003, Correlation between lava-pond drainback, seismicity, and ground deformation at Pu u O O, U.S. Geological Survey Professional Paper 1676, 53–62.

Bernard, A., Escobar, C. D., Mazot, A. and Guttierez, R. E. 2004. The acid volcanic lake of Santa Ana volcano, El Salvador. Geological Society of America, Special paper 375: 121-133.

Bernard, A., 2005, The use of Multispectral Satellite Data to retrieve temperatures from Volcanic Lakes, published online at http://www.ulb.ac.be/sciences/cvl/multispectral/multispectral2.htm.

Brown, G.C., Rymer, H., Dowden, J., Kapadia, P. Stevenson, D., Barquero, J., and Morales, L.D., 1989, Energy budget analysis for Poas crater lake: Implications for predicting volcanic activity, Nature, 339, 370-373.

Carr, M. J., Rose, W. I., and Mayfield, D. G., 1979, Potassium content of lavas and depth to the seismic zone in Central America, Journal of Volcanology and Geothermal Research, 5, 3-4, 387-401.

Carr, M.J., Mayfield, D.G., and Walker, J.A., 1981, Relation of lava compositions to volcano size and structure in El Salvador, JVGR, 10, 35-48.

Carr, M.J., and N.K. Pontier, 1981, Evolution of a young parasitic cone towards a mature central vent: Izalco and Santa Ana volcanoes in El Salvador, Central America , J. Volcanol. Geotherm. Res., 11: 277-292.

Carr, M.J., W.I. Rose, and R.E. Stoiber, 1982, Central America in Andesites, edited by R.S. Thorpe,pp. 149-166, Wiley, New York.

Carr, M.J., 1984, Symmetrical and segmented variation of physical and geochemical characteristics of the Central American volcanic front, JVGR, 20, 231-252.

Casadevall, T.J., De la Cruz-Reyna, A., Rose, W.I., Bagley, S., Finnegan, D.L., and Zoller, W.H., 1984. Crater lake and post-eruption hydrothermal activity, El Chichon volcano, Mexico. J. Volcanol. Geotherm. Res., 23, 169-191.

Christenson, B.W., and Wood, C.P., 1993, Evolution of a vent-hosted hydrothermal system beneath Ruapehu Crater Lake, New Zealand, Bulletin of Volcanology, 55, 547-565.

Christenson, B.W., 2000, Geochemistry of fluids associated with the 1995-1996 eruption of Mt. Ruapehu, New Zealand: signatures and processes in the magmatic-hydrothermal system, JVGR, 97, 1-30.

Delmelle, P., and Bernard., A., 1994, Geochemistry, mineralogy, and chemical modeling of the acid crater lake of Kawah Ijen Volcano, Indonesia, Geochimica et Cosmochimica Acta, 58, 11, 2445-2460.

Delmelle, P., and Bernard, A., 2000, *Volcanic Lakes*, in eds., Sigurdsson, H. et al., Encyclopedia of Volcanoes: Academic Press, San Diego, 877-895.

DeMets, C. Gordon, R.G., Argus, D.F. and Stein, S., 1990, Current plate motions, Geophysical Journal International, 101, 425–478.

Dirección General de Estadísticas y Censos (DIGESTYC), 2007, "CIFRAS OFICIALES, CENSOS NACIONALES, VI Censo de Población y V de Vivienda 2007," [Official Results, National Censuses, 4th Population Census and 5th Housing Census 2007], http://www.digestyc.gob.sv/.

Eaton, A.D., Clesceri, L.S., and Greenberg, A.E., eds., Standard Methods for the Examination of Water and Wastewater, 19th edition. 1995. American Public Health Association: Washington, D.C.

Garcia-Aristizabal, A., Kumagai, H., and Nakano, M., 2004, Source process of tremor at Guagua Pichincha Volcano, Ecuador, inferred from waveform inversion, American Geophysical Union, Fall Meeting 2004, abstract #V14B-03.

Giggenbach, W.F., 1974. The chemistry of crater lake, Mt. Ruapehu (New Zealand) during and after the 1971 active period. N.Z. J. Sci. 17, 33–45.

Giggenbach, W.F., 1983, Chemical surveillance of active volcanoes in New Zealand, *in*: Tazieff, H., Sabroux, J.C., eds., *Forecasting volcanic events*: Elsevier, Amsterdam, 311–322.

Giggenbach, W.F., Garcia, N., Rodriguez, L., Londoño, A., Rojas, N., Calvache, M.L., 1990, The chemistry of fumarolic vapor and thermal-spring discharges from the Nevado del Ruiz volcanic-magmatic-hydrothermal system, Colombia, Journal of Volcanology and Geothermal Research, 42, 13–39.

Gresta, S., Privitera, E., Leotta., A., and Gasperini, P., 1996, Analysis of the intermittent volcanic tremor observed at Mt. Etna, Sicily during March-May 1987, Annali di Geofisica, 39, 421-428.

Grodecki, J., and Dial, G., 2003, Block Adjustment of High Resolution Satellite Images Described by Rational Functions, PE&RS, v. 69, no., 1, 59-70.

Halsor, S.P. and Rose, W.I., 1988, Common Characteristics of Paired volcanoes in Northern Central America, Journal of Geophysical Research, 93, B5, 4467-4476.

Hernandez, P.A., Perez, N.M., Varekamp, J.C., Henriquez, B., Hernandez, A., Barrancos, J., Padron, E., Calvo, D., Melian, G., 2007, Crater Lake Temperature Changes of the 2005 Eruption of Santa Ana Volcano, El Salvador, Central America Pure and Applied Geophysics, 164, 2507-2522.

Handal, S., and Barrios, L.A., 2004, Hydrothermal eruptions in El Salvador: A review, *in* Natural Hazards in El Salvador. Geological Society of America, Special Paper 375: 245–255.

Heiken, G., Crowe, B., McGetchin, T., West, F., Eichelberger, J., Bartram, D., Peterson, R., and. Wohletz, K., 1980, Phreatic eruption clouds: the activity of La Soufrière de Guadeloupe, French West Indies, August–October 1976. Bull. Volc. 43, 383–395.

Hurst, A.W., Bibby, H.M., Scott, B.J., McGuinness, M.J., 1991, The heat source of Ruapehu volcanic lake: deductions from energy and mass balances. J Volcanol. Geotherm. Res., 46, 1–20.

Ingebritson, S.E., and Sorey, M.L., 1988, Vapor-dominated zones within hydrothermal systems: Evolution and natural state, Journal of Geophysical Research, 93, B11, 13635-13655.

ITT Visual Information Solutions, 2008, ENVI Tutorial: Orthorectifying Imagery using Rational Polynomial Coefficients (RPCs). Accessible online at: http://www.ittvis.com/ProductServices/ENVI/Tutorials.aspx

Kieffer, S.W., 1984, Seismicity at Old Faithful Geyser; an isolated source of geothermal noise and possible analogue of volcanic seismicity, Journal of Volcanology and Geothermal Research, 22, 59–95.

Kling, G.W., Clark, M., Compton, H.R., Devine, J.D., Evans, W.C., Humphrey, A.M., Lockwood, J.P. and Tuttle, M.L., 1987, Science, The 1986 Lake Nyos gas disaster, Cameroon, West Africa, 236, 169-175.

Kutterolf, S., Freundt, A., Perez, W., Morz, T., Schact, U., Wehrmann, H., Schmincke, H.-U., 2008, Pacific offshore record of plinian volcanism in Central America: 1. Along-arc correlations, Geochemistry, Geophysics, Geosystems, 9, Q02S01, doi:10.1029/2007GC001631.

Lahr, J.C., Chouet, B.A., Stephens, C.D., Power, J.A., and Page, R.A., 1994, Earthquake classification, location, and error analysis in a volcanic environment: implications for the magmatic system of the 1989-1990 eruptions at Redoubt Volcano, Alaska, JVGR, 62, 137-151.

Leet, R.C., 1988, Saturated and subcooled hydrothermal boiling in groundwater flows channels as a source of harmonic tremor. J. Geophys. Res., 95, 12927–12945.

Linacre, E., 1992: *Climate Data and Resources: A Reference and Guide.* Routledge, 366 pp.

Martinelli, B., 1990, Analysis of seismic patterns observed at Nevado del Ruiz volcano, Colombia during August – September 1985, JVGR, 41, 297-314.

McBirney, A.R., 1980, Mixing and unmixing of magmas, JVGR, 7, 357-371.

McKee, C.O., Wallace, D.A., Almond, R.A., and Talai, B., 1981, Fatal hydro-eruption of Karkar volcano in 1979: development of a maar-like crater, Geological Survey of Papua New Guinea Memoir, 10, 63-84.

McNutt, S.R., 1989, Volcanic tremor from around the world, IAVCEI abstract of New Mexico Bureau of Geology and Mineral Resources Bulletin 131, 183 pp.

Meyer-Abich, H., Los Volcanes Activos do Guatemala y El Salvador, 1956, Anales Serv. Geol. Nacl. El Salvador Bd., 3, 42-62.

Montalvo, A., 1995, Seismic assessment of phreatic-explosion hazard at ‘La Fossa’ Volcano (Island of Vulcano, Italy), Natural Hazards, 11, 57-73.

Moore, D.M., and Reynolds, R.C., 1989, X-Ray diffraction and the identification and analysis of clay minerals. Oxford University Press: New York, 332 pp.

NASA Earth Observatory, 2005, Eruption of Santa Ana (Ilamatepec) Volcano, http://earthobservatory.nasa.gov/NaturalHazards/natural_hazards_v2.php3?img_id=13191.

Njoku, E.G., 1990, Satellite remote sensing of sea surface temperature, *in* Surface Waves and Fluxes: Volume II – Remote Sensing. G.L. Geernaert and W.J. Plant (eds.). Kluwer Academic Publishers: Dordrecht, 311-338.

Obha, T., Hirabayashi, J., and Nogami, K., 1994, Water, heat and chloride budgets of the crater lake, Yugama at Kusatsu-Shirane volcano, Japan, Geochemical Journal, 28, 217-231.

Olmos, R., Barrancos, J., Rivera, C., Barahona, F., López, D.L., Henriquez, B., Hernández, A., Benitez, E., Hernández, P.A., Pérez, N.M., and Galle, B., 2007, Anomalous emissions of SO_2 during the recent eruption of Santa Ana volcano, El Salvador, Central America, Pure and Applied Geophysics, 164, 2489-2506.

Oppenheimer, C., 1993, Infrared surveillance of crater lakes using satellite data, Journal of Volcanology and Geothermal Research, 55, 117-128.

Oppenheimer, C., 1996, Crater lake heat losses estimated by remote sensing, Geophysical Research Letters, 23, 14, 1793-1796.

Oppenheimer, C., 1997, Remote sensing of the colour and temperatura of volcanic lakes, Int. J. Remote Sensing, 18, 1, 5-37.

Ouimette, A.P., 2000, Hydrothermal processes at an active volcano, Copahue, Argentina; unpublished MSc Thesis. Wesleyan University, Middletown, 220p.

Parkhurst, D.L. and Appelo, C.A.J., 1999, User's guide to PHREEQC (version 2)--A computer program for speciation, batch-reaction, one-dimensional transport, and inverse geochemical calculations, U.S. Geological Survey Water-Resources Investigations Report 99-4259, 312 p.

Pasternack, G.B., and Varekamp, J.C., 1994. The geochemistry of the Keli Mutu crater lakes, Flores, Indonesia. Geochem. J. 28, 243–262.

Pasternack, G.B., and Varekamp, J.C., 1997, Volcanic lake systematics I. Physical constraints, Bulletin of Volcanology, 58, 528-538.

Pieri, D., Abrams, M., 2004. ASTER Watches the World's Volcanoes: A New Paradigm for Volcanological Observations from Orbit. Journal of Volcanology and Geothermal Research, 135: 13-28.

Pinel, V., and Jaupart, C., 2005, Some consequences of volcanic edifice destruction for eruption conditions, JVGR, 145, 68-80.

Poli, D., 2004, Orientation of satellite and airborne imagery form multi-line pushbroom sensors with a rigorous sensor model, XXth ISPRS Congress Proceedings, Commission I, vol. XXXV-B1, p. 130-135

Pullinger, C. 1998. Evolution of the Santa Ana volcanic complex, El Salvador; [MS Thesis], Houghton, Michigan Technological University, 151p.

Robie, R.A., Hemingway, B.S., and Fisher, J., 1979, Thermodynamic properties of minerals and related substances at 298.15K and 1 bar pressure and at higher temperatures, US Geological Survey Bulletin, 1452:456.

Rodríguez, L.A., Watson, I. M., Rose, W.I., Branan, Y.K., Bluth, G.J.S., Chigna, G., Matías, O., Escobar, D., Carn, S.A., and Fischer, T.B., 2004, SO_2 emissions to the atmosphere from active volcanoes in Guatemala and El Salvador, 1999–2002, Journal of Volcanology and Geothermal Research, 138, 3-4, 325-344.

Roman, D.C., and Cashman, K.V., 2006, The origin of volcanotectonic earthquake swarms, Geology, 34, 457-460.

Rose, W. I., Conway, F. M., Pullinger, C. R., Deino, A., and McIntosh, W. C., 1999, An improved age framework for late Quaternary silicic eruptions in northern Central America, Bulletin of Volcanology, 61, 106–120.

Rose, W. I., Bommer, J. J. and Sandoval, C. A. 2004. Natural hazards and risk mitigation in El Salvador: An introduction, *in* Natural Hazards in El Salvador, Geological Society of America, Special paper 375: 1-4.

Rouwet, D., Taran, Y.A., Varley, N.R., 2004, Dynamics and mass balance of El Chichón crater lake, Mexico, Geofísica Internacional, 43, 3, 427-434.

Rowe, G.L., Brantley, S.L., Fernandez, M., Fernandez, J.F., Borgia, A., Barquero, J., 1992, Fluid-volcano interaction in an active stratovolcano: the volcanic lake system of Poás Volcano, Costa Rica, J. Volcanol. Geotherm. Res., 49, 23–51.

Ryan, P.J., and Harleman, D.R.F., 1973, Analytical and experimental study of transient cooling pond behavior. Technical report no. 161, Ralph M. Parsons Laboratory for Hydrodynamics and Water Resources, MIT.

Salazar, J.M.L. Hernández, P.A., Pérez, N.M., Olmos, R., Barahona, F., Cartagena, R., Soriano, T., López, D.L., Sumino, H., and Notsu, K., 2004, Spatial and temporal variations of diffuse CO_2 degassing at the Santa Ana–Izalco–Coatepeque volcanic

complex, El Salvador, Central America *in* El Salvador: An introduction. Geological Society of America, Special paper 375, 135-146.

Servicio Nacional de Estudios Territoriales (SNET), Informe Especial No. 1, 2005a, Emisión de ceniza del volcán de Santa Ana.

Servicio Nacional de Estudios Territoriales (SNET), Informe Especial No. 2, 2005b, Vulcanólogos realizan inspección Volcán Ilamatepec en Santa Ana.

Siebert, L., Kimberly, P., and Pullinger, C.R., 2004, The voluminous Acajutla debris avalanche from Santa Ana volcano, western El Salvador, and comparison with other Central American edifice-failure events *in* El Salvador: An introduction. Geological Society of America, Special paper 375, 5-24.

Simkin, T., and Siebert, L., 1994, *Volcanoes of the World*: Geoscience Press, Tucson, 349 p.

Smithsonian Eruptive History, Santa Ana volcano, http://www.volcano.si.edu/world/volcano.cfm?vnum=1403-02=&volpage=erupt.

Smithsonian Institution, 1990, Apaneca Range, El Salvador. Bulletin of the Global Volcanism Network, 15 (11).

Smithsonian Institution, 1992, Mount Spurr, Alaska, USA. Bulletin of the Global Volcanism Network, 17(09).

Smithsonian Institution, 1994, Pagan, Mariana Islands, USA, Bulletin of the Global Volcanism Network, 19(02).

Smithsonian Institution, 2001, Santa Ana, El Salvador. Bulletin of the Global Volcanism Network, 26 (04).

Smithsonian Institution, 2005, Santa Ana, El Salvador. Bulletin of the Global Volcanism Network, 30 (09).

Smithsonian Institution, 2006, Nyiragongo, Democratic Republic of the Congo. Bulletin of the Global Volcanism Network, 31 (01).

Smithsonian Institution, 2007, Santa Ana, El Salvador. Bulletin of the Global Volcanism Network, 32 (04).

Sparks, R.S.J., 2000, The causes and consequences of eruptions of andesite volcanoes: opening remarks, Philosophical Transactions: Mathematical, Physical and Engineering Sciences, v. 358, no. 1770, 1435-1440.

Stoiber, R.E., Williams, S.N., Malinconico, L.L., Jr., Johnston, D.A. and Casadevall, T.J., 1981, Mt. St. Helens: evidence of increased magmatic gas component, Journal of Volcanology and Geothermal Research, 11, 203-212.

Symonds, R.B., Rose, W.I., Bluth, G., and Gerlach, T.M., 1994, Volcanic gas studies: methods, results, and applications, in Carroll, M.R., and Holloway, J.R., eds., Volatiles in Magmas: Mineralogical Society of America Reviews in Mineralogy, 30, 1-66.

Tait, S., Jaupart, C., Vergniolle, S., Pressure, gas content and eruption periodicity of a shallow crystallising magma chamber, Earth and Planetary Science Letters, 92, 107-123.

Takano, B., Saitoh, H., Takano, E., 1994, Geochemical implications of subaqueous molten sulfur at Yugama, Kusatsu-Shirane Volcano, Japan, Geochem J., 28, 199–216.

Takano, B., Watanuki, K., 1990, Monitoring of volcanic eruptions at Yugama crater lake by aqueous sulfur oxyanions. J. Volcanol. Geotherm. Res., 40, 71–87.

Taran, Y., and Rouwet, D., 2008, Estimating thermal inflow to El Chichón crater lake using the energy budget, chemical and isotope balance approaches, JVGR, in review.

Tonooka, H., Sakuma, F., Kudoh, M., and Iwafune, K., 2003, ASTER/TIR onboard calibration status and user-based recalibration, Proceedings of SPIE, 5234, 191-201.

Trunk, L., 2005, Investigating crater lake warming using ASTER thermal imagery: case studies at Ruapehu, Poas, Kawah Ijen, and Copahue volcanoes, unpublished MSc Thesis. University of Washington, 71 p.

Trunk, L., and Bernard, A., 2008, Investigating Crater Lake Warming Using ASTER Thermal Imagery: Case Studies at Ruapehu, Poas, Kawah Ijen, and Copahue Volcanoes, JVGR, in press.

Trusdell, F.A., Sako, M.K., Moore, R.B., Koyanagi, R.Y., Schilling, S., 2001, Preliminary studies of seismicity, ground deformation, and geology, Commonwealth of the Northern Mariana Islands, May 20 to June 8, 2001. Report prepared for Office of the Governor, CMNI, http://www.cnmiemo.org/Preliminary%20Studies%20Northern%20Mariana%20Islands.htm.

Varekamp, J.C., Pasternack, G.B., and Rowe, G.L, 2000, Volcanic lake systematics II. Chemical constraints, Journal of Volcanology and Geothermal Research, 97, 161-179.

Walker, J.A., Templeton, S., and Cameron, B.I., 2006, The chemistry of spring waters and fumarolic gases encircling Santa Maria volcano, Guatemala: Insights into regional hydrothermal activity and implications for volcano monitoring, *in* Geological Society of America Special Paper, 412, 59-83.

Watanabe, H., 1987. Eruption mechanism of Izu-Oshima volcano from the viewpoint of volcanic tremors. *Earth Mon* **9**, pp. 475–480.

Wohletz, K, and Heiken, G., 1992, *Volcanology and Geothermal Energy*: University of California Press, Berkeley, 432 p.

Wolfe, E.W., and Hoblitt, R.P., 1996, Overview of the eruption. *in*: Newhall, C.G., Punongbayan, R.S, eds., *Fire and Mud: Eruptions and Lahars of Mount Pinatubo, Philippines*: Quezon City, Philippines: Philippine Inst Volc Seism, and Seattle: Univ Wash Press, p 3-20.

Yamamoto, T., Nakamura, Y., Glicken, H., 1999, Pyroclastic density current from the 1888 phreatic eruption of Bandai volcano, NE Japan, JVGR, 90, 191-207.

Yu, T., Rose, W.I., and Prata, A.J., 2002, Atmospheric correction for satellite-based volcanic ash mapping and retrievals using "split window" IR data from GOES and AVHRR, J Geophys Res, 106: No D16, 10.1029.

Appendix A: Correction for degradation of the ASTER sensor

The correction for sensor degradation must be applied to TIR values in radiance with units of µm, but AST04 brightness temperature at sensor values are given in scaled temperatures with units ofºC (scale factor of 100), so several conversions must be applied.

First, scaled TIR temperatures (ºC*100) are converted to unscaled temperatures (ºC), then converted fromºC to Kelvin. Second, Band 13 and Band 14 temperatures ($T_{Band\ 13}$ and $T_{Band\ 14}$) are converted to spectral radiances ($L_{Band\ 13}$ and $L_{Band\ 14}$) using the wavelength dependent Planck equation:

$L_{Band\ 13}$ = $c1_{Band\ 13}$ / e^($c2_{Band\ 13}$/($T_{Band\ 13}$)-1)

$L_{Band\ 14}$ = $c1_{Band\ 14}$ / e^($c2_{Band\ 14}$/($T_{Band\ 14}$)-1)

where spectral radiances ($L_{Band\ 13}$ and $L_{Band\ 14}$) have units of meters and c1 and c2 are wavelength dependent constants with values of:

$c1_{Band\ 13}$ = 1252453293 W m^-3

$c2_{Band\ 13}$ = 1453.37 K

$c1_{Band\ 14}$ = 890037255 W m^-3

$c2_{Band\ 13}$ = 1357.39 K

Constants c1 and c2 are defined by Planck's constant (h), speed of light (c), Boltzmann's constant (k), Band 13 central wavelength (λ_{c13}), and Band 14 central wavelength (λ_{c14}):

$c1_{Band\ 13}$ = (2*h*(c^2))/λ_{c13})

$c2_{Band\ 13}$ = (h*c)/(k*λ_{c13})

$c1_{Band\ 14}$ = (2*h*(c^2))/λ_{c14})

$c2_{Band\ 14}$ = (h*c)/(k*λ_{c14})

where Planck function constants have the following values: Planck's constant = 6.6262 * 10^-34 J s, speed of light = 2.99793 * 10^8 m s^-1, Boltzmann's constant = 1.38062 *10^-23 J K^-1, Band 13 central wavelength = 9.9 * 10^-6 m, Band 14 central wavelength =10.6 * 10^-6 m.

Third, spectral radiances are converted from units of meters (m) to units of µm. Fourth, the recalibrated radiances are obtained for Band 13 and Band 14 lake pixels using equations given in lookup tables on the Japan ASTER Science Team website (http://deco.cis.ibaraki.ac.jp/RECAL/) (*Tonooka, 2003).* Fifth, recalibrated radiances are converted from units of µm to units of meters (m). The inverse of the Planck equation is applied again to convert from spectral radiance with units of meters to temperature with units of degrees Kelvin:

$$T_{Band\ 13recal} = c2_{\text{Band 13}} / ((\log_e(c1_{\text{Band 13}} / L_{Band\ 13recal}))+1)$$

$$T_{Band\ 14recal} = c2_{\text{Band 14}} / ((\log_e(c1_{\text{Band 14}} / L_{Band\ 14recal}))+1)$$

Lastly, recalibrated temperature ($T_{Band\ 13recal}$ and $T_{Band\ 14recal}$) is converted from degrees Kelvin back to degrees Celsius.

Appendix B: Energy budget model
Annotated and adapted from *Pasternack & Varekamp (1997)*

Perfect Mixing Hydrothermal Steady State
Crater Lake Model for Santa Ana 2000-2007

Clear["global`*"]

The relation between SO2 flux and gas temperature
% choose average arc magmatic gas temperature of 800ºC (Symonds et al., 1994)
gastemp[so2_] := 800;

Determination of the distribution of input mass
% assume volcanic gas is composed of only three major components: H2O, CO2, and SO2.
% choose average arc magmatic gas ratio (H2O:CO2:SO2) of 93:5:2 (Symonds et al., 1994)
% molar mass in units of mol/day
so2molday [so2_] := 10^6 so2/64.07 *%SO2 in tonnes/day*
totlmolday [so2_] := so2molday[so2]/0.02
co2molday [so2_] := 0.05totlmolday[so2]
h2omolday [so2_] := 0.93totlmolday[so2]
% convert molar mass of water to molecular mass of water
h2omassday [so2_] := 18 h2omolday [so2]/10^8

Lake and atmosphere characteristics (equations adapted for El Salvador)
latitude = 13.853;
% units are degrees north
elevation = 2300;
% units are meters
airtsl = 30-0.008*latitude^2;
% air temperature at sea level dependant on latitude (Linacre, 1992)
airtc = airtsl - 0.006*elevation;
% calculate air temperature using ICAO defined global lapse rate of 6ºC/km. Use latitude dependent air temperature only if actual air temperature is unknown
airtc= 16.12;
% VARIABLE, if atmospheric temperature is known, input the value here. 16.12ºC is the average atmospheric temperature for Santa Ana 2000-2007
raintc = airtc;
% assume rain temperature equals air temperature

Temperature conversions to degrees Kelvin
raintemp = raintc + 273;
airtemp = airtc + 273;

Air Pressure at Volcano

airpresspascal = 101300 ((airtemp - .0065 elevation)/airtemp)^5.2586;
airpressmbar = 769;

Basin characteristics

lakeradius = 100;
% units are meters
windspeed = 2.5;
% units are meters per second
catchradius = 2.5 lakeradius;
% units are meters
catcharea = 3.141592654 catchradius^2;
% units are meters^2
lakearea = 3.141592654 lakeradius^2;
% units are meters^2
p = 5.4;
% VARIABLE; 5.4 m/yr is the average precipitation rate for Santa Ana 2000-2007
pday = p 0.002739726;
% precipitation rate in meters/day
meth2oday = catcharea*pday/100;
*% catchment area in m^2 * precipitation rate in meters/day*

Heat influx algorithm

*% The energy flux from the volcanic input is the sum of the mass (moles) of a component * the specific enthalpy (J/mol) of a component, for the three components: H2O, CO2, SO2.*
%qwjday is the volcanic inputs from H2O
%qgcjday is the volcanic inputs from CO2
% qgsjday is the volcanic inputs from SO2
% Specific enthalpy (J/mol) is defined as the integral from the temperature of the liquid (i.e. lake temperature) to the temperature of the gas evaluated from the heat capacity of a component (J/mol K) for the given gas temperature (K)

Water vapor

*% energy flux from the volcanic input from water takes into account the phase change of water from gas to liquid and is equal to the change in enthalpy of formation at standard state * molar mass of water*
qwjday [x_,so2_] := 38.75*(gastemp[so2] - 372.8)*h2omolday[so2] +
75.5*(372.8 - x)*h2omolday[so2] +
40866*h2omolday[so2];
% 38.75 J/mol K is the average heat capacity for water vapor between 500<T<1100K; 75.5 J/mol K is the heat capacity for liquid water; 40866 J is the enthalpy of vaporization (after Robie et al., 1979, p. 172).

Carbon dioxide gas

*% the heat capacity equation for carbon dioxide in J/mol K is given in Robie et al. (1979), p. 147: Cp=87.82 - 2.6442 10^-3 T - 998.86 T^-0.5 + 7.0641 *10^5 T^-2*

% b is the heat capacity of carbon dioxide evaluated at liquid temperature
b [x_] := 87.82 x - (2.6442 10^-3)*.5 x^2 - 998.86*2 x^(0.5) - 706410 x^(-1)

% qgcb is heat capacity for carbon dioxide evaluated at gas temperature
qgcb [gastemp_] := 87.82 gastemp - (2.6442 10^-3)*.5 gastemp^2 -
998.86*2 gastemp^(0.5) - 706410 gastemp^(-1)

% qgcc is the specific enthalpy for carbon dioxide
qgcc [x_, gastemp_] := qgcb[gastemp] - b[x]

*% qgcjday is the volcanic input from carbon dioxide=specific enthalpy CO2 * molar mass CO2*
qgcjday [x_,so2_] := qgcc[x,gastemp[so2]] * co2molday[so2]

Sulfur dioxide gas

*% the heat capacity equation for sulfur dioxide in J/mol K is given in Robie et al. (1979), p. 212: Cp=86.219 – 4.3073 10^-3 T – 886.46 T^-0.5 + 5.5769 *10^5 T^-2*

% c is the heat capacity of sulfur dioxide evaluated at liquid temperature
c [x_] := 86.219 x - (4.3073 10^-3)*.5 x^2 - 886.46*2 x^(0.5) - 557690 x^(-1)

% qgsb is heat capacity for sulfur dioxide evaluated at gas temperature
qgsb [gastemp_] := 86.219 gastemp - (4.3073 10^-3)*.5 gastemp^2 -
886.46*2 gastemp^(0.5) - 557690 gastemp^(-1)

% qgsc is the specific enthalpy for sulfur dioxide
qgsc [x_, gastemp_] := qgsb[gastemp] - c[x]

*% qgsjday is the volcanic input from sulfur dioxide=specific enthalpy SO2 * molar mass SO2*
qgsjday [x_,so2_] := qgsc [x, gastemp[so2]] * so2molday[so2]

Net shortwave radiation

% average solar flux in J/m^2 s from Linacre (1992)
solarflux = 185 +5.9*latitude - 0.22*latitude^2 + 0.00167*latitude^3;
% integrate flux over of lake area to convert from J/m^2 s to J/day
qsunjday = solarflux*lakearea*86400;
% convert from J/day to MW
*% MW=10^6 W and W=J/s and 1 day=86400 seconds, so MW=(J*10^-6)/86400s*
qsunmw = (1 10^-6) qsunjday/86400;

Longwave radiation influx

% average cloud cover from Linacre (1992)

clouds = 5.1946 - 0.23227*latitude + 0.0067727*latitude^2 -
(4.9495 10^-5)*latitude^3;

% lradinjday is the longwave radiation from the atmosphere reaching the lake, taking into account cloud cover and integrating over lake area

radina = 208 + 6*airtc;

lradinjday = radina*(1 + 0.0034 clouds^2)*lakearea*86400;

% convert from J/day to MW

*% MW=10^6 W and W=J/s and 1 day=86400 seconds, so MW=(J*10^-6)/86400s*

lradinmw=lradinjday*(1*10^-6)/86400;

Summation of influx terms

% total heat influx to the lake is the summation of the volcanic flux + long and short wave solar radiation

heatinjday [x_,so2_]:= qwjday[x,so2] + qgcjday[x,so2] + qgsjday[x,so2] +
qsunjday + lradinjday;

% energy input from the volcanic input only

gasinjday [x_,so2_]:= qwjday[x,so2] + qgcjday[x,so2] + qgsjday[x,so2]

% convert from J/day to MW

*% MW=10^6 W and W=J/s and 1 day=86400 seconds, so MW=(J*10^-6)/86400s*

volgasmw [x_,so2_]:= (1 10^-6)*gasinjday[x,so2]/86400;

heatmw [x_,so2_]:= (1 10^-6) heatinjday[x,so2]/86400;

Heat outflux algorithm

Net radiative heat loss

% long wavelength radiation from lake in J/day (Stefan-Boltzmann law)

radoutjday [x_] := (5.67 10^-8)*(x^4)*lakearea*86400

% 5.67X10^-8 J/s m^2 K^4 (Stefan-Boltzmann constant)

% x is lake temperature in K

% lakearea in m^2

% 86400 is time interval in seconds = 1 day

Evaporation outflux (by wind and buoyancy)

% evaporation energy flux after Ryan and Harleman (1973)

% e0 is the saturation water vapor pressure (mb) at absolute lake temperature

d [x_] := (-0.00019899 x^2) + (0.179064 x) - 32.23339;

e0 [x_] := E^(d[x]);

% E is the base of natural logarithms (e) and has a value of 2.71828

% x is lake temperature in K

% virtlaktemp is the virtual lake temperature of surface water

virtlaktemp [x_] := x/(1-(0.378 e0[x])/airpressmbar);

```
        % e0 is the water vapor pressure (mb) at absolute lake temperature
        % x is lake temperature in K
        % airpressmbar is the ambient air pressure (mb)

% ea is the saturated vapor pressure 2 m above the lake
ewa = (-0.00019899 airtemp^2) + (0.179064 airtemp) - 32.23339;
ea = E^(ewa);
        % E is the base of natural logarithms (e) and has a value of 2.71828
        % airtemp is atmospheric temperature in K

% virtairtemp is the virtual air temperature of ambient air
virtairtemp = airtemp/(1- (0.378 ea)/airpressmbar);
        % airtemp is atmospheric temperature in K
        % ea is the saturated vapor pressure 2 m above the lake
        % airpressmbar is the ambient air pressure (mb)

% evapjday is evaporation energy flux in joules per day
evapjday [x_] := (2.7*((virtlaktemp[x] - virtairtemp)^1/3) + 3.2 windspeed)*(e0[x] -
            ea)*lakearea*86400
        % virtairtemp is the virtual air temperature of ambient air
        % virtlaktemp is the virtual lake temperature of surface water
        % windspeed in meters per second
        % e0 is the saturation water vapor pressure (mb) at absolute lake
            temperature
        % ea is the saturated vapor pressure 2 m above the lake
        % lakearea in meters^2
        % 86400 s = 1 day

% evapmolday is evaporation mass flux in moles per day
evapmolday [x_] :=evapjday [x] / 40866
        % 40866 is a conversion factor with units of J/mol
% convert from molar mass to molecular mass
evapmassday [x_] := 18 evapmolday [x]/10^8
% evapdis is evaporation mass flux in m^3 per day
evapdis [x_] := evapmolday [x] / 55555.6
        % 55555.6 is a conversion factor with units of mol/m^3
```

Rain water heating term

```
% heatrainjday is the rain water heating term in joules per day
heatrainjday [x_] := (x - raintemp)*75.42*55555.6*meth2oday;
        % x is lake temperature in K
        % raintemp is the temperature of rainwater in K
        %75.42 J/mol K is the average heat capacity of water (Robie et al., 1979)
        % 55555.6 is a conversion factor with units of mol/m^3
        % meth2oday is the catchment area in m^2 * precipitation rate in meters per day
```

Conductive loss

% condjday is the conductive heat loss, or sensible heat loss, in joules per day as defined by Bowen's ratio

condjday [x_] := 0.61 evapjday [x] * (x - airtemp) / (e0[x] - ea)

% 0.61 m/ºC is Bowen's constant
% evapjday is evaporation energy flux in joules per day
% x is lake temperature in K
% airtemp is atmospheric temperature in K
% e0 is the saturation water vapor pressure (mb) at absolute lake temperature
% ea is the saturated vapor pressure 2 m above the lake

Summation of outflux terms

% total heat flux leaving the lake in joules per day

heatoutjday [x_] := radoutjday[x] + evapjday[x] + heatrainjday[x] + condjday[x]

%convert from joules per day to MW
*% MW=10^6 W and W=J/s and 1 day=86400 seconds, so MW=(J*10^-6)/86400s*

radoutmw [x_]:= (1 10^-6) radoutjday[x]/86400
evapmw [x_]:= (1 10^-6) evapjday[x]/86400
heatrainmw [x_]:= (1 10^-6) heatrainjday[x]/86400
condmw [x_]:= (1 10^-6) condjday[x]/86400

% calculate net radiative flux in MW

netlradmw[x_]:= radoutmw[x] – lradinmw

Apply mass conservation for heat and water

Water conservation

% total water influx in m^3/day equals meteoric water flux (meth2oday) – evaporative water flux (evapmassday) + volcanic water flux (h2omolday)

watgain [so2_] := meth2oday - evapmassday[x] + 18h2omolday[so2]/10^8

% meth2oday in m^3/day
% evapmassday in molecular mass/day
% 18h2omolday[so2]/10^8 in molecular mass/day

% lake level in m/day equals total water influx per lake area

lakelevel[so2_] :=100*watgain[so2] / lakearea

Solve equations

% solve the energy balance equation with two unknowns: SO2 and lake temperature (x). solves equation iteratively based on SO2. For example, starts at 0.3, ends at 200, and uses steps of 10. outputs data in table format.

data = Table [{lake, airtc, so2, x-273, volgasmw[x,so2], p, h2omassday[so2],

```
evapmassday[x],  watgain[so2], lakelevel[so2], radoutmw[x], lradinmw, evapmw[x],
condmw[x]} /. FindRoot [{heatoutjday[x] == heatinjday[x, so2]}, {x, 295},
AccuracyGoal->5], {so2, 0.3, 200, 10}];
```

Appendix C: Copyright permission

SPRINGER LICENSE
TERMS AND CONDITIONS

Nov 18, 2008

This is a License Agreement between Anna S Colvin ("You") and Springer ("Springer"). Please note that you are liable to account for Value Added Tax (VAT). The license consists of your order details, the terms and conditions provided by Springer, and the payment terms and conditions.

License Number

2054990257451

License date

October 23, 2008

Licensed content publisher

Springer

Licensed content publication

Bulletin of Volcanology

Licensed content title

Volcanic lake systematics I. Physical constraints

Licensed content author

Gregory B. Pasternack

Licensed content date

May 1, 1997

Volume number

58

Issue number

7

Pages

528 - 538

Type of Use

Thesis / Dissertation

Details of use

Print

Requestor Type

Individual

Portion of the article

Figures

Title of your thesis / dissertation

Crater lake evolution during volcanic unrest: case study of the 2005 phreatic eruption at Santa Ana volcano, El Salvador.

Expected completion date

Dec 2008

Total

0.00 USD

Terms and Conditions

Introduction
The publisher for this copyrighted material is Springer Science + Business Media. By clicking "accept" in connection with completing this licensing transaction, you agree that the following terms and conditions apply to this transaction (along with the Billing and

Payment terms and conditions established by Copyright Clearance Center, Inc. ("CCC"), at the time that you opened your Rightslink account and that are available at any time at http://myaccount.copyright.com).

Limited License
With reference to your request to reprint in your thesis material on which Springer Science and Business Media control the copyright, permission is granted, free of charge, for the use indicated in your enquiry. Licenses are for one-time use only with a maximum distribution equal to the number that you identified in the licensing process.

This License includes use in an electronic form, provided it is password protected or on the university's intranet, destined to microfilming by UMI and University repository. For any other electronic use, please contact Springer at (permissions.dordrecht@springer.com or permissions.heidelberg@springer.com)

The material can only be used for the purpose of defending your thesis, and with a maximum of 100 extra copies in paper.

Although Springer holds copyright to the material and is entitled to negotiate on rights, this license is only valid, provided permission is also obtained from the (co) author (address is given with the article/chapter) and provided it concerns original material which does not carry references to other sources (if material in question appears with credit to another source, authorization from that source is required as well). Permission free of charge on this occasion does not prejudice any rights we might have to charge for reproduction of our copyrighted material in the future.

Altering/Modifying Material: Not Permitted
However figures and illustrations may be altered minimally to serve your work. Any other abbreviations, additions, deletions and/or any other alterations shall be made only with prior written authorization of the author(s) and/or Springer Science + Business Media. (Please contact Springer at permissions.dordrecht@springer.com or permissions.heidelberg@springer.com)

Reservation of Rights
Springer Science + Business Media reserves all rights not specifically granted in the combination of (i) the license details provided by you and accepted in the course of this licensing transaction, (ii) these terms and conditions and (iii) CCC's Billing and Payment terms and conditions.

Copyright Notice:
Please include the following copyright citation referencing the publication in which the material was originally published. Where wording is within brackets, please include verbatim.
"With kind permission from Springer Science+Business Media: <book/journal title,

chapter/article title, volume, year of publication, page, name(s) of author(s), figure number(s), and any original (first) copyright notice displayed with material>."

Warranties: Springer Science + Business Media makes no representations or warranties with respect to the licensed material.

Indemnity
You hereby indemnify and agree to hold harmless Springer Science + Business Media and CCC, and their respective officers, directors, employees and agents, from and against any and all claims arising out of your use of the licensed material other than as specifically authorized pursuant to this license.

No Transfer of License
This license is personal to you and may not be sublicensed, assigned, or transferred by you to any other person without Springer Science + Business Media's written permission.

No Amendment Except in Writing
This license may not be amended except in a writing signed by both parties (or, in the case of Springer Science + Business Media, by CCC on Springer Science + Business Media's behalf).

Objection to Contrary Terms
Springer Science + Business Media hereby objects to any terms contained in any purchase order, acknowledgment, check endorsement or other writing prepared by you, which terms are inconsistent with these terms and conditions or CCC's Billing and Payment terms and conditions. These terms and conditions, together with CCC's Billing and Payment terms and conditions (which are incorporated herein), comprise the entire agreement between you and Springer Science + Business Media (and CCC) concerning this licensing transaction. In the event of any conflict between your obligations established by these terms and conditions and those established by CCC's Billing and Payment terms and conditions, these terms and conditions shall control.

Jurisdiction
All disputes that may arise in connection with this present License, or the breach thereof, shall be settled exclusively by the country's law in which the work was originally published.